Nanomaterials for Biodiagnostic

- Nucleic Acid
  - Genetic information for identification
  - Diseases, bacterium, virus, pathogen
  - PCR with molecular fluorophore, State of the Art
  - Expansive, Non-portable, Non-multiplexing
- Proteins
  - Cancers and diseases, unusual high concentration of marker
  - ELISA (~pM) with molecular fluorophore
  - No PCR version

ELISA (Enzyme-Linked Immunosorbent Assay)

is a biochemical technique used mainly in immunology to detect the presence of an antibody or an antigen in a sample. It utilizes two antibodies, one of which is specific to the antigen and the other of which is coupled to an enzyme. This second antibody gives the assay its "enzyme-linked" name, and will cause a chromogenic or fluorogenic substrate to produce a signal.

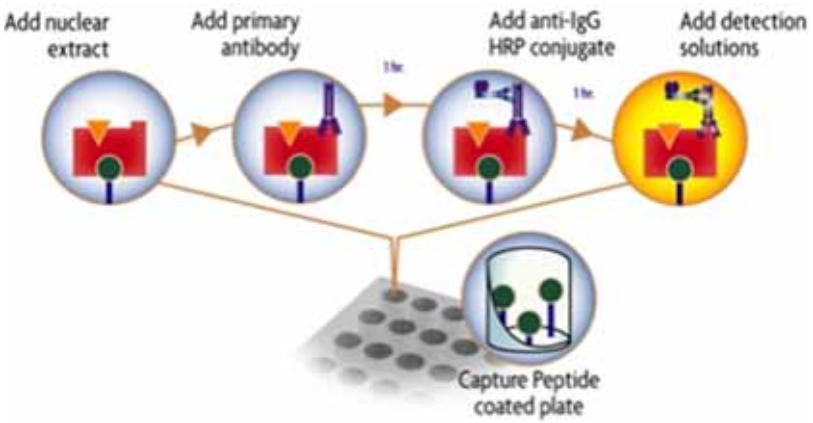

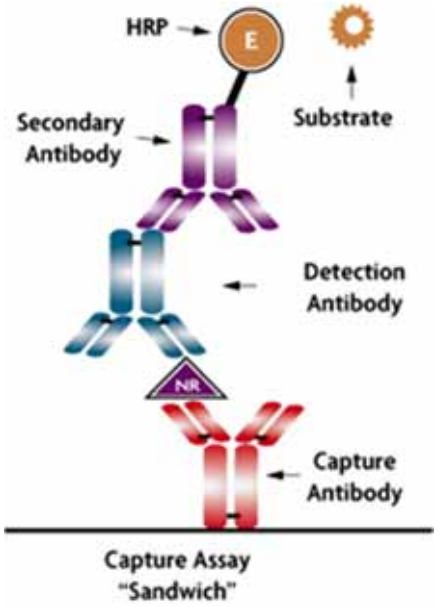

Why Nanomaterials?

- Molecular fluorophores
  - Limited spectral response
  - photostability
- Nanomaterials
  - Small size (1-100 nm)
  - Chemically tailorable physical properties
  - Unusual target binding properties
  - Structure robustness

Tailorable Physical Properties

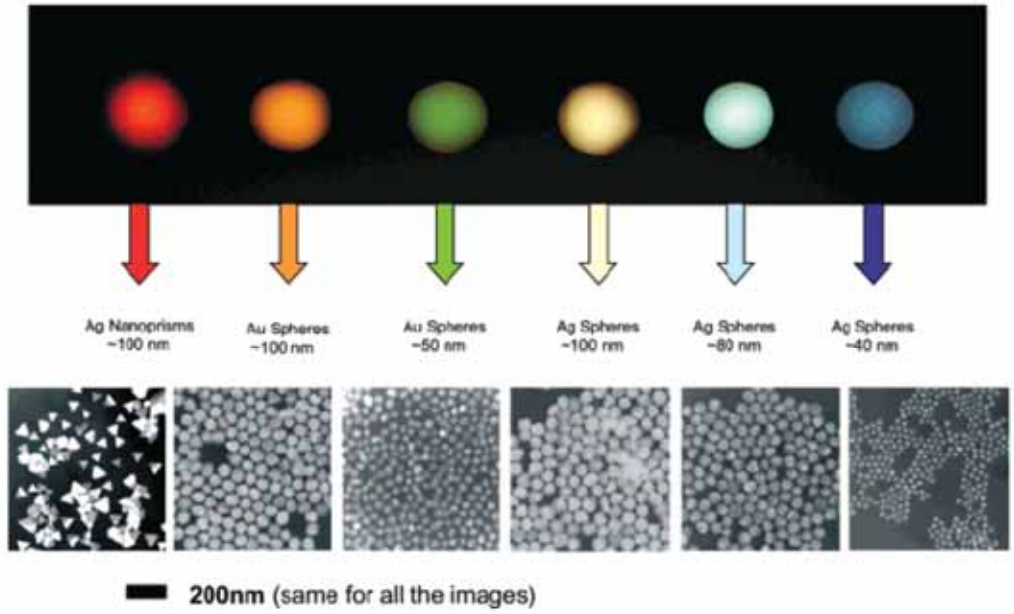

Figure 1. Sizes, shapes, and compositions of metal nanoparticles can be systematically varied to produce materials with distinct light-scattering properties.

Nanomaterial Detection

- Optical
- Electrical and electrochemical
- Magnetic
- Nanowire and Nanotubes
- Nanofabrication

Colorimetric Detection of DNA

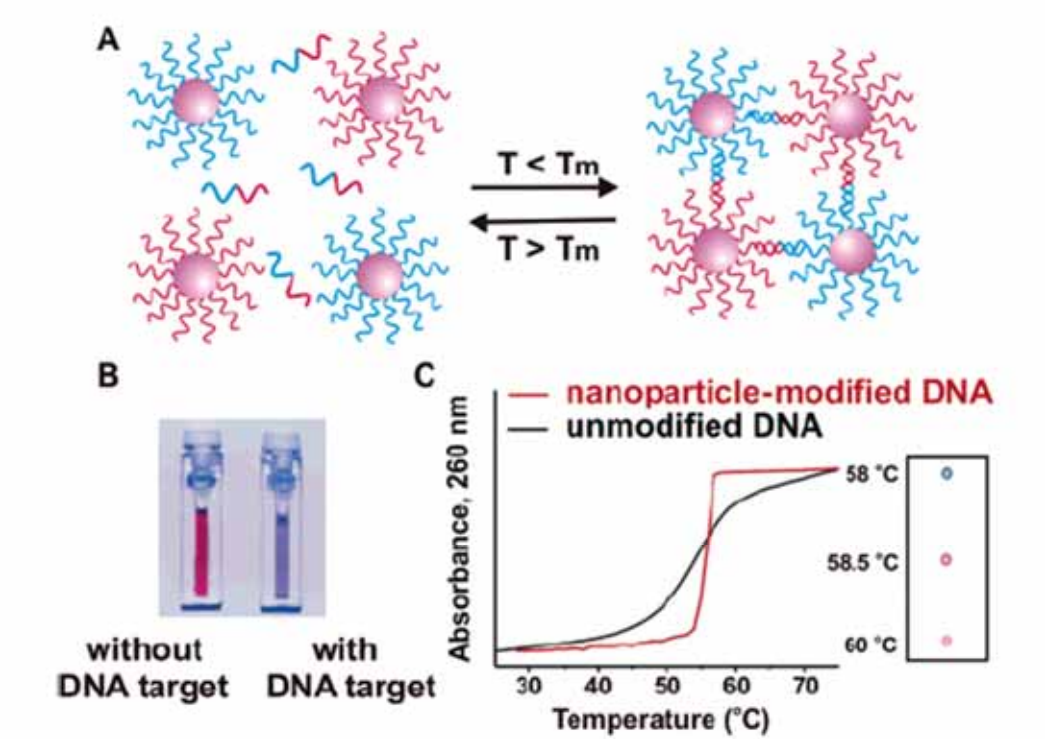

Figure 2. In the presence of complementary target DNA, oligonucleotide-functionalized gold nanoparticles will aggregate (A), resulting in a change of solution color from red to blue (B). The aggregation process can be monitored using UV−vis spectroscopy or simply by spotting the solution on a silica support (C). (Reprinted with permission from *Science* (http://www.aaas.org), ref 29. Copyright 1997 American Association for the Advancement of Science.)

A DNA-based method for rationally assembling nanoparticles into macroscopic materials

Chad A. Mirkin, Robert L. Letsinger, Robert C. Mucic & James J. Storhoff

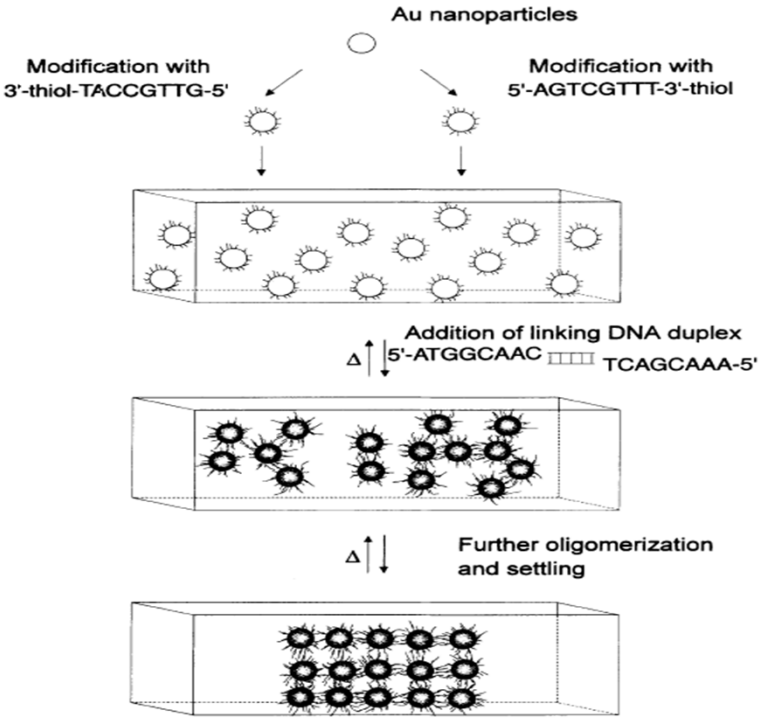

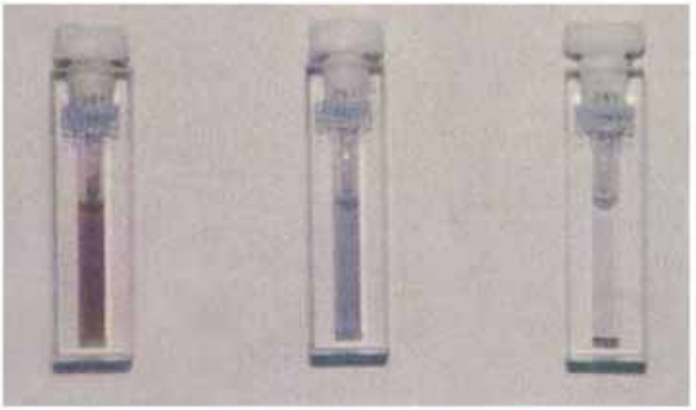

FIG. 2 Cuvettes with the Au colloids and the four DNA strands responsible for the assembly process. Left cuvette, at 80 °C with DNA-modified colloids in the unhybridized state; centre, after cooling to room temperature but before the precipitate settles; and right, after the polymeric precipitate settles to the bottom of the cuvette. Heating either of these cool solutions results in the reformation of the DNA-modified colloids in the unhybridized state (shown in the left cuvette).

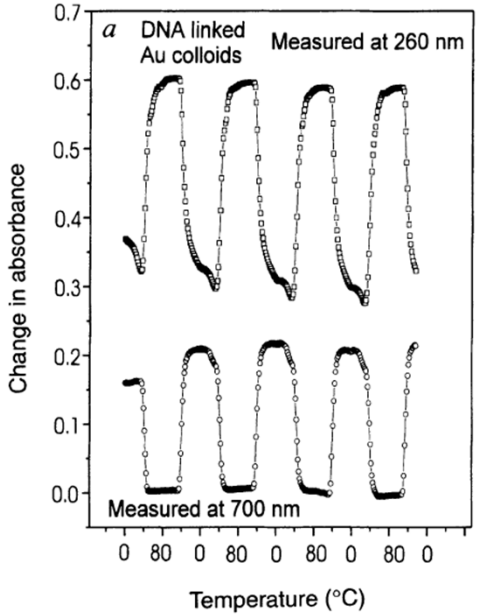

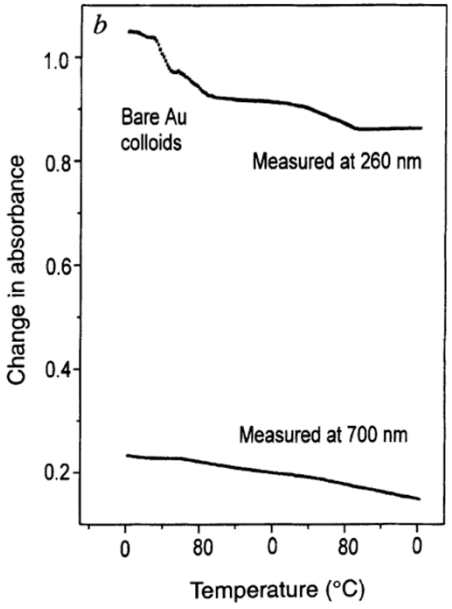

Nature, 1996, 382, 607

Selective Colorimetric Detection of Polynucleotides Based on the Distance-Dependent Optical Properties of Gold Nanoparticles

Robert Elghanian, James J. Storhoff, Robert C. Mucic,
Robert L. Letsinger,* Chad A. Mirkin*

SCIENCE • VOL. 277 • 22 AUGUST 1997

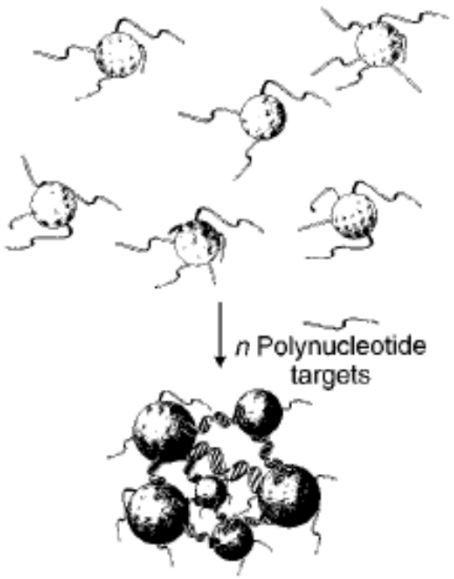

Fig. 1. Schematic representation of the concept for generating aggregates signaling hybridization of nanoparticle-oligonucleotide conjugates with oligonucleotide target molecules. The nanoparticles and the oligonucleotide interconnects are not drawn to scale, and the number of oligomers per particle is believed to be much larger than depicted.

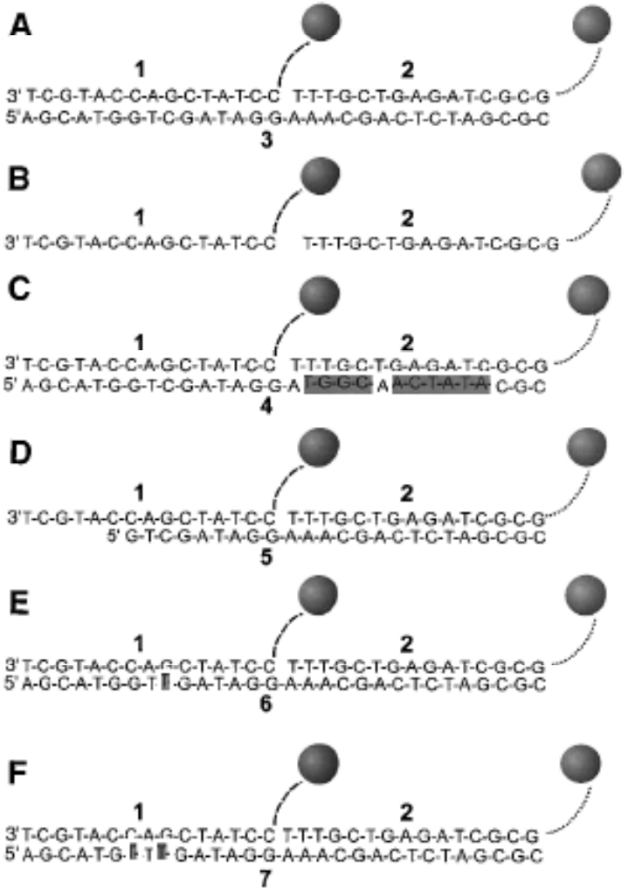

Fig. 2. Mercaptoalkyloligonucleotide-modified 13-nm Au particles and polynucleotide targets used for examining the selectivity of the nanoparticle-based colorimetric polynucleotide detection system. (**A**) Complementary target; (**B**) probes without the target; (**C**) a half-complementary target; (**D**) a 6-bp deletion; (**E**) a 1-bp mismatch; and (**F**) a 2-bp mismatch. For the sake of clarity, only two particles are shown; in reality a polymeric aggregate with many particles is formed. Dashed lines represent flexible spacer portions of the mercaptoalkyloligonucleotide strands bound to the nanoparticles; note that these spacers, because of their noncomplementary nature, do not participate in hybridization. The full sequences for the two probes, **1** and **2**, which bind to targets **3** through **7**, are

1-5′SH-$(CH_2)_6$-$\underset{\text{spacer}}{}$[CTA-ATC-CGC-ACA-G]

$\underset{\text{probe}}{}$[CC-TAT-CGA-CCA-TGC-T]

2-5′SH-$(CH_2)_6$-$\underset{\text{spacer}}{}$[ATG-GCA-ACT-ATA-C]

$\underset{\text{probe}}{}$[GC-GCT-AGA-GTC-GTT-T]

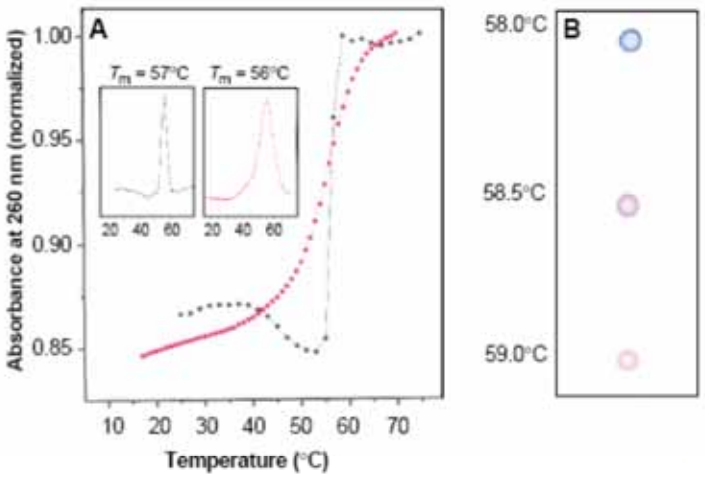

Fig. 3. (**A**) Comparison of the thermal dissociation curves for complexes of mercaptoalkyloligonucleotide-modified Au nanoparticles (black circles) and mercaptoalkyloligonucleotides without Au nanoparticles (red squares) with the complementary target, **3**, in hybridization buffer (0.1 M NaCl, 10 mM phosphate buffer, pH 7.0). For the first set (black circles), a mixture of 150 μl of each colloid conjugate and 3 μl of the target oligonucleotide in hybridization buffer (0.1 M NaCl, 10 mM phosphate, pH 7.0) was frozen at the temperature of dry ice, kept for 5 min, thawed over a period of 15 min, and diluted to 1.0 ml with buffer (final target concentration, 0.02 μM). The absorbance was measured at 1-min intervals with a temperature increase of 1°C per minute. The increase in absorption at 260 nm (A_{260}) was ~0.3 absorption units (AU). In the absence of the oligonucleotide targets, the absorbance of the nanoparticles did not increase with increasing temperature. For the second set, the mercaptoalkyloligonucleotides and complementary target (each 0.33 μM) were equilibrated at room temperature in 1 ml of buffer, and the changes in absorbance with temperature were monitored as before. The increase in A_{260} was 0.08 AU. (**Insets**) Derivative curves for each set (*15*). (**B**) Spot test showing T_c (thermal transition associated with the color change) for the Au nanoparticle probes hybridized with complementary target. A solution prepared from 150 μl of each probe and 3 μl of the target (0.06 μM final target concentration) was frozen for 5 min, allowed to thaw for 10 min, transferred to a 1-ml cuvette, and warmed at 58°C for 5 min in the thermally regulated cuvette chamber of the spectrophotometer. Samples (3 μl) were transferred to a C_{18} reverse phase plate with an Eppendorf pipette as the temperature of the solution was increased incrementally 0.5°C at 5-min intervals.

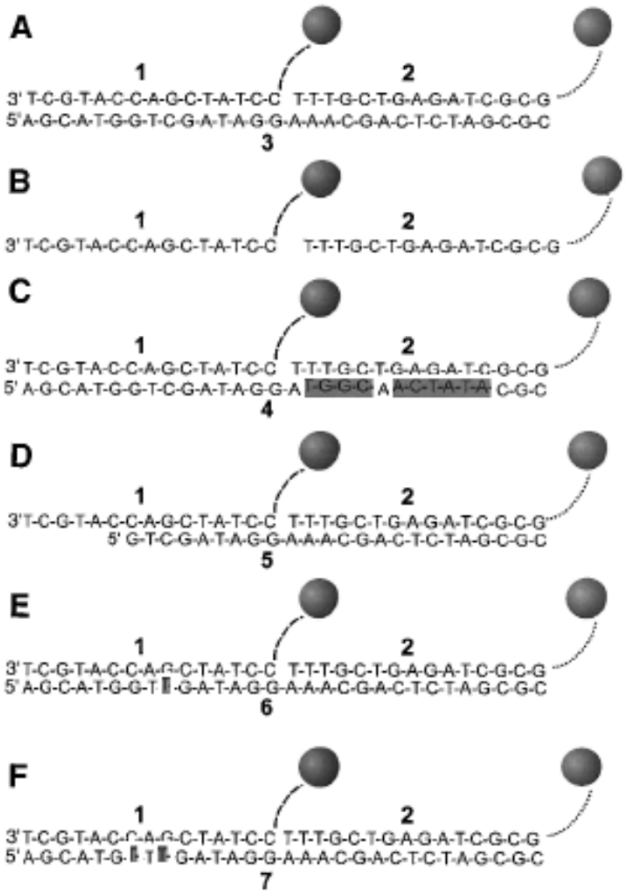

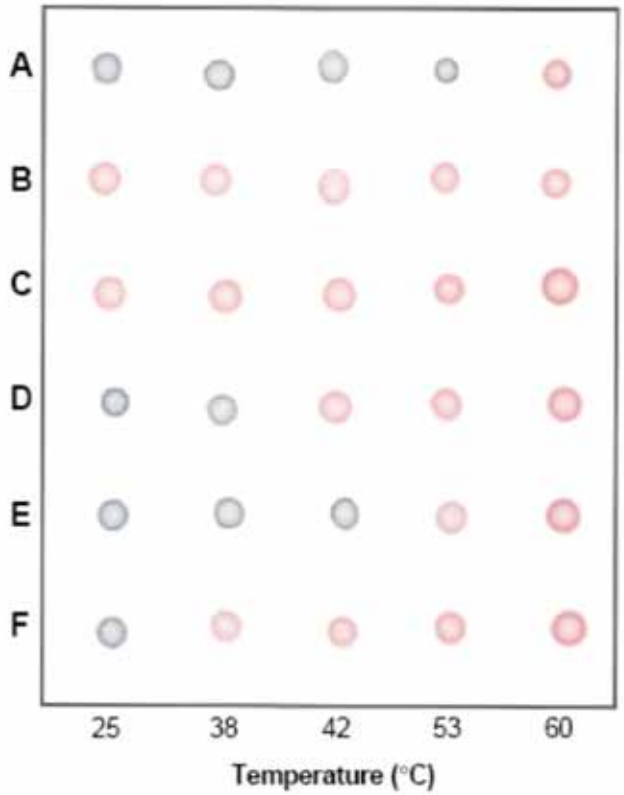

Fig. 4. Selective polynucleotide detection for the target probes shown in Fig. 2: (**A**) complementary target; (**B**) no target; (**C**) complementary to one probe; (**D**) a 6-bp deletion; (**E**) a 1-bp mismatch; and (**F**) a 2-bp mismatch. Nanoparticle aggregates were prepared in a 600-μl thin-walled Eppendorf tube by addition of 1 μl of a 6.6 μM oligonucleotide target to a mixture containing 50 μl of each probe (0.06 μM final target concentration). The mixture was frozen (5 min) in a bath of dry ice and isopropyl alcohol and allowed to warm to room temperature. Samples were then transferred to a temperature-controlled water bath, and 3-μl aliquots were removed at the indicated temperatures and spotted on a C_{18} reverse phase plate.

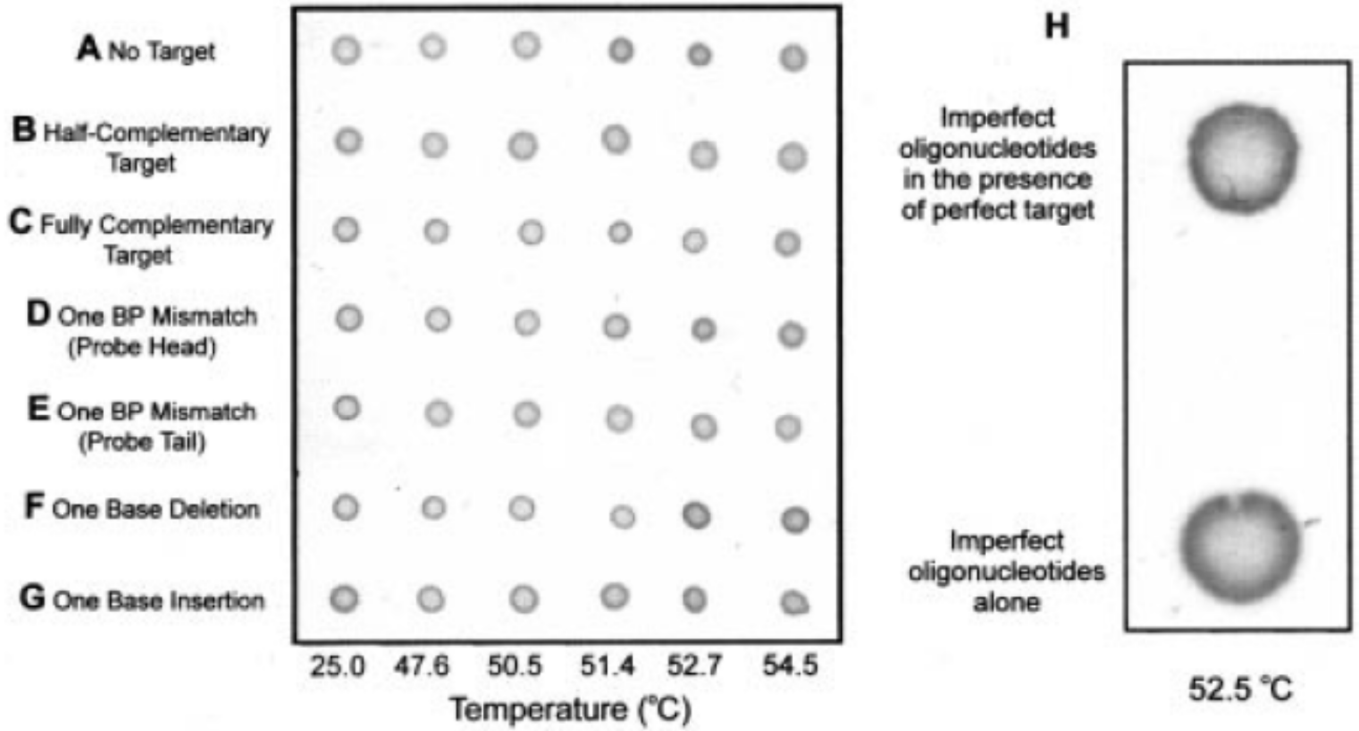

Figure 5. (A–G) The spot method for polynucleotide detection which demonstrates the selectivity of the Au nanoparticle based detection system toward single base imperfections. The probes and corresponding polynucleotide targets are listed in Figure 2. (H) Spot test demonstrating the detection and differentiation by color of a polynucleotide target in the presence of polynucleotides with single base imperfections.

1nM => 50pM

Rapid Aggregation of Gold Nanoparticles Induced by Non-Cross-Linking DNA Hybridization

Kae Sato, Kazuo Hosokawa, and Mizuo Maeda*

8102 ■ J. AM. CHEM. SOC. 2003, *125*, 8102−8103

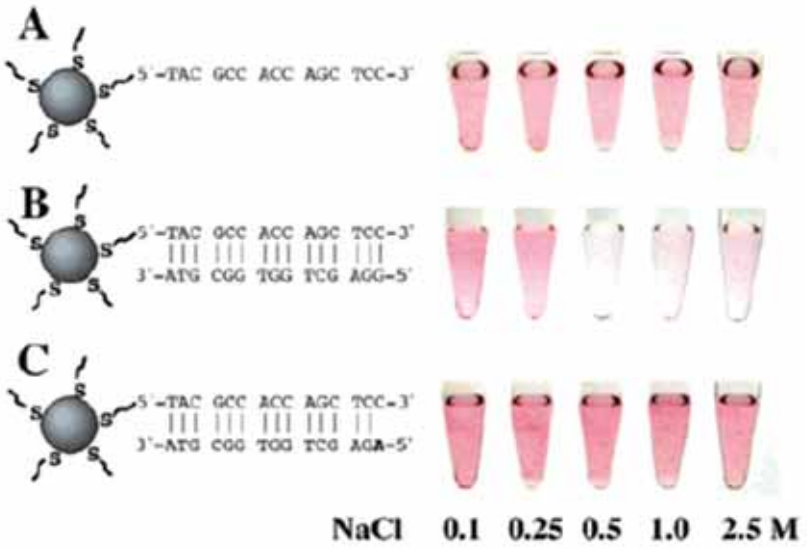

Figure 1. Aggregation behaviors of the DNA-gold nanoparticles at various NaCl concentrations at room temperature: (A) without a target DNA, (B) with the complementary target, and (C) with a target containing a single-base mismatch at its 5′ terminus. The final concentrations of the particle, the probe DNA, and the targets were 2.3, 500, and 500 nM, respectively.

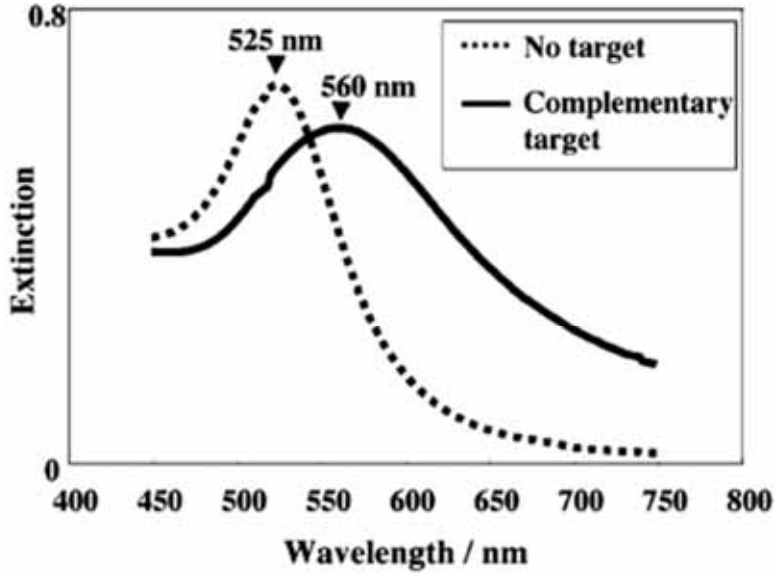

Figure 2. Visible spectra corresponding to Figure 1A (dotted line, no target) and 1B (solid line, complementary target) at 0.5 M NaCl.

60-500 nM

J. Am. Chem. Soc. **2000,** *122,* 9071−9077

Colloidal Au-Enhanced Surface Plasmon Resonance for Ultrasensitive Detection of DNA Hybridization

Lin He, Michael D. Musick, Sheila R. Nicewarner, Frank G. Salinas, Stephen J. Benkovic, Michael J. Natan, and Christine D. Keating*

Scheme 1. SPR Surface Assembly

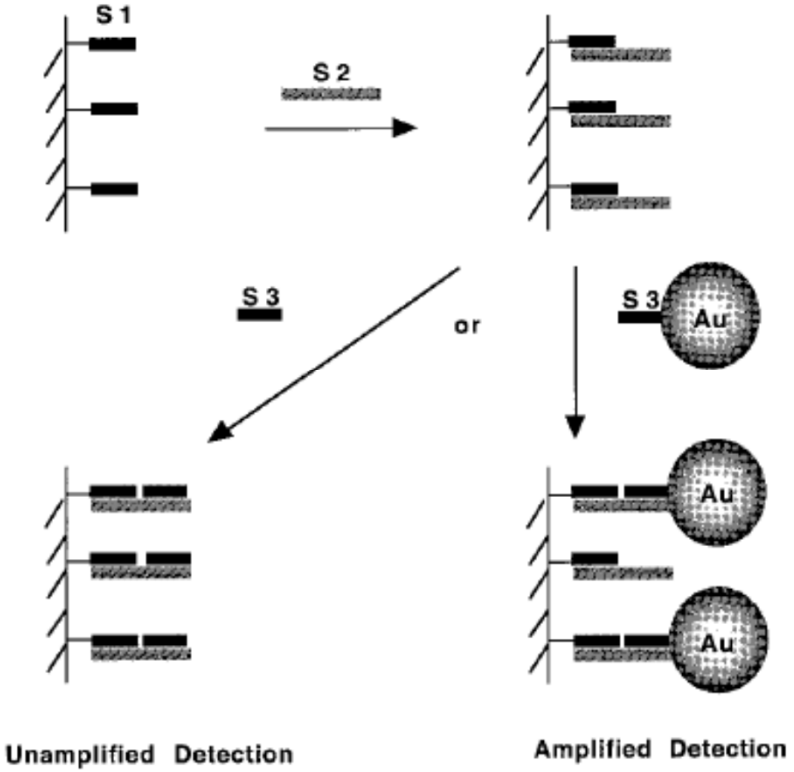

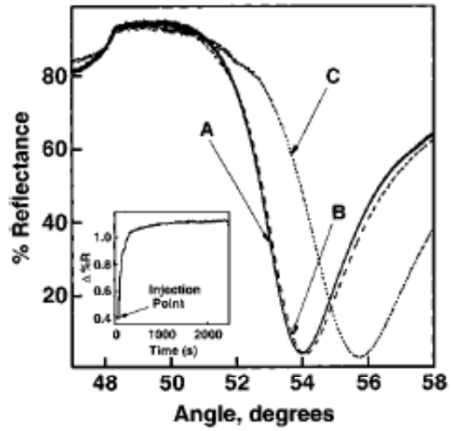

Figure 1. SPR curves of surfaces prepared in sequential steps as illustrated in Scheme 1: a MHA-coated Au film modified with a 12-mer oligonucleotide S1(A), after hybridization with its complementary 24-mer target S2 (B), and followed by introduction of S3:Au conjugate (C) to the surface. Inset: surface plasmon reflectance changes at 53.2° for the oligonucleotide-coated Au film measured during a 60-min exposure to S3:Au conjugates.

Scheme 2. SPR Surface Assembly in the Digestion Experiment

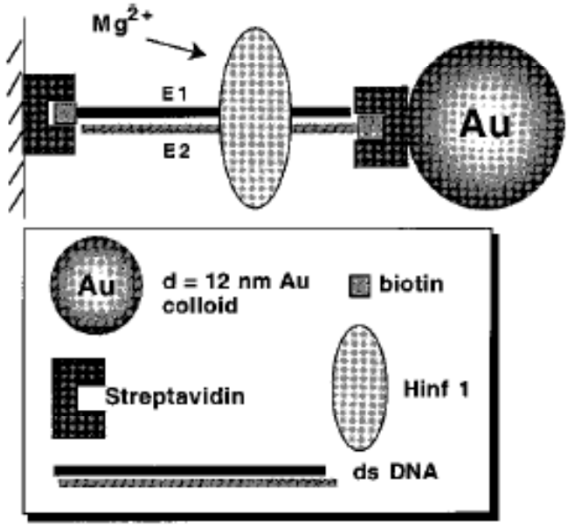

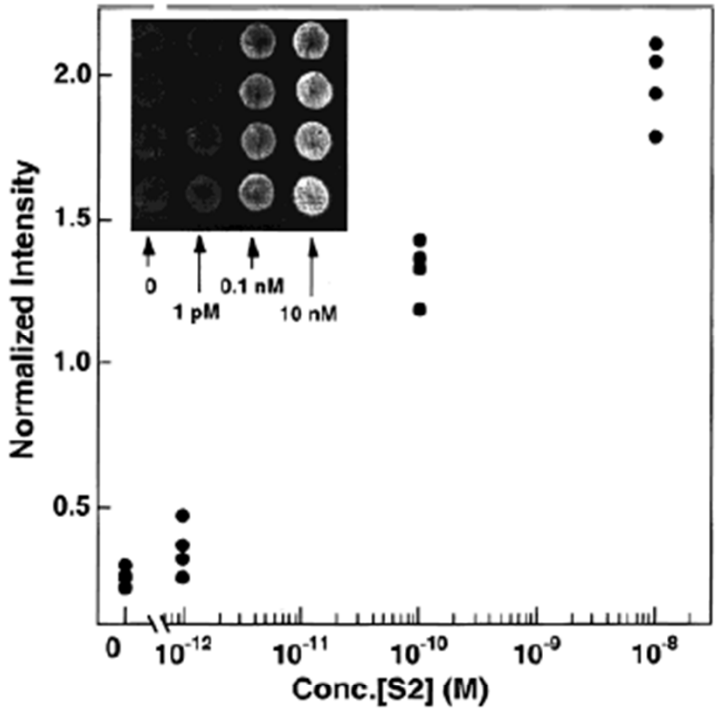

Figure 5. Plot of normalized intensity of SPR reflectance as a function of logarithmic concentration of the analyte 24-mer oligo (S2). Each spot represents one data point at the corresponding concentration. CCD parameters: exposure time = 0.3 s, 16 bit resolution, spot size = 4.5 mm in diameter. Inset: a 2-D SPR image of a Au surface derivatized with 20 μL of buffer blank, 1 pM, 0.1 nM, and 10 nM S2 oligos (from left to right, respectively).

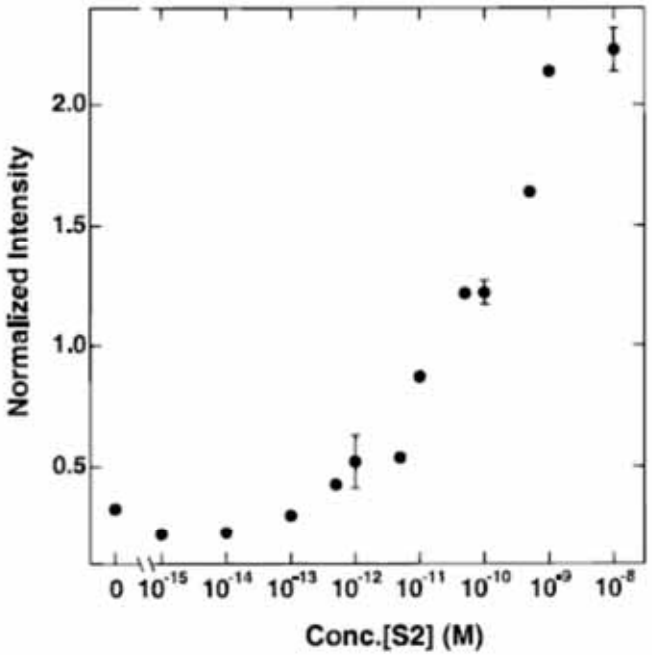

Figure 7. Plot of normalized intensity of SPR reflectance as a function of logarithmic concentration of the analyte 24-mer oligo (S2) from the image shown in Figure 6. The error bars are standard deviations from the data in Figure 5.

Table 1. Comparison of Sensitivity for Au−Amplified SPR in DNA Analysis with Other Techniques

detection method	detection limit of target DNA	refs
radiolabeling	100 fg	71
fluorescence	1.2×10^7 probes/cm^2	36
unamplified scanning SPR	100 fg/100 μm^2 for 10-mer oligos, 150 nM ~120 bp DNA	33, 35
unamplified imaging SPR	10 nM 16-mer oligos	63
Au-amplified scanning SPR	lower than 10 pM 24-mer oligos[a]	this work
Au-amplified imaging SPR	10 pM 24-mer oligos, ≤12 pg/cm^2 ($\leq 8 \times 10^8$ oligonucleotides/cm^2)[b]	this work

[a] The spots on SPR imaging surface can be detected by scanning SPR with ease, which demonstrated a lower detection limit can be achieved with the scanning instrument. Considering an instrumental angle resolution limit of 0.005°, a theoretical detection limit of 2×10^7 particles/cm^2 can be realized.[21] [b] The oligonucleotide surface coverage reported for these experiments is an upper limit, determined by assuming 100% of the molecules in solution hybridized to the surface.

A Gold Nanoparticle Based Approach for Screening Triplex DNA Binders

Min Su Han, Abigail K. R. Lytton-Jean, and Chad A. Mirkin*

4954 ■ J. AM. CHEM. SOC. 2006, *128*, 4954−4955

Scheme 1. Representation of Structure and Color Change of Nanoassembly in the Presence of Triplex Binder at Room Temperature

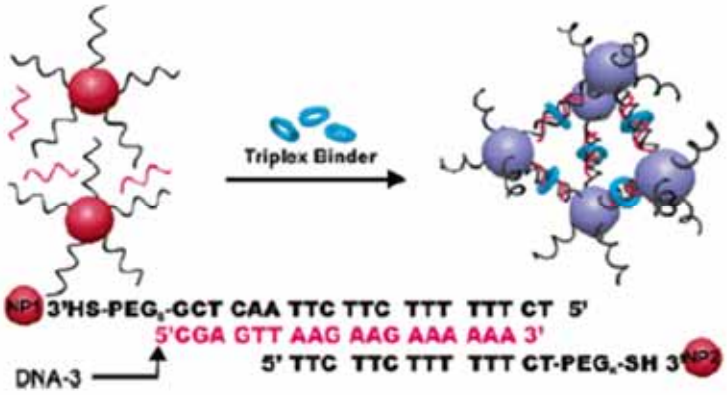

Figure 3. The color change of nanoassembly (NP-1, NP-2, and DNA-3) in the absence and presence of DNA binders at room temperature.

Sequence specific

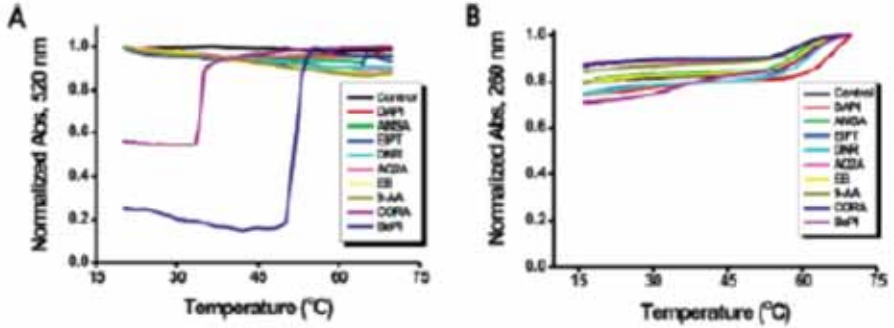

Figure 2. Melting curves of (A) NP-1, NP-2, and DNA-3 assemblies in the presence of DNA binders, (B) DNA-1, DNA-2, and DNA-3 (no nanoparticles) in the presence of DNA binders.

Self-Assembled Nanoparticle Probes for Recognition and Detection of Biomolecules

Dustin J. Maxwell, Jason R. Taylor, and Shuming Nie*,†

9606 ■ J. AM. CHEM. SOC. 2002, *124*, 9606−9612

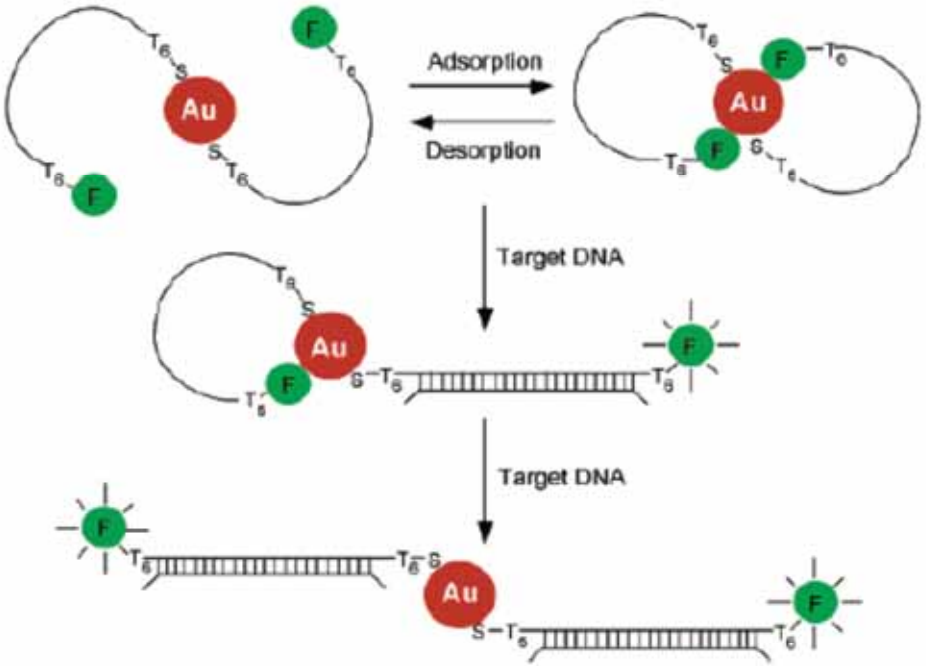

Figure 1. Nanoparticle-based probes and their operating principles. Two oligonucleotide molecules (oligos) are shown to self-assemble into a constrained conformation on each gold particle (2.5 nm diameter). A T_6 spacer (six thymines) is inserted at both the 3′- and 5′-ends to reduce steric hindrance. Single-stranded DNA is represented by a single line and double-stranded DNA by a cross-linked double line. In the assembled (closed) state, the fluorophore is quenched by the nanoparticle. Upon target binding, the constrained conformation opens, the fluorophore leaves the surface because of the structural rigidity of the hybridized DNA (double-stranded), and fluorescence is restored. In the open state, the fluorophore is separated from the particle surface by about 10 nm. See text for detailed explanation. Au, gold particle; F, fluorophore; S, sulfur atom.

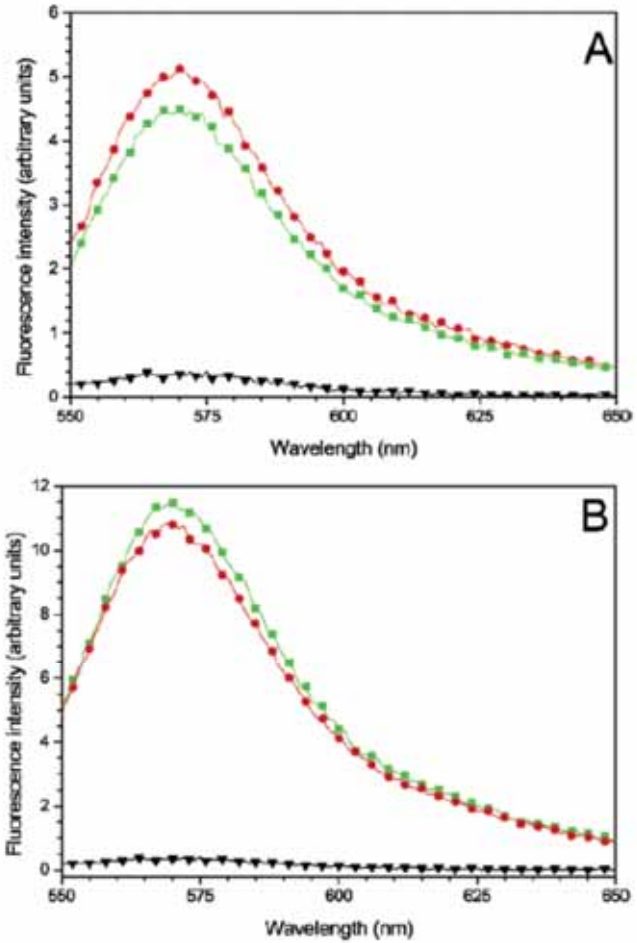

Figure 5. Fluorescence responses and the lack of sequence recognition abilities observed for nonthiolated nanoparticle probes. (A) Fluorescence spectra of nonthiolated probes generated by a complementary target (red curve), a noncomplementary target (green curve), and no target (black curve). These probes are considered nonfunctional because they do not recognize specific DNA sequences. (B) Fluorescence signals obtained from the supernatant solution when the probes were treated with a complementary target (red curve) or a noncomplementary target (green curve). The result revealed that the oligos were released into solution by nonspecific adsorption of the target on the particle surface. With a thiol group, this release was not observed (little or no signal in solution, black curve in B). The nonfunctional probes were prepared in the same way as the functional probes, except that the 3′-end thiol group was deleted. The intensity differences for the red and green curves were within experimental errors and had no particular significance.

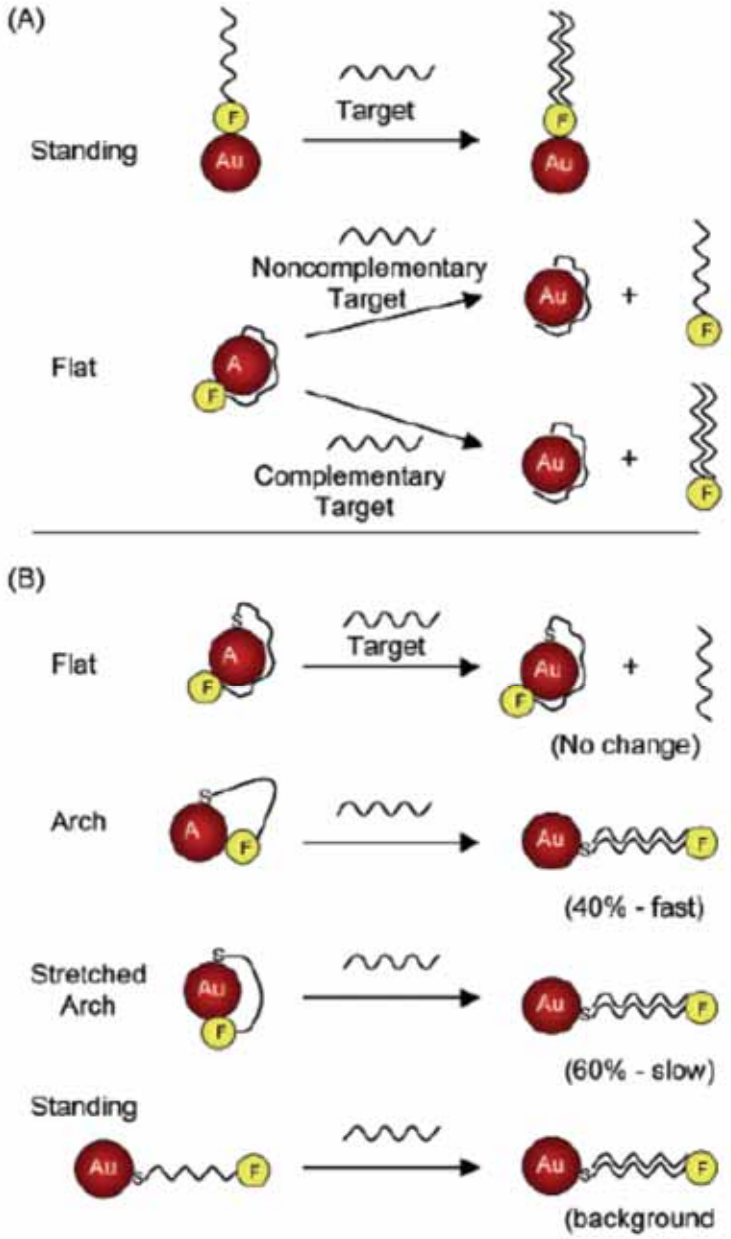

Figure 6. Schematic illustration of possible configurations for (a) nonthiolated and (b) thiolated oligonucleotides adsorbed on colloidal gold nanocrystals. Detailed discussion in text.

Silver Amplification

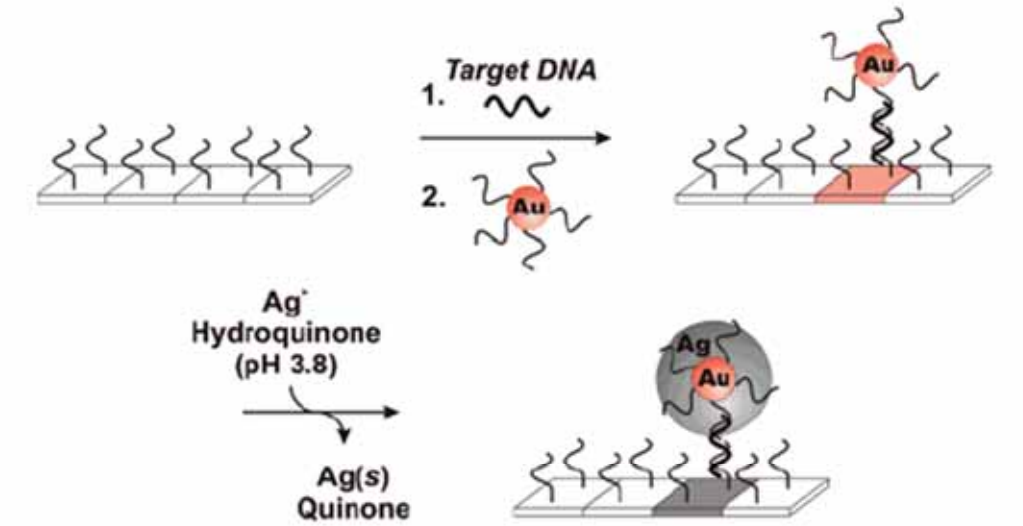

Figure 4. Scanometric DNA assay. In this assay a surface-bound capture oligonucleotide binds one-half of the target of interest, and an oligonucleotide-functionalized gold nanoparticle probe binds to the other half. Catalytic reduction of silver onto the capture/target/probe sandwich results in a signal that can be detected scanometrically. (Reprinted with permission from *Science* (http://www.aaas.org), ref 66. Copyright 2000 American Association for the Advancement of Science.)

Catalytic reduction of Ag on Au

Scanometric DNA Array Detection with Nanoparticle Probes

SCIENCE VOL 289 8 SEPTEMBER 2000

T. Andrew Taton,[1,2] Chad A. Mirkin,[1,2]* Robert L. Letsinger[1]*

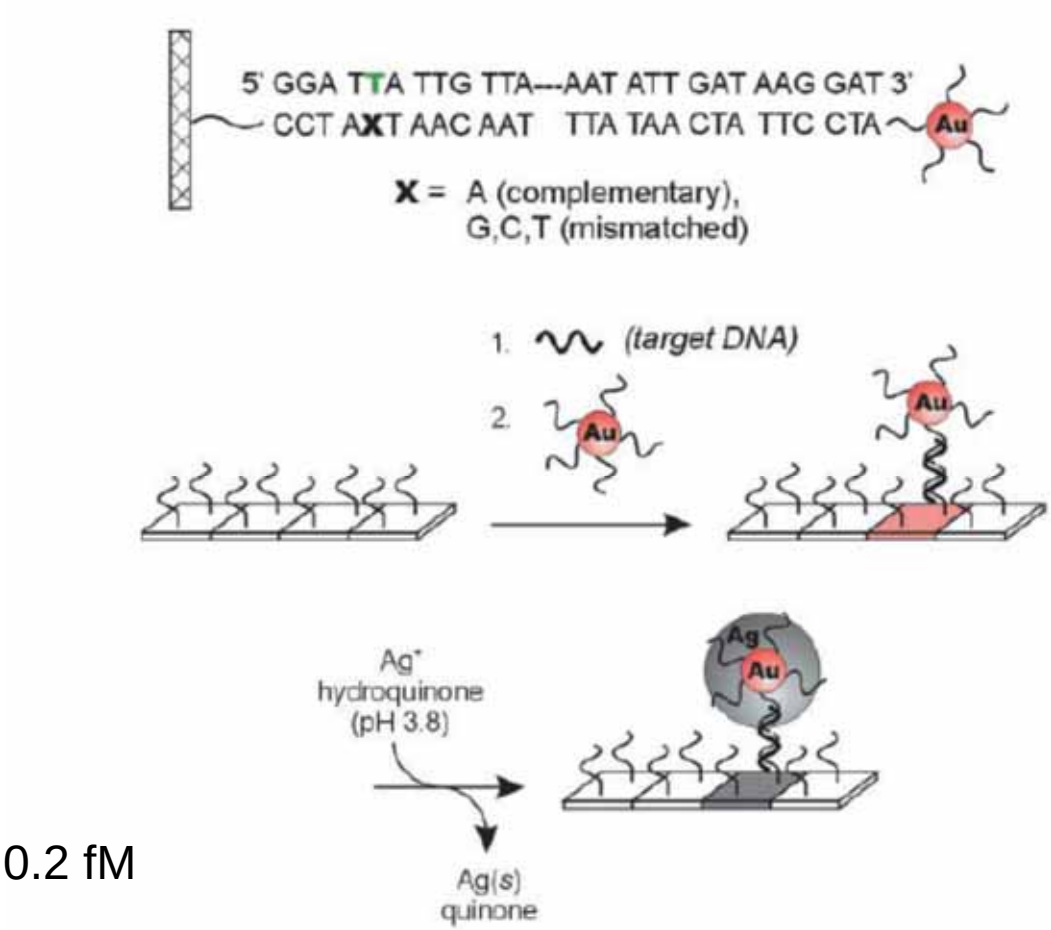

50 fM => 0.2 fM

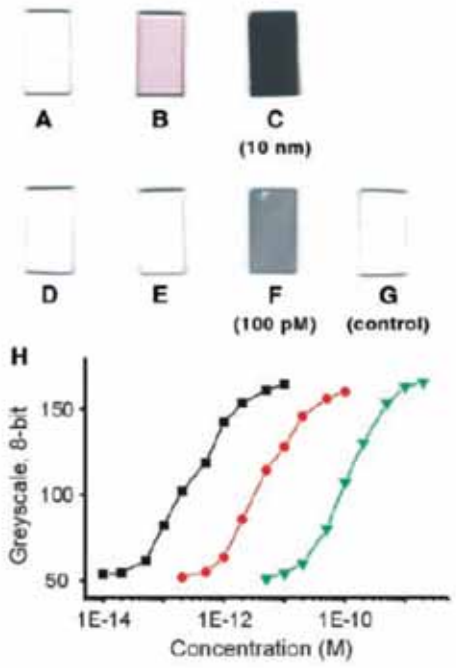

Fig. 1. Images of 7 mm by 13 mm, oligonucleotide-functionalized, float glass slides, obtained with a flatbed scanner. (**A**) Slide before hybridization of target and nanoparticle probe. (**B**) A slide identical to (A) after hybridization with oligonucleotide target (10 nM) and then nanoparticle probes (5 nM in particles). The pink color derives from the Au nanoparticle probes. (**C**) A slide identical to (B) after exposure to silver amplification solution for 5 min. (**D**) Slide before hybridization of target and nanoparticle probe. (**E**) A slide identical to (D) after hybridization with target (100 pM) and then nanoparticle probe (5 nM). The extinction of the submonolayer of nanoparticles is too low to be observed visually or with a flatbed scanner. (**F**) A slide identical to (E) after exposure to silver amplification solution for 5 min. Slide (F) is lighter than slide (C), indicating a lower concentration of target. (**G**) A control slide exposed to 5 nM nanoparticle probe and then exposed to silver amplification solution for 5 min. No darkening of the slide is observed. (**H**) Graph of 8-bit gray scale values as a function of target concentration. The gray scale values were taken from flatbed scanner images of oligonucleotide-functionalized glass surfaces that had been exposed to varying concentrations of oligonucleotide target, labeled with 5 nM oligonucleotide probe and immersed in silver amplification solution. For any given amplification time, the grayscale range is limited by surface saturation at high grayscale values and the sensitivity of the scanner at low values. Therefore, the dynamic range of this system can be adjusted by means of hybridization and amplification conditions (that is, lower target concentrations require longer amplification periods). Squares: 18-base capture-target overlap (*5*), 8× PBS hybridization buffer [1.2 M NaCl and 10 mM NaH_2PO_4/Na_2HPO_4 buffer (pH 7)], 15 min amplification time. Circles: 12-base capture-target overlap, 8× PBS hybridization buffer, 10 min amplification time. Triangles: 12-base capture-target overlap, 2× PBS hybridization buffer [0.3 M NaCl, 10 mM NaH_2PO_4/Na_2HPO_4 buffer (pH 7)], 5 min amplification time. The lowest target concentration that can be effectively distinguished from the background baseline is 50 fM.

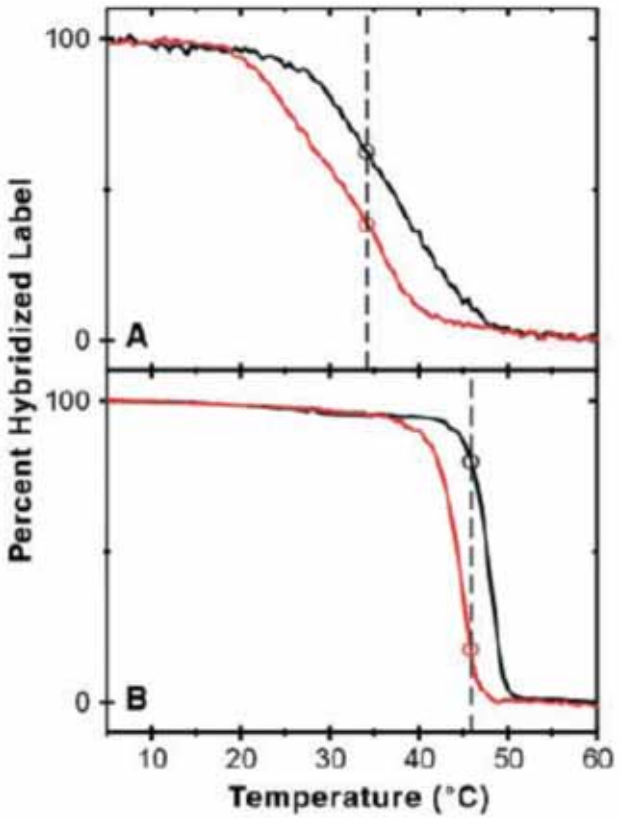

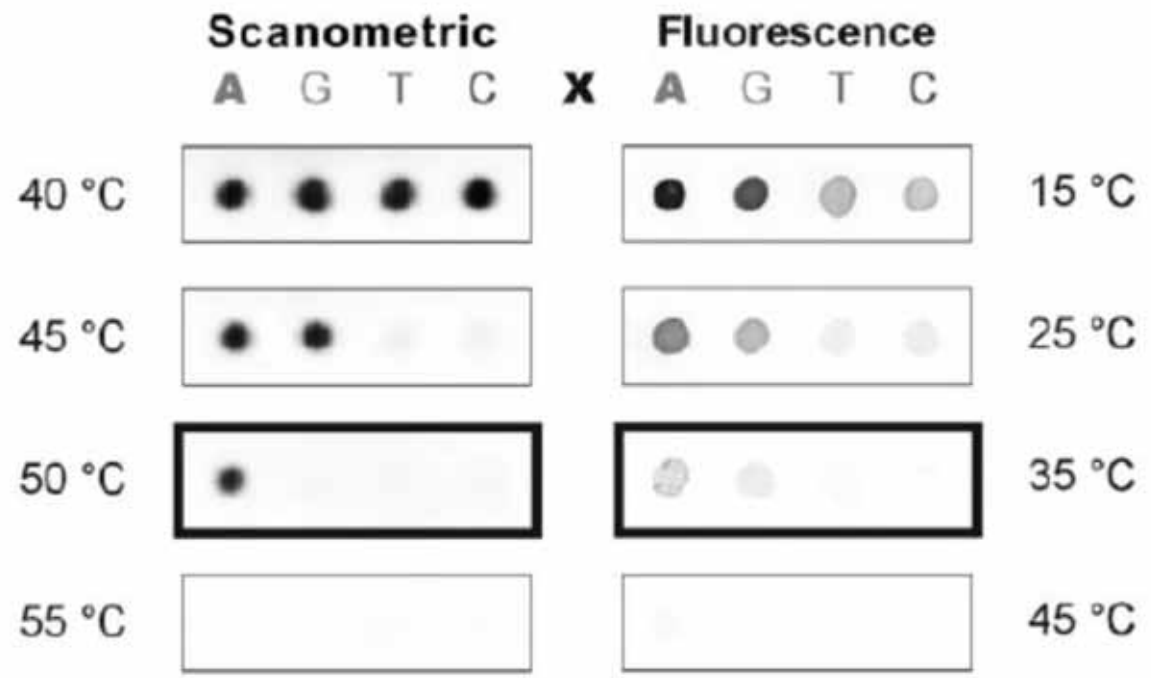

Fig. 3. (**Left**) Nanoparticle-labeled arrays developed at different stringency temperatures. Model oligonucleotide arrays (with the capture sequences shown in Scheme 1) were treated with oligonucleotide target and nanoparticle probes, followed by a 2-min buffer wash at the temperatures shown and subsequent silver amplification (*13*). Images were obtained with an Epson Expression 636 (600 dots per inch) flatbed scanner (Epson America, Long Beach, California). The darkened border indicates the array that showed optimum selectivity for the perfectly complementary target; at this temperature, the ratio of background-subtracted, 8-bit gray scale values for elements A:G:T:C, obtained from histogram averages in Adobe Photoshop (Adobe Systems, San Jose, California), is 96:9:7:6. (**Right**) Fluorophore-labeled arrays washed at different stringency temperatures. Model oligonucleotide arrays identical to those shown at left were treated with oligonucleotide target and Cy3-labeled oligonucleotide probes, followed by a 2-min buffer wash at the temperatures shown. Images were obtained with a ScanArray Confocal Microarray Scanner (GSI Lumonics, Billerica, Massachusetts). The darkened border indicates the array that showed the highest selectivity for the perfectly complementary target, as calculated by the QuantArray Analysis software package (GSI Lumonics); at this temperature, the intensity ratio (in percent, with the intensity of the X = A element at 15°C set to 100%) for elements A:G:T:C is 18:7:1:1.

Nanoparticles with Raman Spectroscopic Fingerprints for DNA and RNA Detection

YunWei Charles Cao, Rongchao Jin, Chad A. Mirkin*

30 AUGUST 2002 VOL 297 SCIENCE

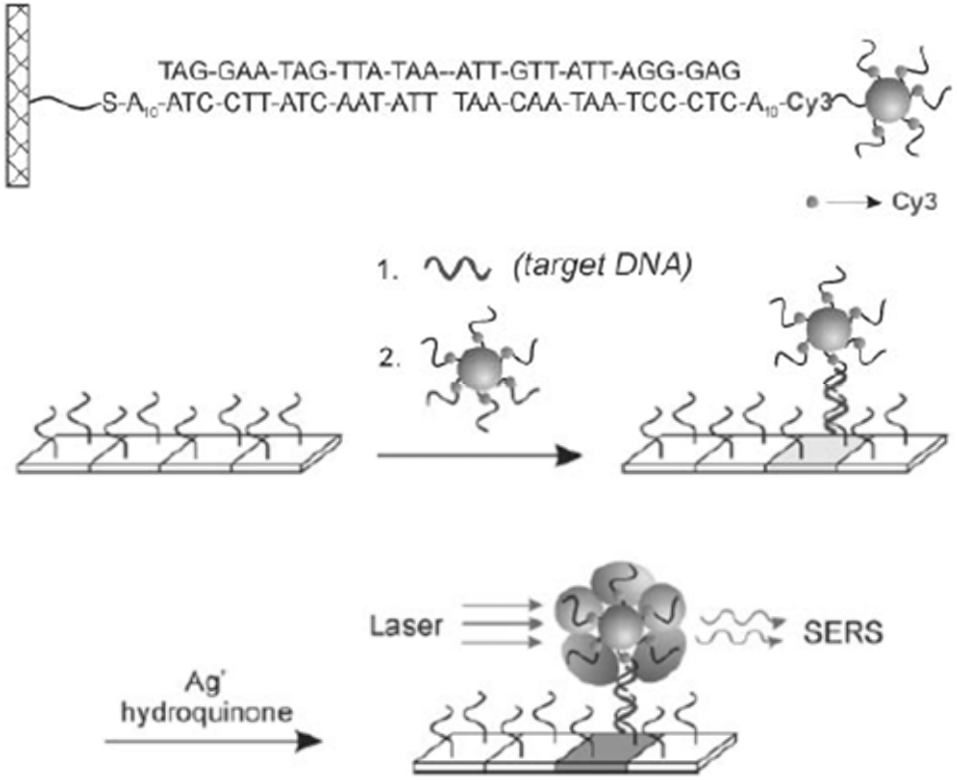

1 fM

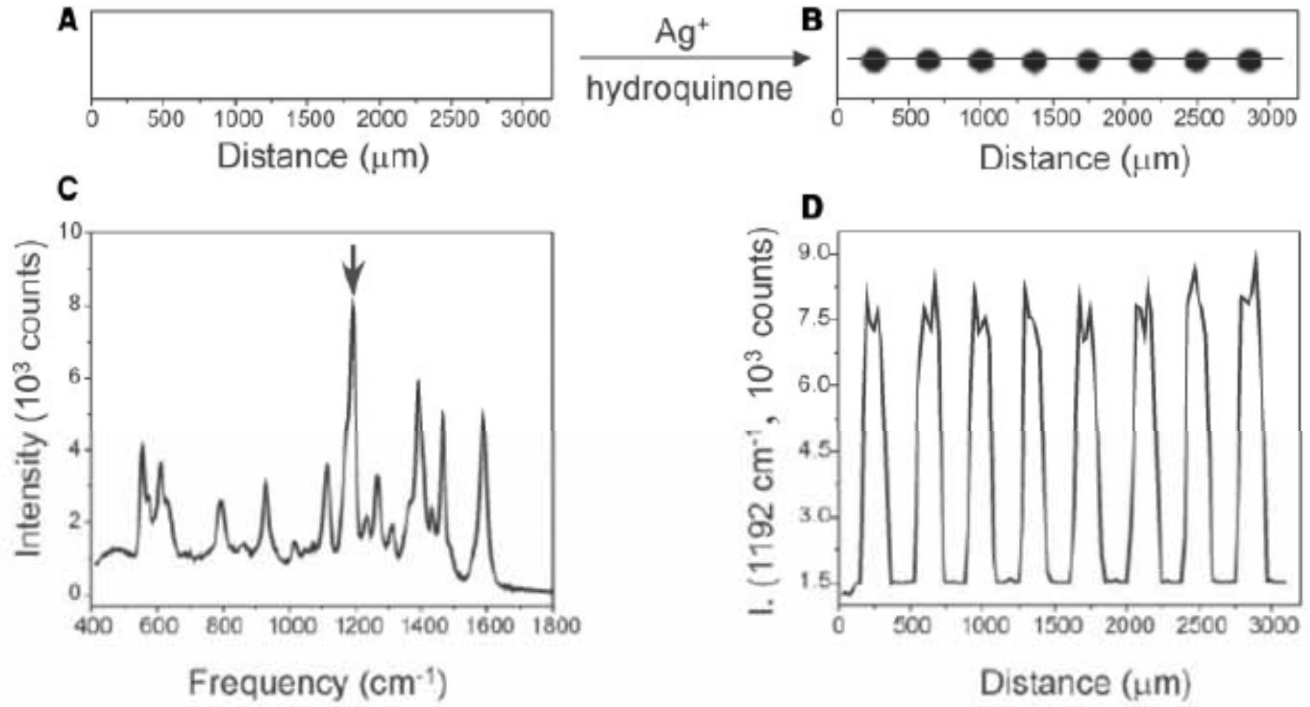

Fig. 1. Flatbed scanner images of microarrays hybridized with nanoparticles (**A**) before and (**B**) after Ag enhancing. (**C**) A typical Raman spectrum acquired from one of the Ag spots. (**D**) A profile of Raman intensity at 1192 cm^{-1} as a function of position on the chip; the laser beam from the Raman instrument is moved over the chip from left to right as defined by the line in (B).

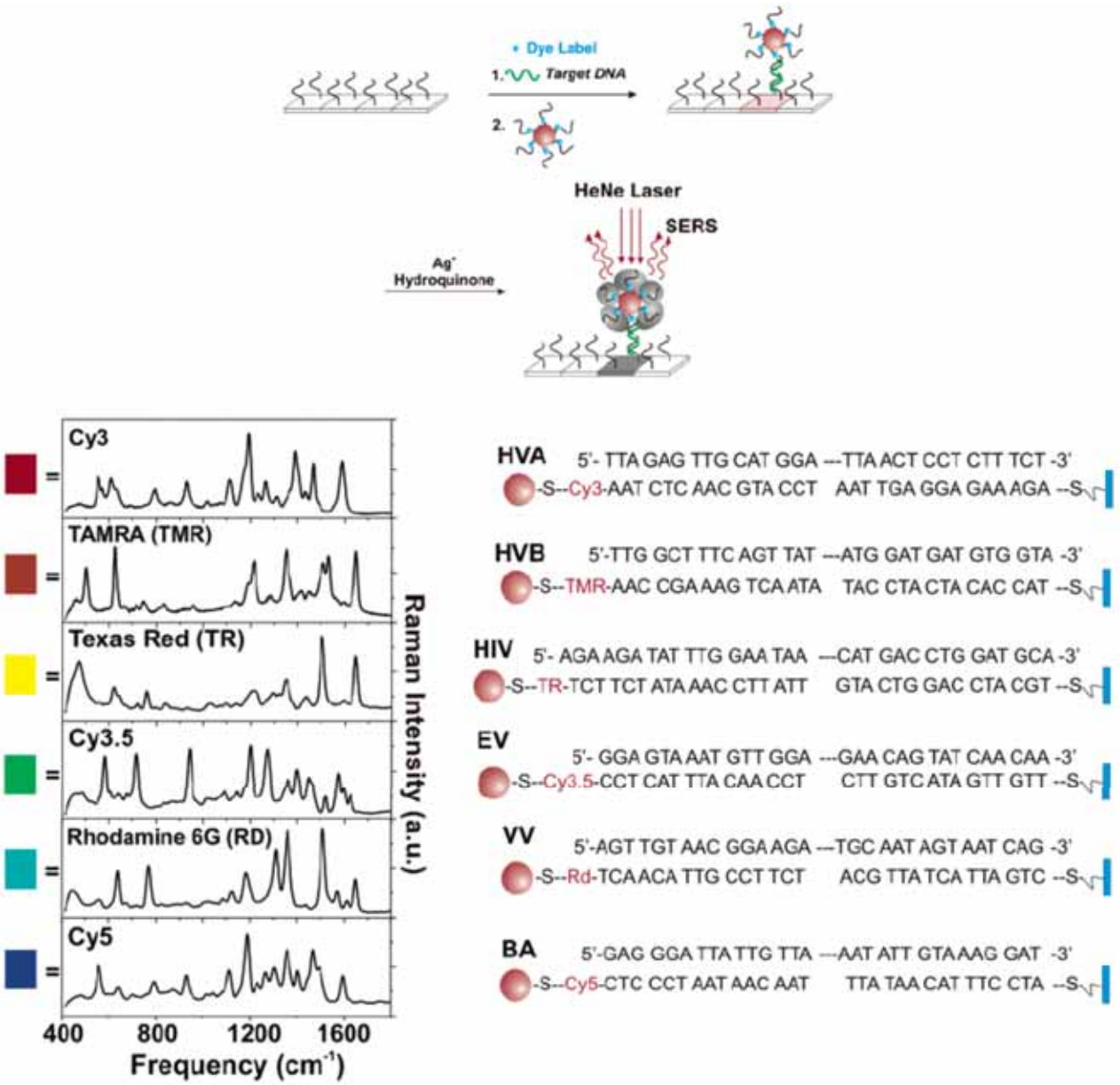

Figure 5. If Raman dyes (blue spheres) are attached to the labeling probe in the scanometric assay, the targets can be encoded and detected via the Raman signal of their labels. (Reprinted with permission from *Science* (http://www.aaas.org), ref 68. Copyright 2002 American Association for the Advancement of Science.)

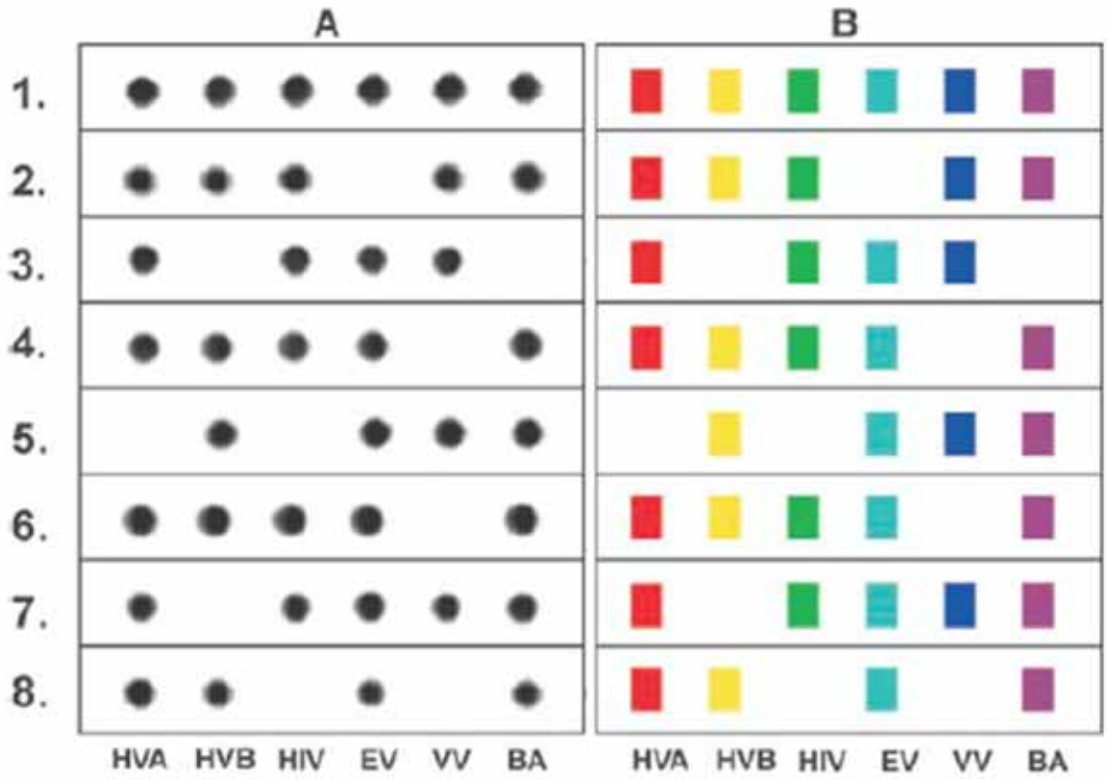

Fig. 3. (**A**) Flatbed scanner images of Ag-enhanced microarrays and (**B**) corresponding Raman spectra. The colored boxes correlate with the color-coded Raman spectra in Fig. 2. No false-positives or false-negatives were observed.

Bio-Bar-Code-Based DNA Detection with PCR-like Sensitivity

Jwa-Min Nam, Savka I. Stoeva, and Chad A. Mirkin*

J. AM. CHEM. SOC. 2004, *126*, 5932−5933

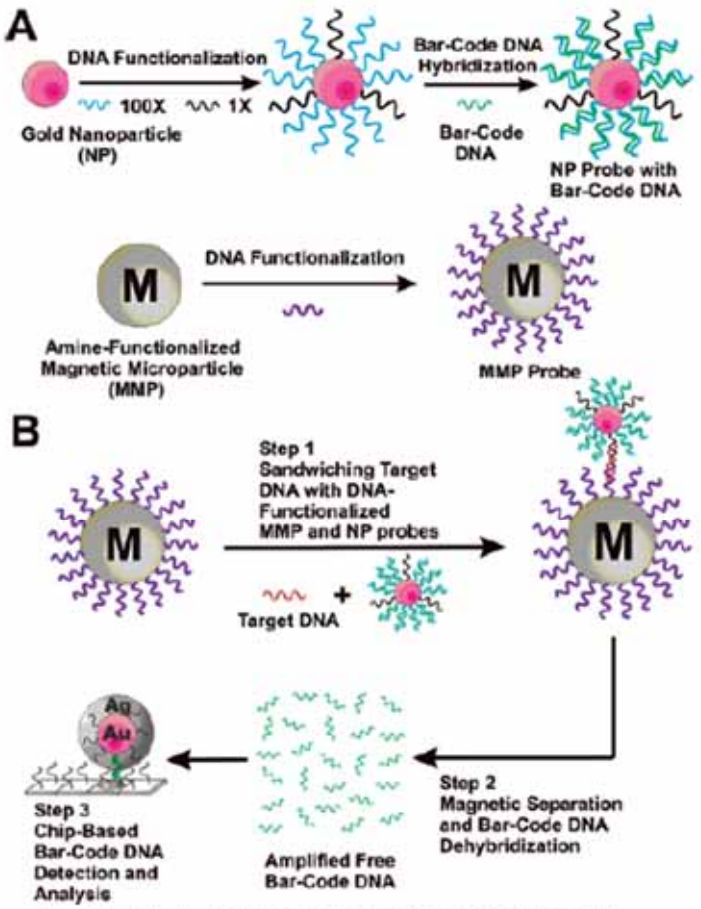

Figure 1. The DNA-BCA assay. (A) Nanoparticle and magnetic microparticle probe preparation. (B) Nanoparticle-based PCR-less DNA amplification scheme.

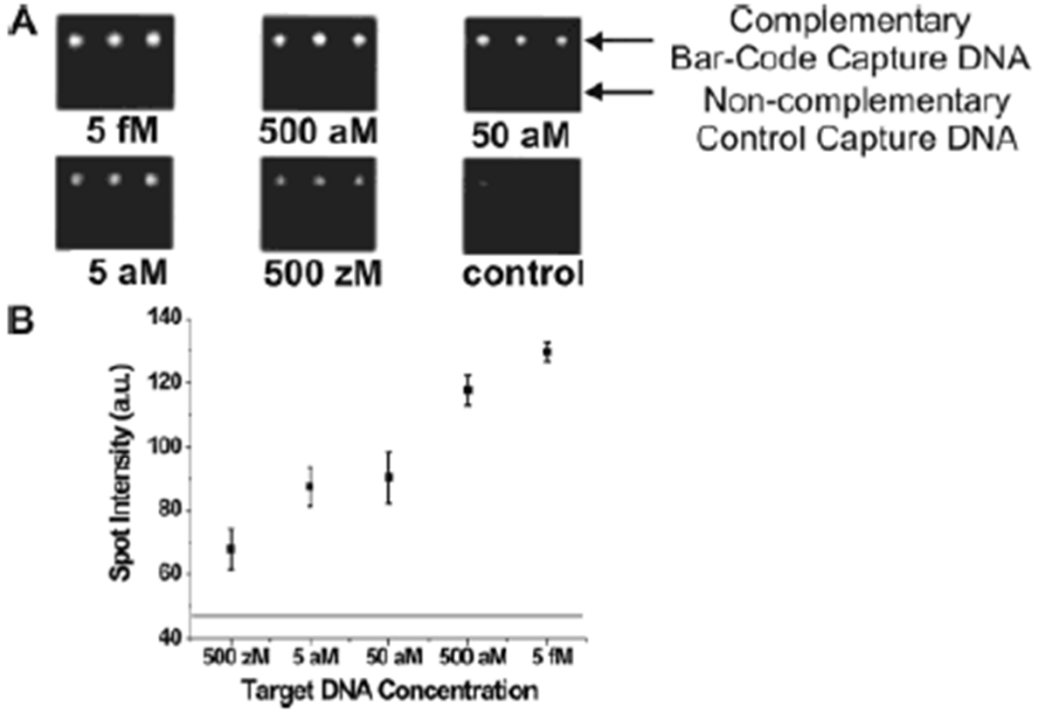

Figure 2. Amplified anthrax bar-code DNA detection with the Verigene ID system. (A) Anthrax bar-code DNA detection with 30 nm NP probes. (B) Quantitative data of spot intensities with 30 nm NP probes (Adobe Photoshop, Adobe Systems, Inc., San Jose, CA). The horizontal line represents control signal intensity (47 ± 2).

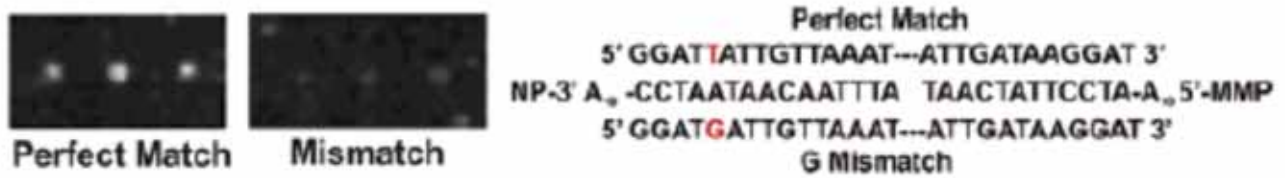

Figure 3. Single base mismatch experiment.

Nanoparticle-Based Bio–Bar Codes for the Ultrasensitive Detection of Proteins

26 SEPTEMBER 2003 VOL 301 SCIENCE

Jwa-Min Nam,* C. Shad Thaxton,* Chad A. Mirkin†

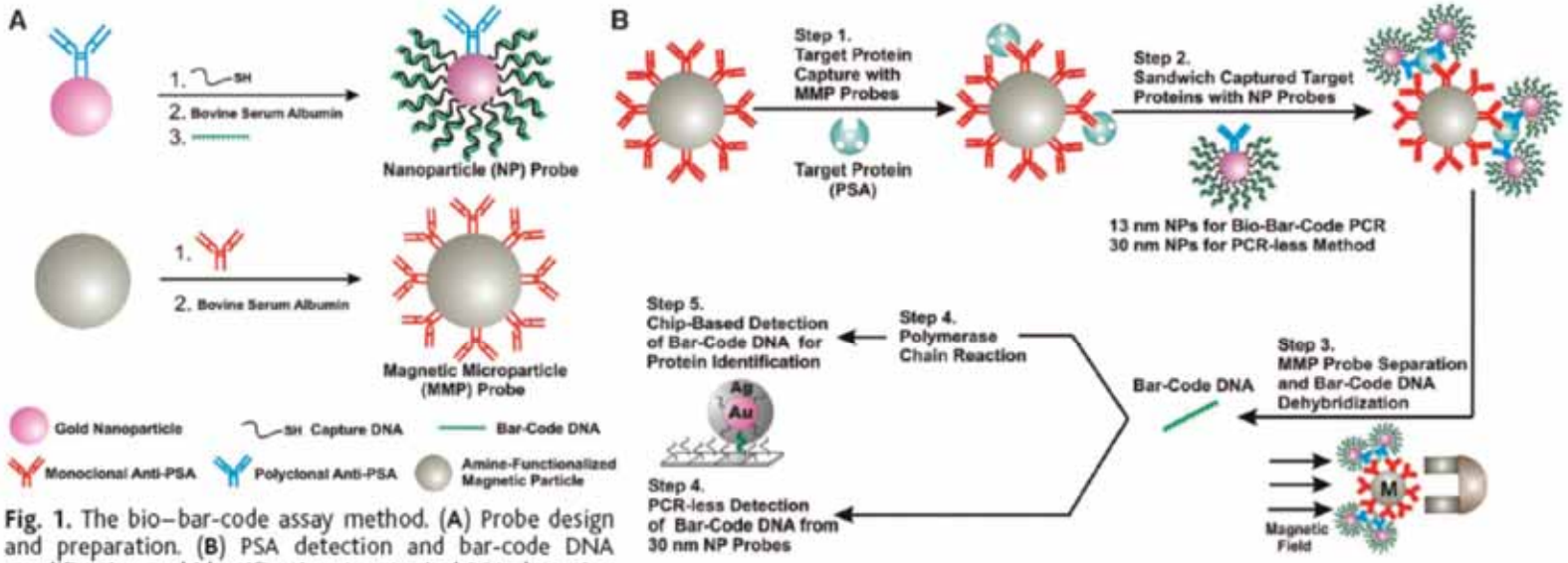

Fig. 1. The bio–bar-code assay method. (**A**) Probe design and preparation. (**B**) PSA detection and bar-code DNA amplification and identification. In a typical PSA-detection experiment, an aqueous dispersion of MMP probes functionalized with mAbs to PSA (50 μl of 3 mg/ml magnetic probe solution) was mixed with an aqueous solution of free PSA (10 μl of PSA) and stirred at 37°C for 30 min (Step 1). A 1.5-ml tube containing the assay solution was placed in a BioMag microcentrifuge tube separator (Polysciences, Incorporated, Warrington, PA) at room temperature. After 15 s, the MMP-PSA hybrids were concentrated on the wall of the tube. The supernatant (solution of unbound PSA molecules) was removed, and the MMPs were resuspended in 50 μl of 0.1 M phosphate-buffered saline (PBS) (repeated twice). The NP probes (for 13-nm NP probes, 50 μl at 1 nM; for 30-nm NP probes, 50 μl at 200 pM), functionalized with polyclonal Abs to PSA and hybridized bar-code DNA strands, were then added to the assay solution. The NPs reacted with the PSA immobilized on the MMPs and provided DNA strands for signal amplification and protein identification (Step 2). This solution was vigorously stirred at 37°C for 30 min. The MMPs were then washed with 0.1 M PBS with the magnetic separator to isolate the magnetic particles. This step was repeated four times, each time for 1 min, to remove everything but the MMPs (along with the PSA-bound NP probes). After the final wash step, the MMP probes were resuspended in NANOpure water (50 μl) for 2 min to dehybridize bar-code DNA strands from the nanoparticle probe surface. Dehybridized bar-code DNA was then easily separated and collected from the probes with the use of the magnetic separator (Step 3). For bar-code DNA amplification (Step 4), isolated bar-code DNA was added to a PCR reaction mixture (20-μl final volume) containing the appropriate primers, and the solution was then thermally cycled (*20*). The bar-code DNA amplicon was stained with ethidium bromide and mixed with gel-loading dye (*20*). Gel electrophoresis or scanometric DNA detection (*24*) was then performed to determine whether amplification had taken place. Primer amplification was ruled out with appropriate control experiments (*20*). Notice that the number of bound NP probes for each PSA is unknown and will depend upon target protein concentration.

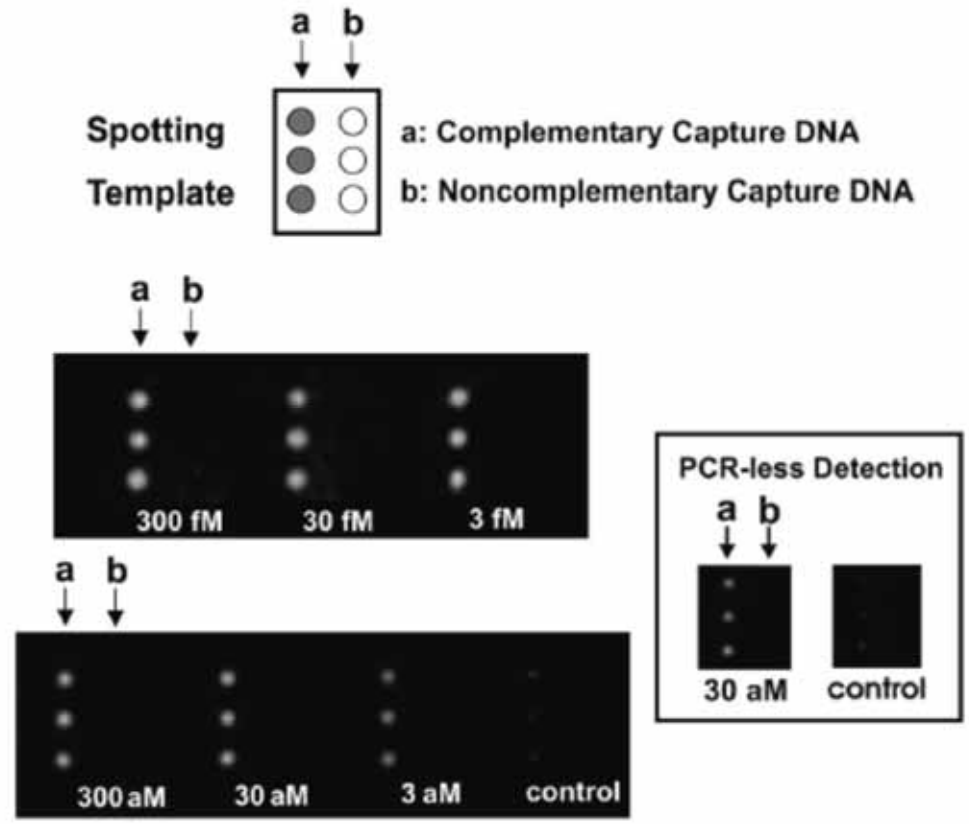

Fig. 2. Scanometric detection of PSA-specific bar-code DNA. PSA concentration (sample volume of 10 μl) was varied from 300 fM to 3 aM and a negative control sample where no PSA was added (control) is shown. For all seven samples, 2 μl of antidinitrophenyl (10 pM) and 2 μl of β-galactosidase (10 pM) were added as background proteins. Also shown is PCR-less detection of PSA (30 aM and control) with 30 nm NP probes (inset). Chips were imaged with the Verigene ID system (*20*).

Table 1. Detection Limits of Nucleic Acid Assays[a]

	assay	ss DNA	PCR products	genomic DNA
nanostructure-based methods	colorimetric[29] (cross-linked Au nanoparticles)	~10 nM		
	colorimetric[36] (non-cross-linked Au nanoparticles)	60 nM		
	magnetic relaxation[97] (iron oxide nanoparticles)	20 pM		
	electrochemical[96] (nanoparticles)	270 pM		
	scanometric[35,66,67] (Au nanoparticles with Ag amplification)	50 fM	100 aM[b]	200 fM
	Raman spectroscopy[68] (Au nanoparticles with Ag amplification)	~1 fM		
	electrical[93] (Au nanoparticles with Ag amplification)	500 fM		
	electrical[99] (Si nanowire)	10 fM		
	electrical[103] (carbon nanotube)	54 aM		
	resonant light-scattering[61–66] (metal nanoparticles)	170 fM[b]		33 fM
	fluorescence[56] (ZnS and CdSe quantum dots)	2 nM		
	surface plasmon resonance[41] (Au nanoparticles)	10 pM		
	quartz crystal microbalance[94] (Au nanoparticles)	~1 fM		
	laser diffraction[42] (Au nanoparticles)	~50 fM		
	fluorescence[45] (fluorescent nanoparticles)	~1 fM		
	bio-bar-code amplification[71] (Au nanoparticles with Ag amplification)	500 zM		
other non-enzymatic based methods	fluorescence[35] (molecular fluorophores)		~600 fM[b]	
	fluorescence (dendrimer amplification)[134]		2.5 μg	
	electrochemical amplification[136] (electroactive reporter molecules)	100 aM		

[a] Detection limits can vary based on target length and sequence; therefore, it is difficult to compare assays without testing them using identical targets and conditions. [b] Values taken from ref 34.

Table 2. Detection Limits of Protein Assays

	assay	target	protein in saline	protein in serum
nanostructure-based methods	optical[72] (Au nanoshells)	rabbit IgG	0.88 ng/mL (~4.4 pM)[a]	0.88 ng/mL (~4.4 pM)[c]
	optical[74] (Au nanoparticles)	IgE and IgG1	~20 nM	
	magnetic relaxation[98] (iron oxide nanoparticles)	adenovirus (ADV) and herpes simplex virus (HSV)	100 ADV/ 100μL	50 HSV/ 100 μL
	scanometric[79] (Au nanoparticles with Ag amplification)	mouse IgG	200 pM	
	Raman[82] (Au nanoparticles with Raman labels)	prostate-specific antigen		30 fM
	surface plasmon resonance[83,84] (triangular Ag particles on surfaces)	streptavidin(S A) and anti-biotin (AB)	~1 pM SA and ~700 pM AB	
	electrical[110] (single-walled carbon nanotubes)	10E3 antibody to U1A RNA splicing factor	~1 nM	
	electrical[20] (Si nanowires)	streptavidin	10 pM	
	bio-bar-code amplification[75] (Au nanoparticles with Ag amplification)	prostate-specific antigen	30 aM (3 aM)[b]	(30 aM)[b]
molecular fluorophore methods	enzyme-linked immunosorbent assay	various	pM range	pM range
electrochemical methods	electrochemical amplification[137] (oligonucleotide reporter molecules)	IgG	13 fM	
enzyme-based amplification methods	immuno-PCR[76]	bovine serum albumin	2 fM	
	rolling circle amplification[77]	prostate-specific antigen	3 fM	

[a] Reported in ng/mL; authors converted to molar concentration for ease of comparison. [b] These values are the lower limits when PCR is used to amplify the bar-code DNA prior to scanometric detection of bar codes.

Surface Plasmon

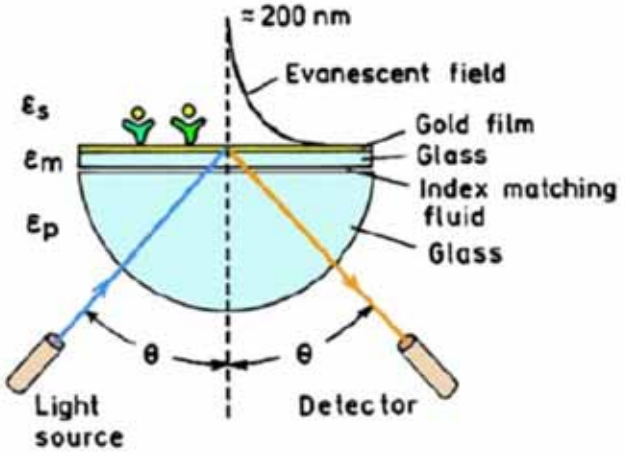

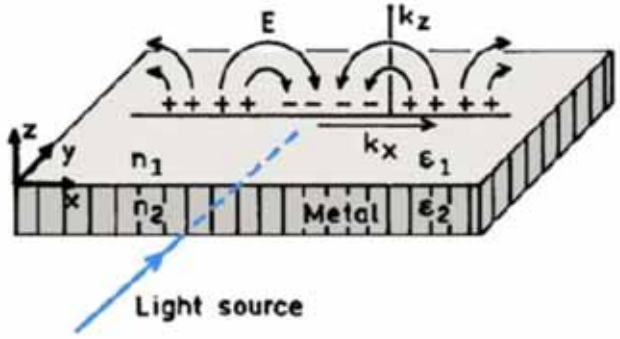

Figure 3. Schematics of an SPR experiment (top) and of the light-induced surface plasmons (bottom).

(b)

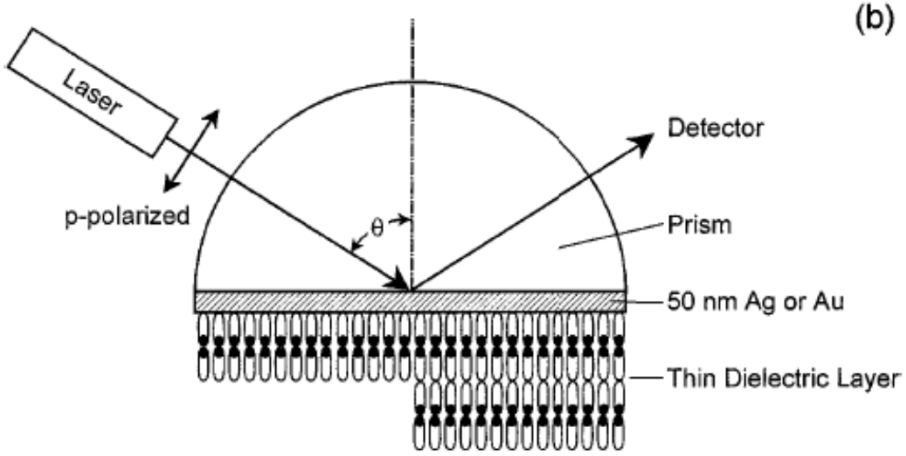

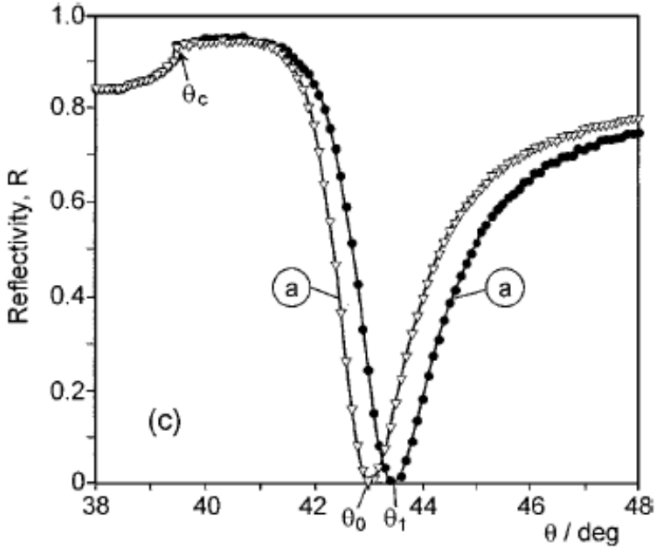

Drift: Drude model

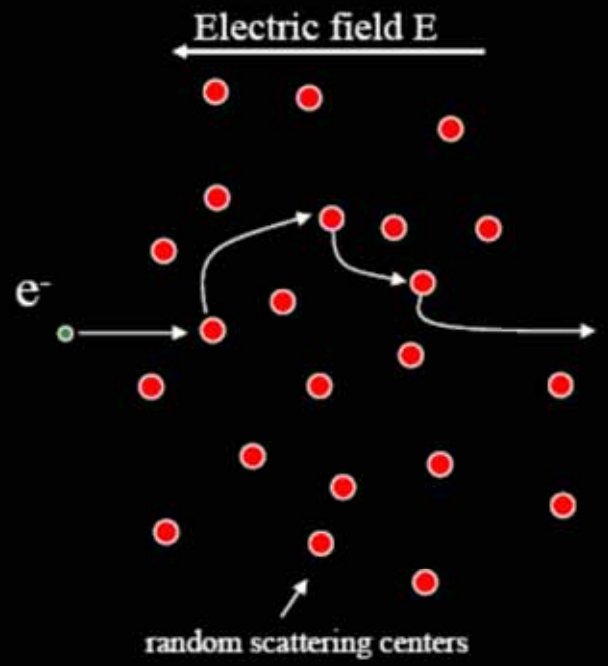

$$F = ma$$

$$eE = m\frac{\partial v}{\partial t}$$

$$v_{avg} = \underbrace{\frac{e\tau}{m}}_{\mu} E$$

$$j = nev_{avg} = \underbrace{\frac{ne^2\tau}{m}}_{\sigma} E$$

$$m\frac{\partial}{\partial t}\langle\vec{v}\rangle = q\vec{E} - \gamma\langle\vec{v}\rangle$$

$$\sigma(\omega) = \frac{\sigma_0}{1 + i\omega\tau}$$

AC Dielectric Response

$$\varepsilon_m = 1 - \frac{\omega_p^2}{\omega^2}$$

Plasma frequency

polarizability of a small metal sphere with dielectric function $\varepsilon(\lambda)$

$$\alpha = R^3 \frac{\varepsilon - 1}{\varepsilon + 2}\,.$$

$$\varepsilon = \varepsilon_\mathrm{b} + 1 - \frac{\omega_\mathrm{p}^2}{\omega^2 + \mathrm{i}\omega\gamma}\,,$$

$$\alpha = \frac{R^3(\varepsilon_\mathrm{b}\omega^2 - \omega_\mathrm{p}^2) + i\omega\gamma\varepsilon_\mathrm{b}}{[(\varepsilon_\mathrm{b} + 3)\omega^2 - \omega_\mathrm{p}^2] + i\omega\gamma(\varepsilon_\mathrm{b} + 3)}\,.$$

$\omega_\mathrm{R} = \frac{\omega_\mathrm{p}}{\sqrt{\varepsilon_\mathrm{b}+3}}$ $\gamma(\varepsilon_\mathrm{b} + 3).$

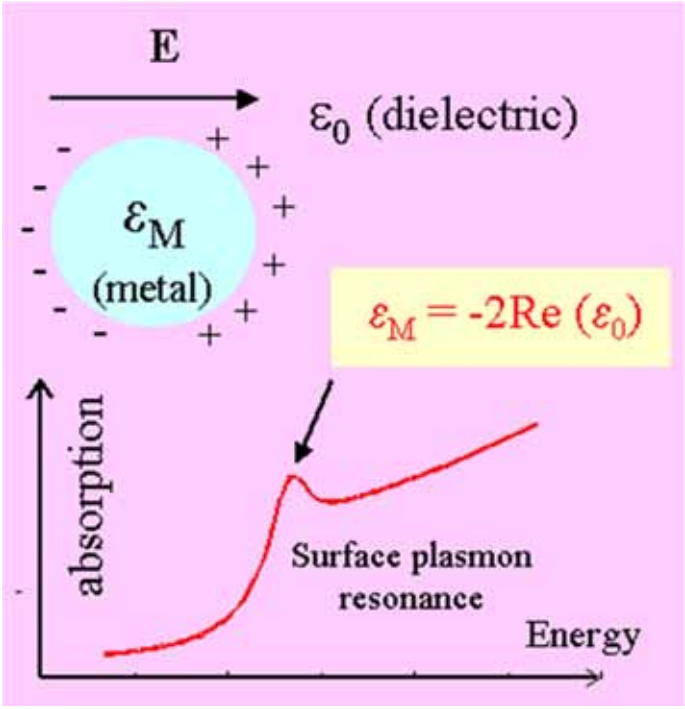

$$\varepsilon_{eff} = \varepsilon_0 + 3N\varepsilon_0 \frac{\varepsilon_M - \varepsilon_0}{\varepsilon_M + 2\varepsilon_0}$$

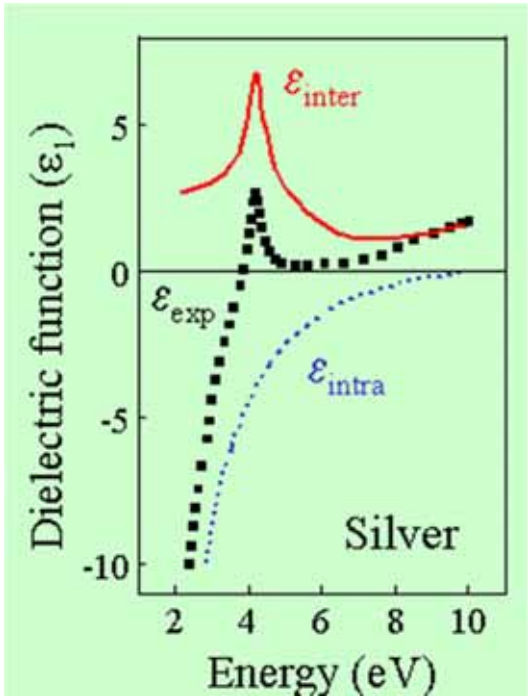

Biomolecular Binding in Real Time

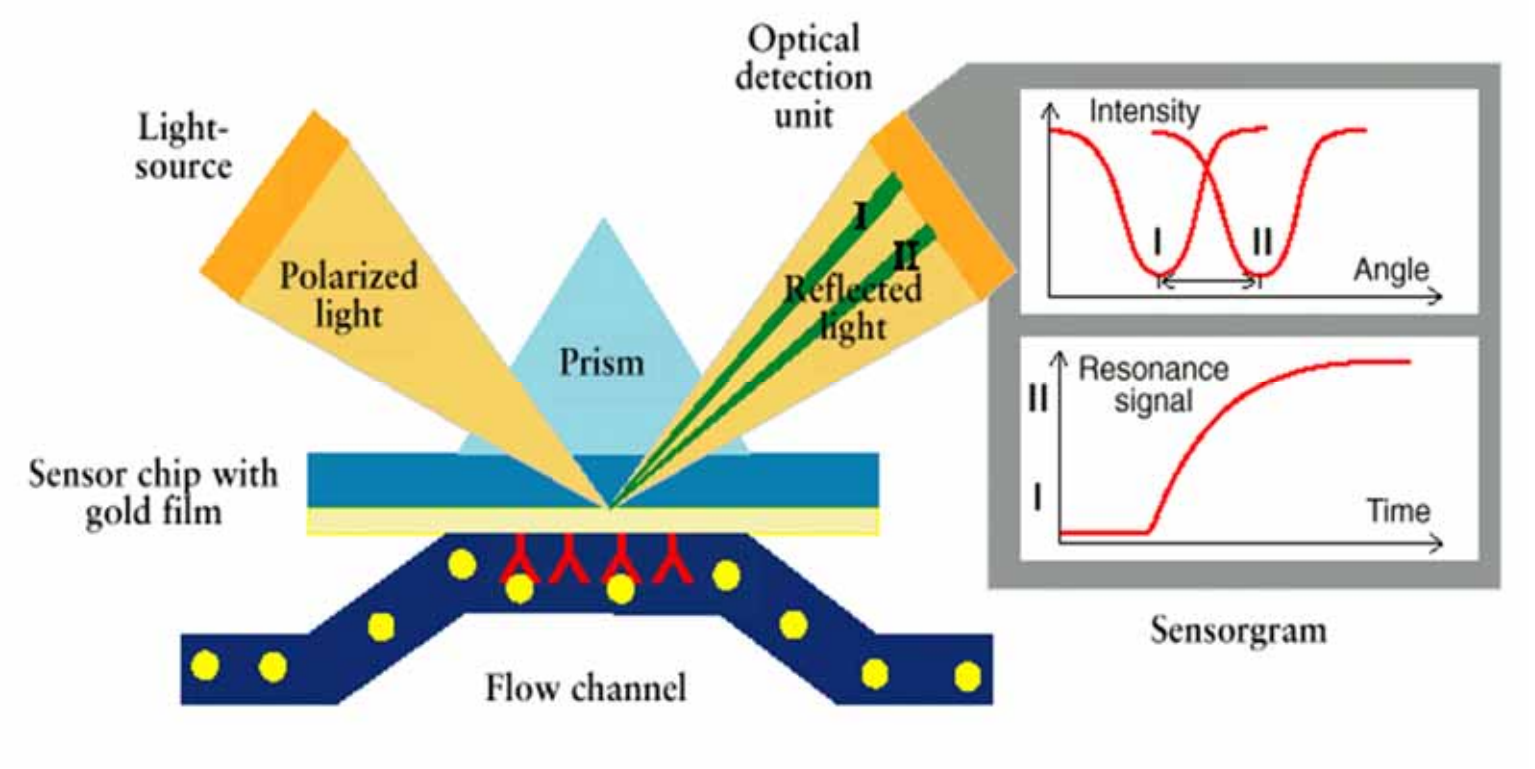

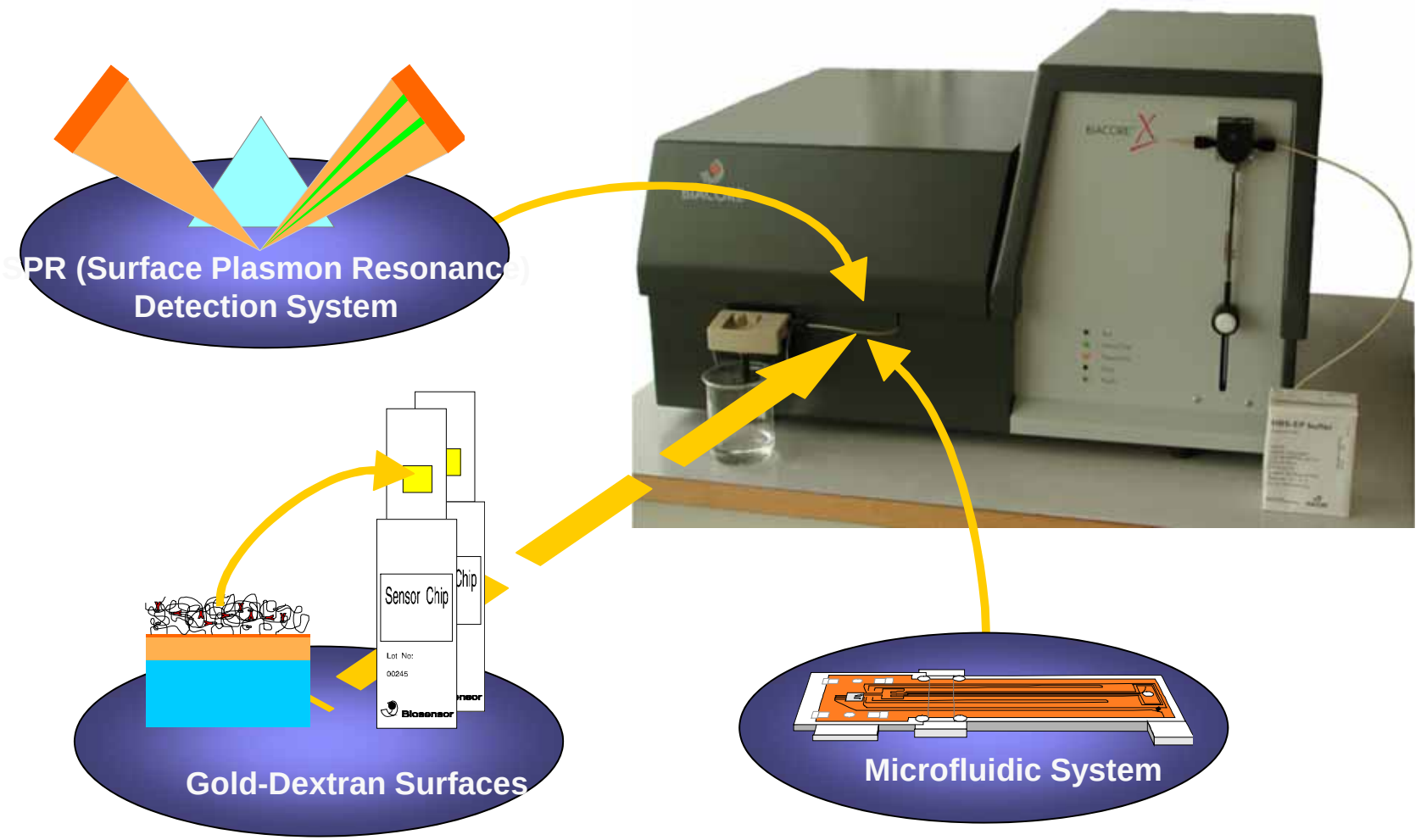
SPR (Surface Plasmon Resonance)
Detection System
Sensor Chip
Lot No:
00245
Biosensor
Gold-Dextran Surfaces
Microfluidic System

SPR Imaging Apparatus

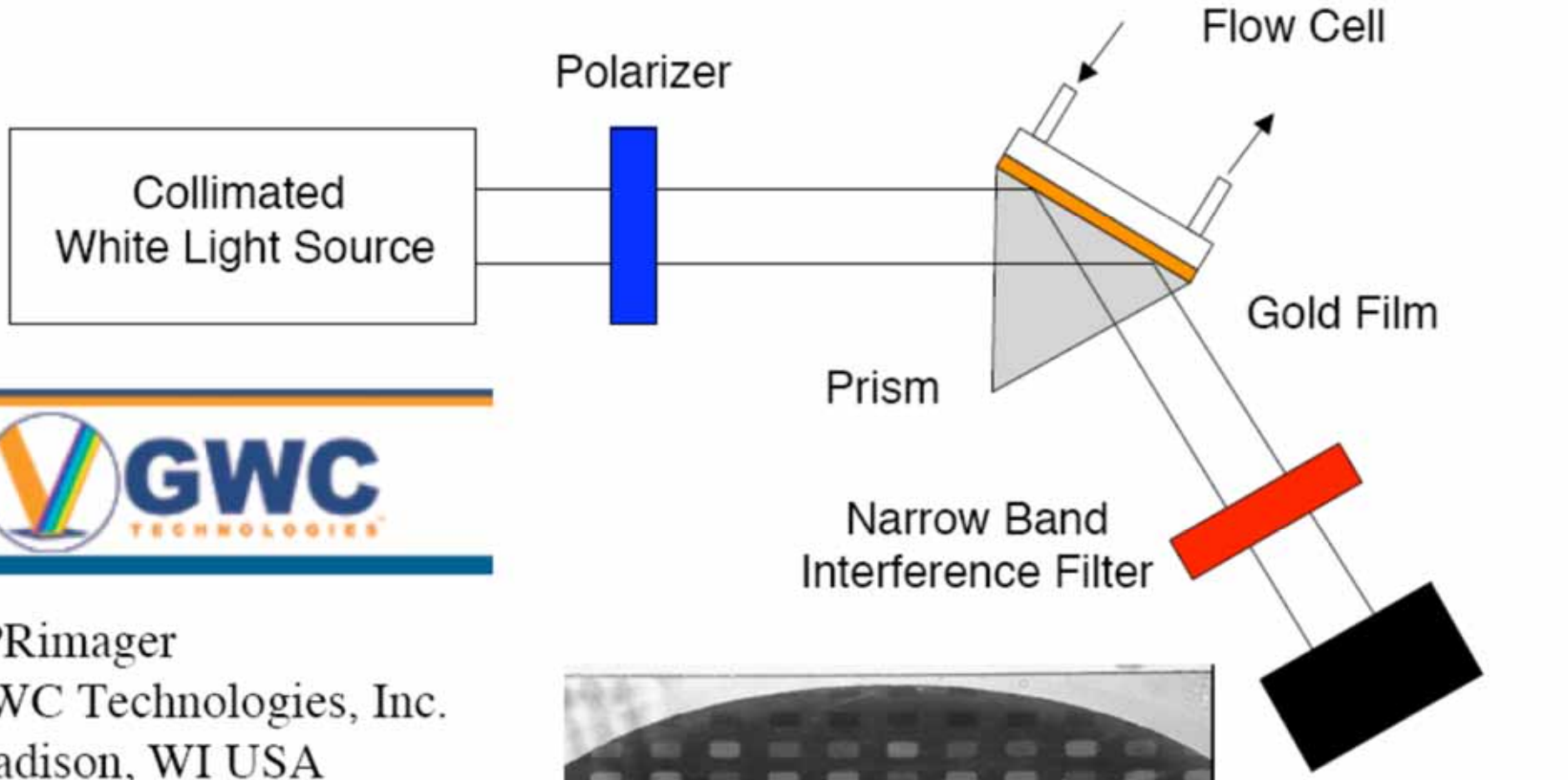

SPRimager
GWC Technologies, Inc.
Madison, WI USA

www.gwctechnologies.com

Raw Image

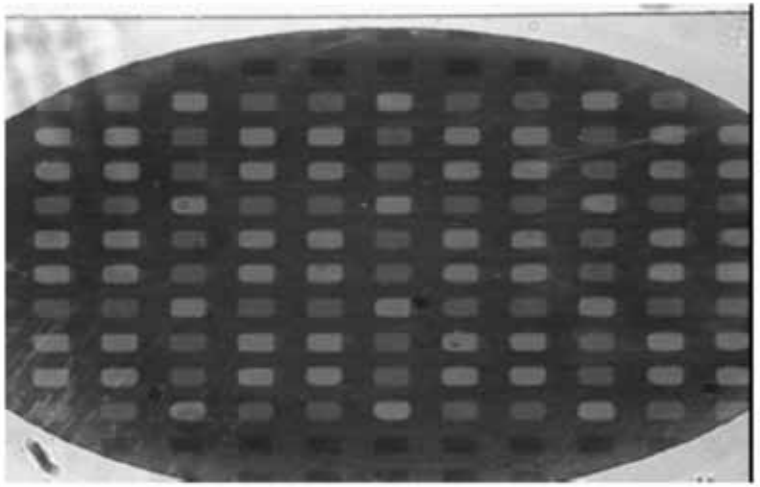

UCIrvin
University of California, Ir

Localized Plasmon

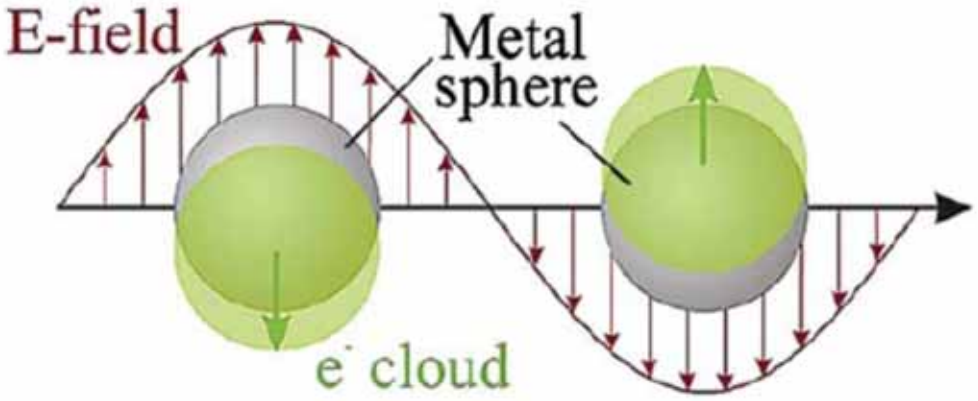

Figure 6. Schematic of plasmon oscillation for a sphere. From [39].

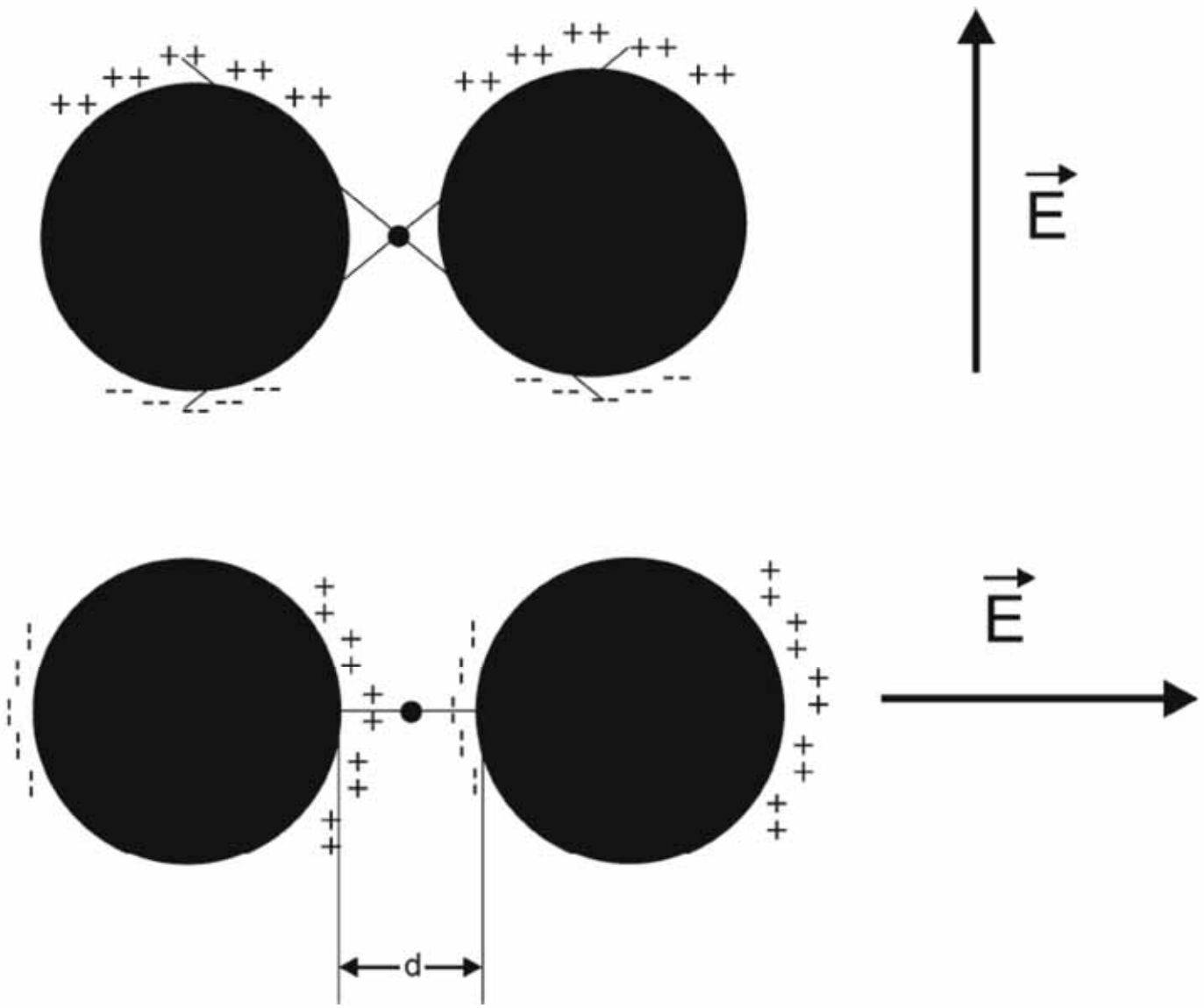
E
E
d

field enhancement

$E_s = gE_0$, where E_0 is the magnitude of the incident field.

$$E_R \propto \alpha_R E_s \propto \alpha_R g E_0$$

$$E_{SERS} \propto \alpha_R g g' E_0$$

$$I_{SERS} \propto |\alpha_R|^2 |gg'|^2 I_0$$

$$g \cong g'$$

$$|E_L|^4 = |g|^4.$$

Probing Single Molecules and Single Nanoparticles by Surface-Enhanced Raman Scattering

SCIENCE • VOL. 275 • 21 FEBRUARY 1997

Shuming Nie* and Steven R. Emory

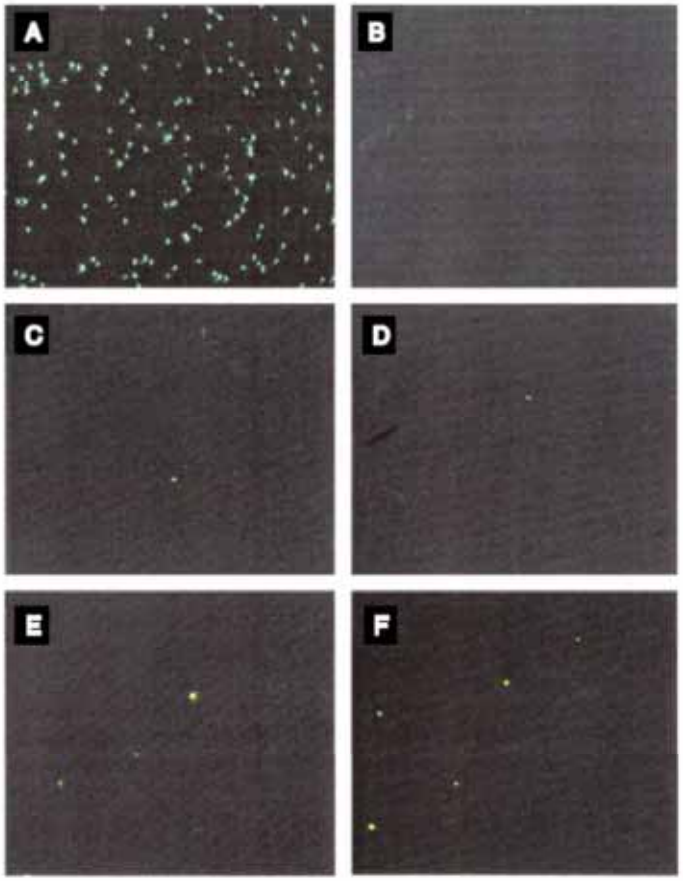

Fig. 1. Single Ag nanoparticles imaged with evanescent-wave excitation. Total internal reflection of the laser beam at the glass-liquid interface was used to reduce the laser scattering background. The instrument setup for evanescent-wave microscopy was adapted from Funatsu *et al.* (*11*). The images were directly recorded on color photographic film (ASA-1600) with a 30-s exposure by a Nikon 35-mm camera attached to the microscope. (**A**) Unfiltered photograph showing scattered laser light from all particles immobilized on a polylysine-coated surface. (**B**) Filtered photographs taken from a blank Ag colloid sample (incubated with 1 mM NaCl and no R6G analyte molecules). (**C**) and (**D**) Filtered photographs taken from a Ag colloid sample incubated with 2×10^{-11} M R6G. These images were selected to show at least one Raman scattering particle. Different areas of the cover slip were rapidly screened, and most fields of view did not contain visible particles. (**E**) Filtered photograph taken from Ag colloid incubated with 2×10^{-10} M R6G. (**F**) Filtered photograph taken from Ag colloid incubated with 2×10^{-9} M R6G. A high-performance bandpass filter was used to remove the scattered laser light and to pass Stokes-shifted Raman signals from 540 to 580 nm (920 to 2200 cm^{-1}). Continuous-wave excitation at 514.5 nm was provided by an Ar ion laser. The total laser power at the sample was 10 mW. Note the color differences between the scattered laser light in (A) and the red-shifted light in (C) through (F).

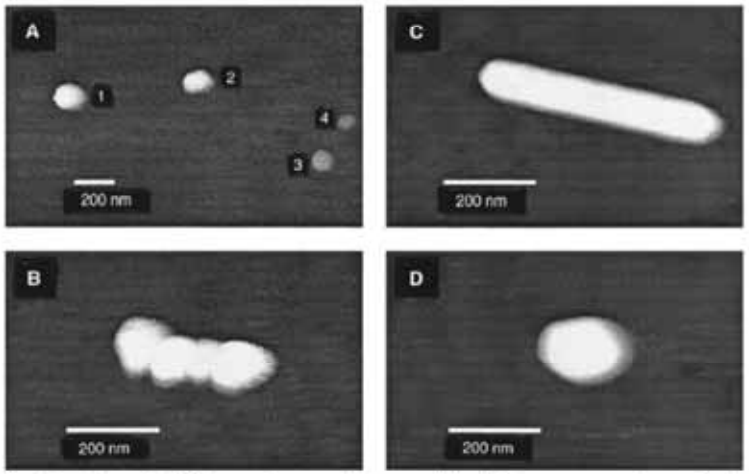

Fig. 2. Tapping-mode AFM images of screened Ag nanoparticles. (**A**) Large area survey image showing four single nanoparticles. Particles 1 and 2 were highly efficient for Raman enhancement, but particles 3 and 4 (smaller in size) were not. (**B**) Close-up image of a hot aggregate containing four linearly arranged particles. (**C**) Close-up image of a rod-shaped hot particle. (**D**) Close-up image of a faceted hot particle.

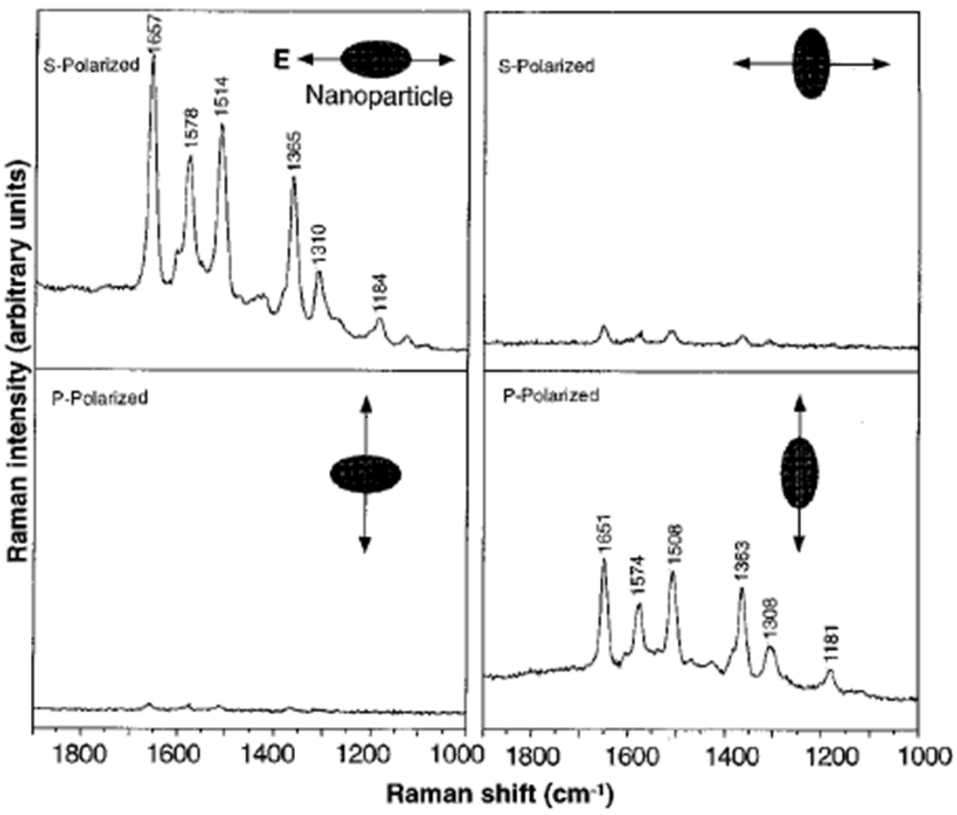

Fig. 3. Surface-enhanced Raman spectra of R6G obtained with a linearly polarized confocal laser beam from two Ag nanoparticles. The R6G concentration was 2×10^{-11} M, corresponding to an average of 0.1 analyte molecule per particle. The direction of laser polarization and the expected particle orientation are shown schematically for each spectrum. Laser wavelength, 514.5 nm; laser power, 250 nW; laser focal radius, ~250 nm; integration time, 30 s. All spectra were plotted on the same intensity scale in arbitrary units of the CCD detector readout signal.

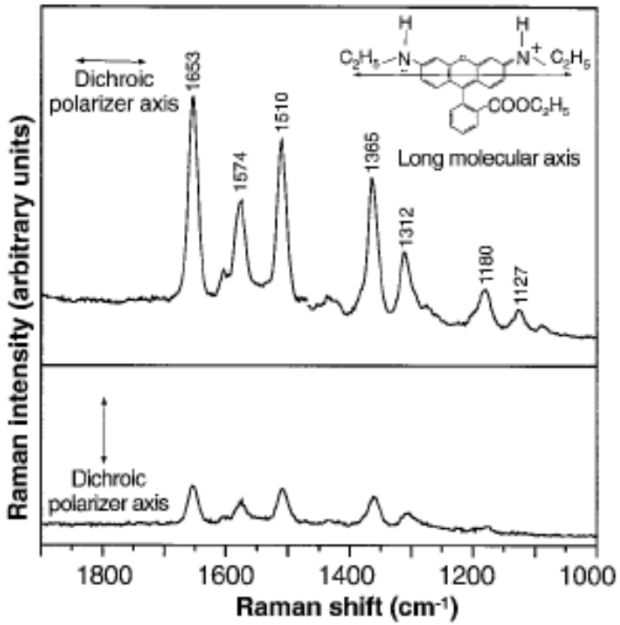

Fig. 4. Emission-polarized surface-enhanced Raman signals of R6G observed from a single Ag nanoparticle with a polarization-scrambled confocal laser beam. A dichroic sheet polarizer was rotated 90° to select Raman scattering signals polarized parallel (upper spectrum) or perpendicular (lower spectrum) to the long molecular axis of R6G. (**Inserts**) Structure of R6G, the electronic transition dipole (along the long axis when excited at 514.5 nm), and the dichroic polarizer orientations. Other conditions as in Fig. 3.

troscopic signatures of adsorbed molecules. For single rhodamine 6G molecules adsorbed on the selected nanoparticles, the intrinsic Raman enhancement factors were on the order of 10^{14} to 10^{15}, much larger than the ensemble-averaged values derived from conventional measurements. This enormous enhancement leads to vibrational Raman signals that are more intense and more stable than single-molecule fluorescence.

Electromagnetic contributions to single-molecule sensitivity in surface-enhanced Raman scattering

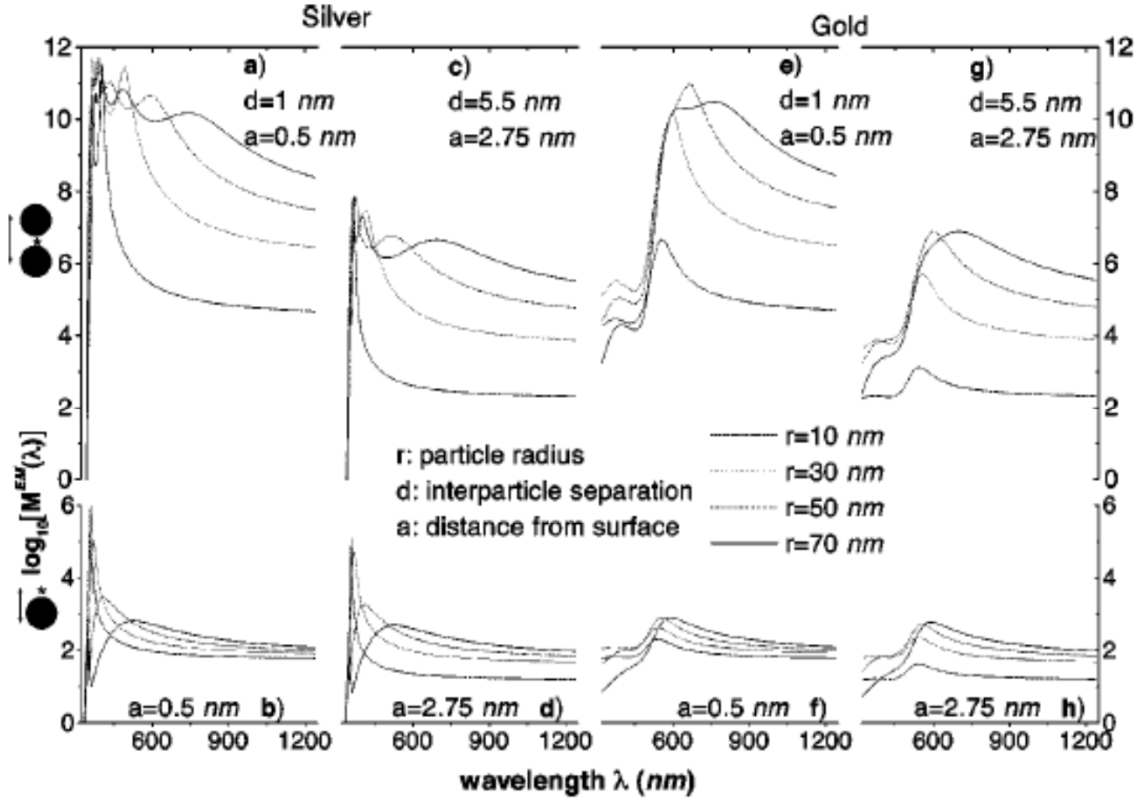

FIG. 3. (Color) EM-enhancement factor M^{EM} at a cross section through six different silver particle configurations. The wavelength of the incident field is $\lambda = 514.5$ nm with vertical polarization. The left-hand column illustrates the EM enhancement for dimer configurations of two spheres (top) and two polygons (bottom) with a separation of 1 nm. The middle column shows the same situation, but with a separation distance of 5.5 nm. The right-hand column shows the case of an isolated single particle. All particles share a common largest dimension of 90 nm. Note that the color scale from dark blue to dark red is logarithmic, covering the interval $10^9 < M^{EM} < 10^8$. Regions with enhancement outside this interval are shown in dark blue and dark red, respectively.

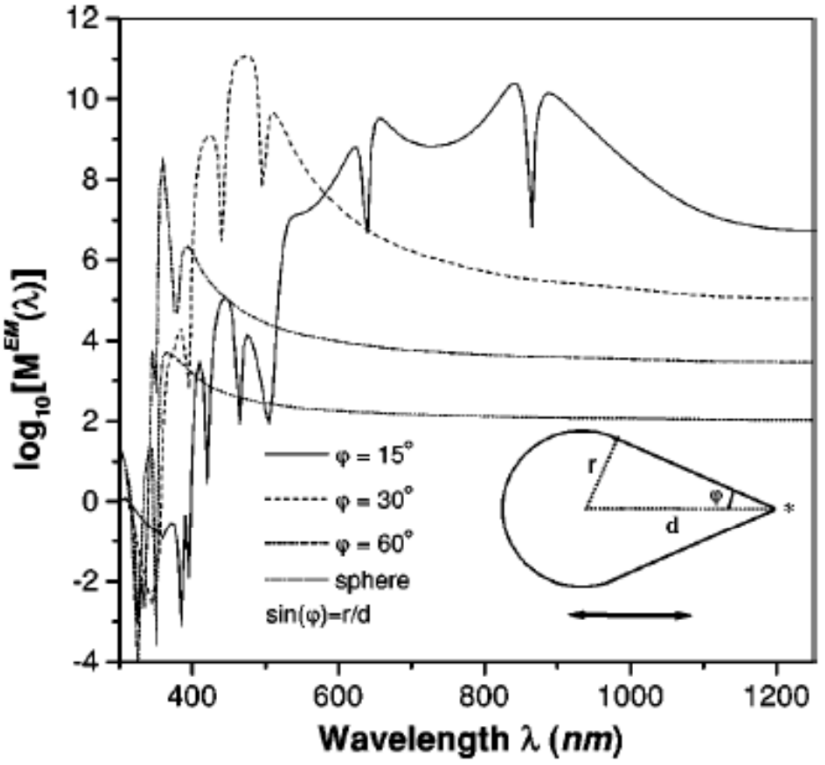

FIG. 5. EM-enhancement factor for a rotationally symmetric silver droplet as a function of the angle defining the opening edge ϕ. The field is polarized parallel to the axis of the droplet and the evaluation position (star) is located 0.5 nm outside the tip. As the droplet becomes sharper the enhancement increases several orders of magnitude.

Nanotechnology in Gene and Drug Delivery

Gene Therapy

- Gene therapy is a technique for correcting defective genes responsible for disease development. Researchers may use one of several approaches for correcting faulty genes:
  - **A normal gene may be inserted into a nonspecific location within the genome to replace a nonfunctional gene. This approach is most common.**
  - **An abnormal gene could be swapped for a normal gene through homologous recombination.**
  - **The abnormal gene could be repaired through selective reverse mutation, which returns the gene to its normal function.**
  - **The regulation (the degree to which a gene is turned on or off) of a particular gene could be altered.**

Vectors in gene therapy

- Viruses
- Envelope protein pseudotyping of viral vectors
- Naked DNA
- Oligonucleotides
- Lipoplexes and polyplexes
- Dendrimers

Envelope protein

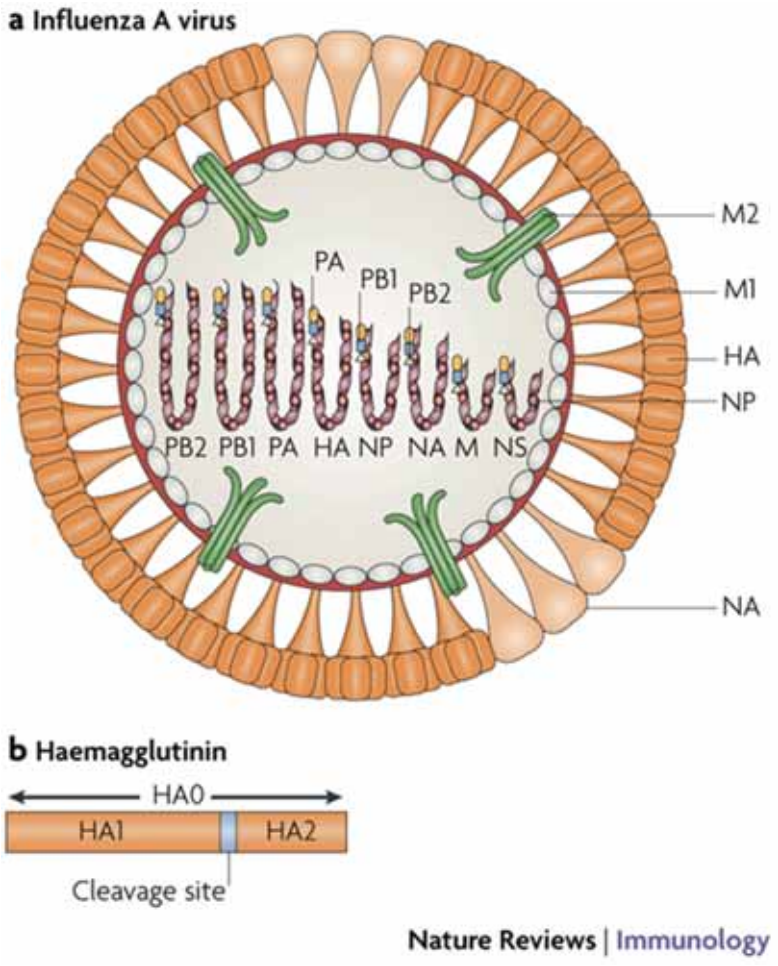

Virus Infection

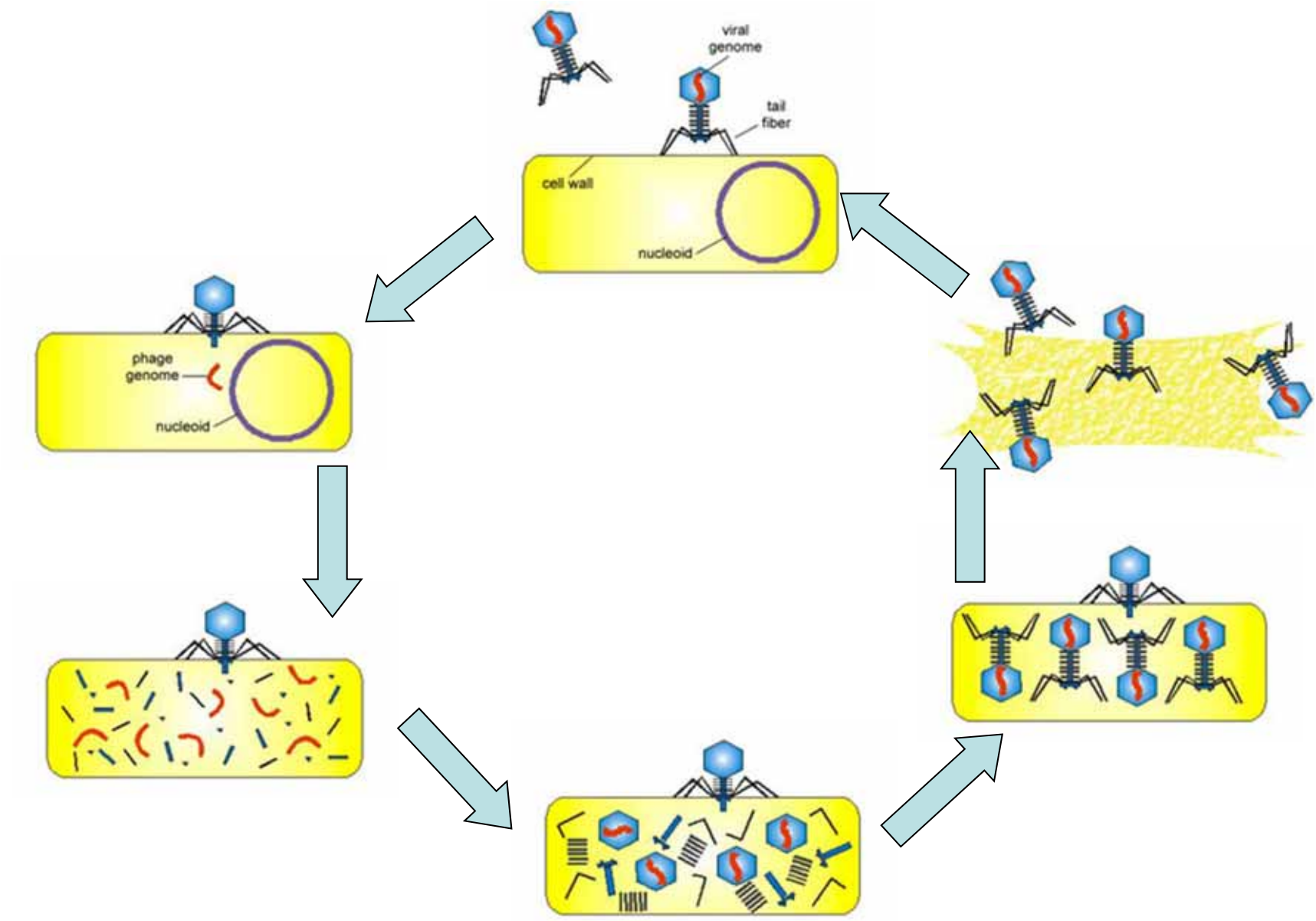

Non-viral Gene Delivery

- Transfection- the delivery of foreign molecules such as DNA and RNA into eukaryotic cells
- Naked DNA is not suitable for in-vivo transport of genetic materials-> degradation by serum nucleases
- Ideal gene delivery system
  - Biocompatible
  - Non-immunogenic
  - Stable in blood stream
  - Protect DNA during transport
  - Small enough to extravagate
  - Cell and tissue specific

CANCER NANOTECHNOLOGY: OPPORTUNITIES AND CHALLENGES

Summary

- Nanotechnology concerns the study of devices that are themselves or have essential components in the 1–1,000 nm dimensional range (that is, from a few atoms to subcellular size).
- Two main subfields of nanotechnology are nanovectors — for the administration of targeted therapeutic and imaging moieties — and the precise patterning of surfaces.
- Nanotechnology is no stranger to oncology: liposomes are early examples of cancer nanotherapeutics, and nanoscale-targeted magnetic resonance imaging contrast agents illustrate the application of nanotechnology to diagnostics.
- Photolithography is a light-directed surface-patterning method, which is the technological foundation of microarrays and the surface-enhanced laser desorption/ionization time-of-flight approach to proteomics. Nanoscale resolution is now possible with photolithography, and will give rise to instruments that can pack a much greater density of information than current biochips.
- The ability of nanotechnology to yield advances in early detection, diagnostics, prognostics and the selection of therapeutic strategies is predicated based on its ability to 'multiplex' — that is, to detect a broad multiplicity of molecular signals and biomarkers in real time. Prime examples of multiplexing detection nanotechnologies are arrays of nanocantilevers, nanowires and nanotubes.
- Multifunctionality is the fundamental advantage of nanovectors for the cancer-specific delivery of therapeutic and imaging agents. Primary functionalities include the avoidance of biobarriers and biomarker-based targeting, and the reporting of therapeutic efficacy.
- Thousands of nanovectors are currently under study. By systematically combining them with preferred therapeutic and biological targeting moieties it might be possible to obtain a very large number of novel, personalized therapeutic agents.
- Novel mathematical models are needed, in order to secure the full import of nanotechnology into oncology.

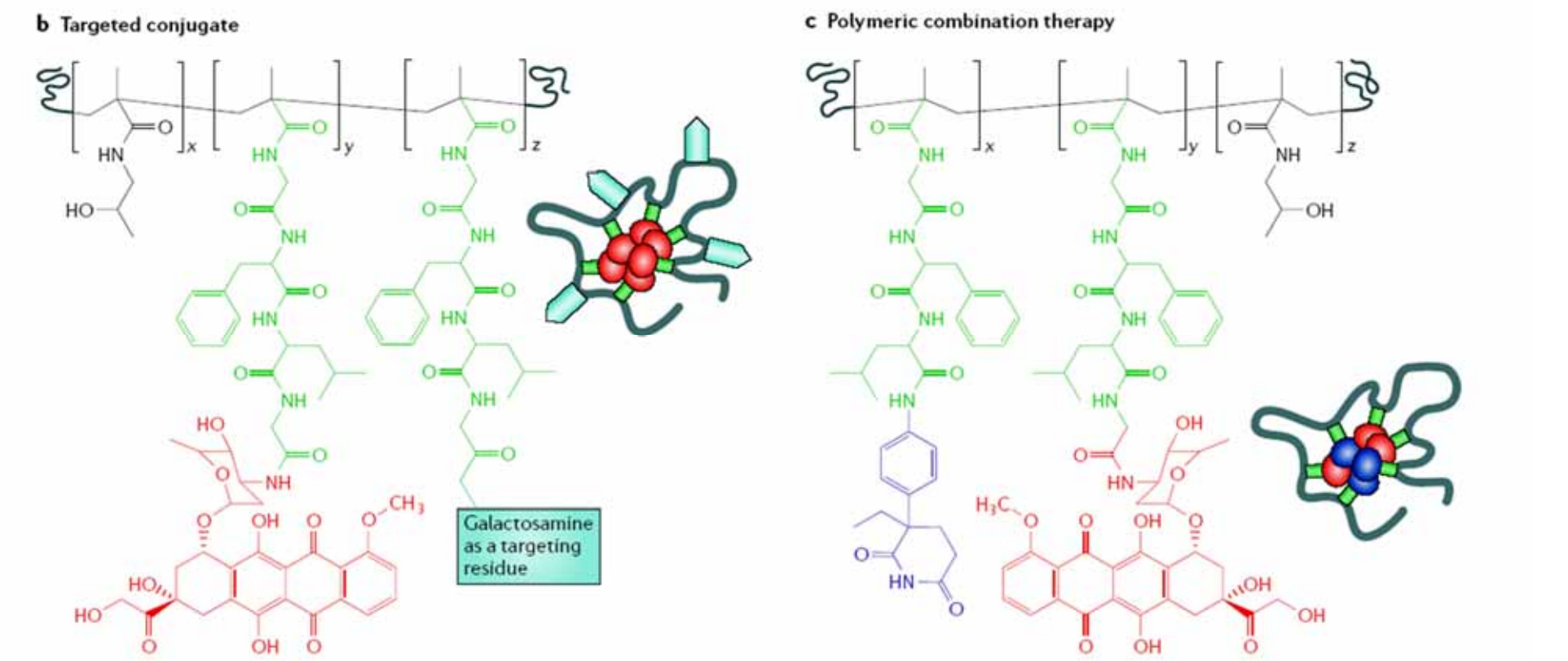

Figure 1 | **Polymer–anticancer drug conjugates.** Each panel shows both the detailed chemical structure and a cartoon of the general structure. The polymer backbone is shown in black, linker region in green, drug in red and additional components (for example, a targeting residue) in blue. **a** | Two examples of more 'simple' polymer–drug conjugates containing doxorubicin (left) and paclitaxel (right) that have progressed to clinical trial. **b** | A multivalent receptor-targeted conjugate containing galactosamine (light blue) to promote liver targeting. **c** | Polymer combination therapy containing the aromatase inhibitor aminogluthethimide (red) and doxorubicin (blue).

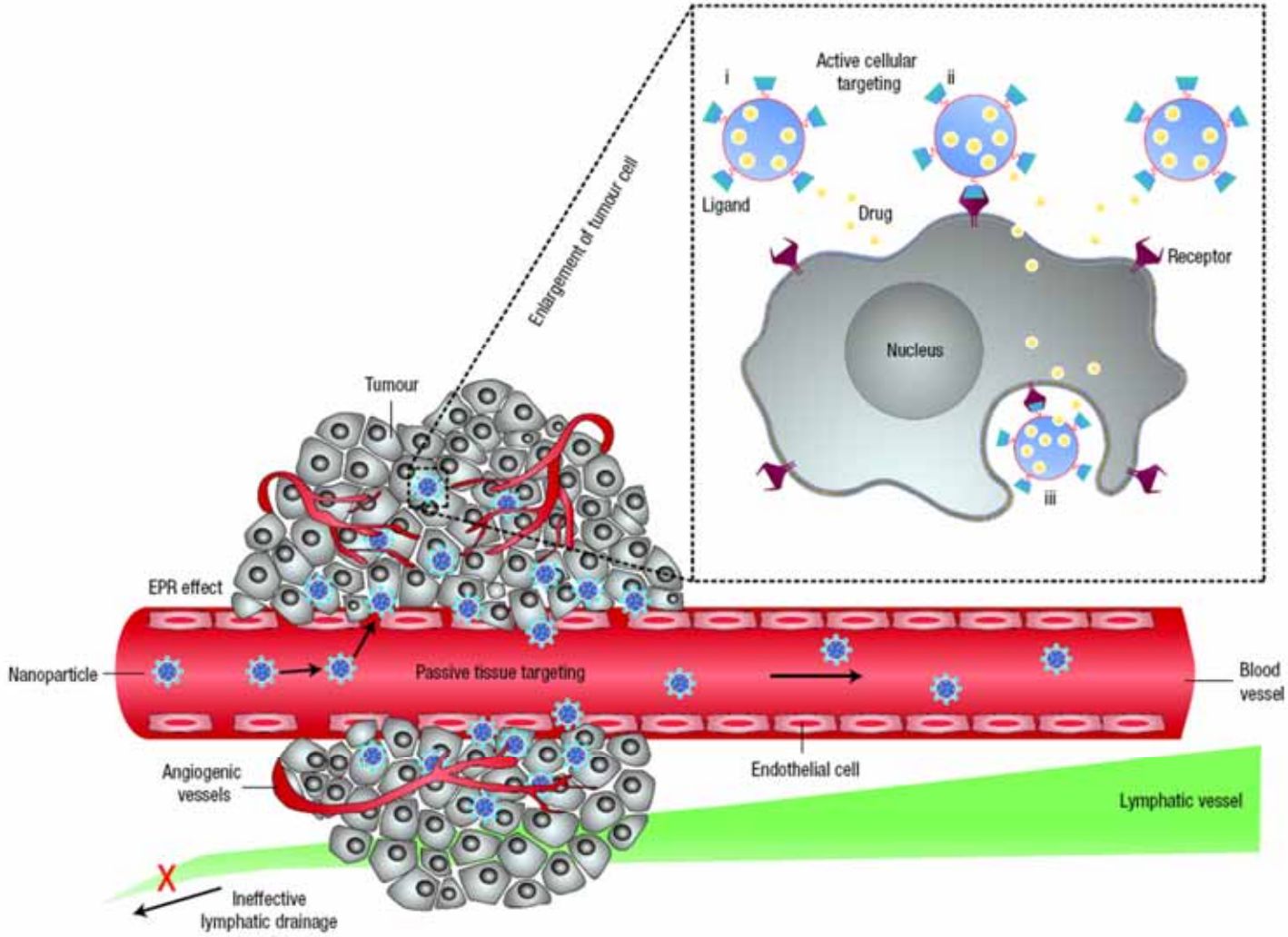

Figure 1 Schematic representation of different mechanisms by which nanocarriers can deliver drugs to tumours. Polymeric nanoparticles are shown as representative nanocarriers (circles). Passive tissue targeting is achieved by extravasation of nanoparticles through increased permeability of the tumour vasculature and ineffective lymphatic drainage (EPR effect). Active cellular targeting (inset) can be achieved by functionalizing the surface of nanoparticles with ligands that promote cell-specific recognition and binding. The nanoparticles can (i) release their contents in close proximity to the target cells; (ii) attach to the membrane of the cell and act as an extracellular sustained-release drug depot; or (iii) internalize into the cell.

Endocytosis

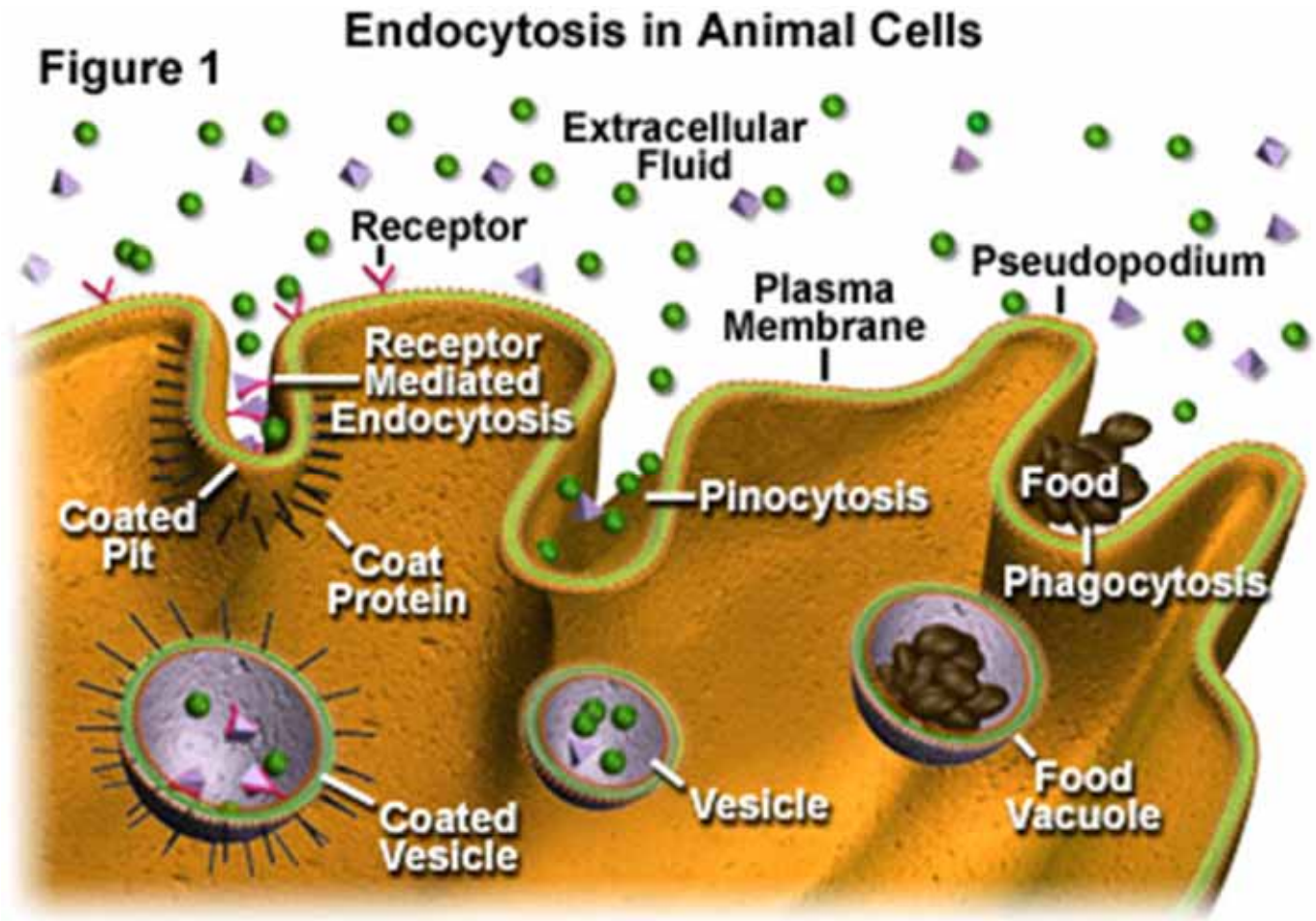

Barrier to non-viral gene delivery

<45 kDa
< 250 bp

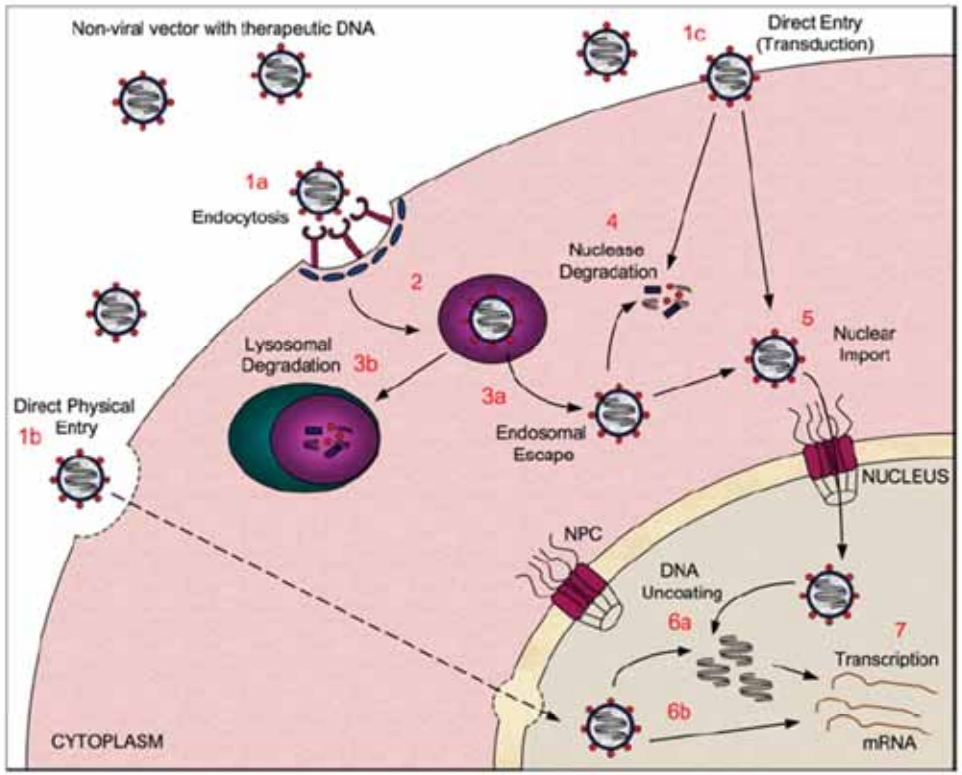

Figure 1 Barriers to non-viral gene delivery

Representation of the route travelled by a non-viral gene-delivery vector carrying therapeutic DNA to the nucleus. A non-viral vector, formed by interaction of the DNA with a carrier compound, must cross the plasma membrane to enter the cell. This can be via several routes, including endocytosis-based entry (1a), direct physical entry routes, such as electroporation or ballistic delivery (1b), or direct entry via protein transduction (1c). Depending on the mode of cellular entry, the vector may become encapsulated in an endosome (2), from which it must escape (3a) or it will become degraded when the endosome fuses with a lysosome (3b). The DNA will at some point be subjected to degradation by cytosolic nucleases (4), as it traverses through the cytoplasm to reach the nucleus. Finally, the vector must undergo nuclear transport (5) through NPCs embedded in the NE in order to gain access to the nucleoplasm. Once in the nucleus, the DNA may (6a) or may not (6b) need to be uncoated, depending upon the vector used, before it can ultimately be transcribed (7).

Biochem. J. (2007) **406**, 185–202 (Printed in Great Britain) doi:10.1042/BJ20070505

NLS-mediated nuclear import

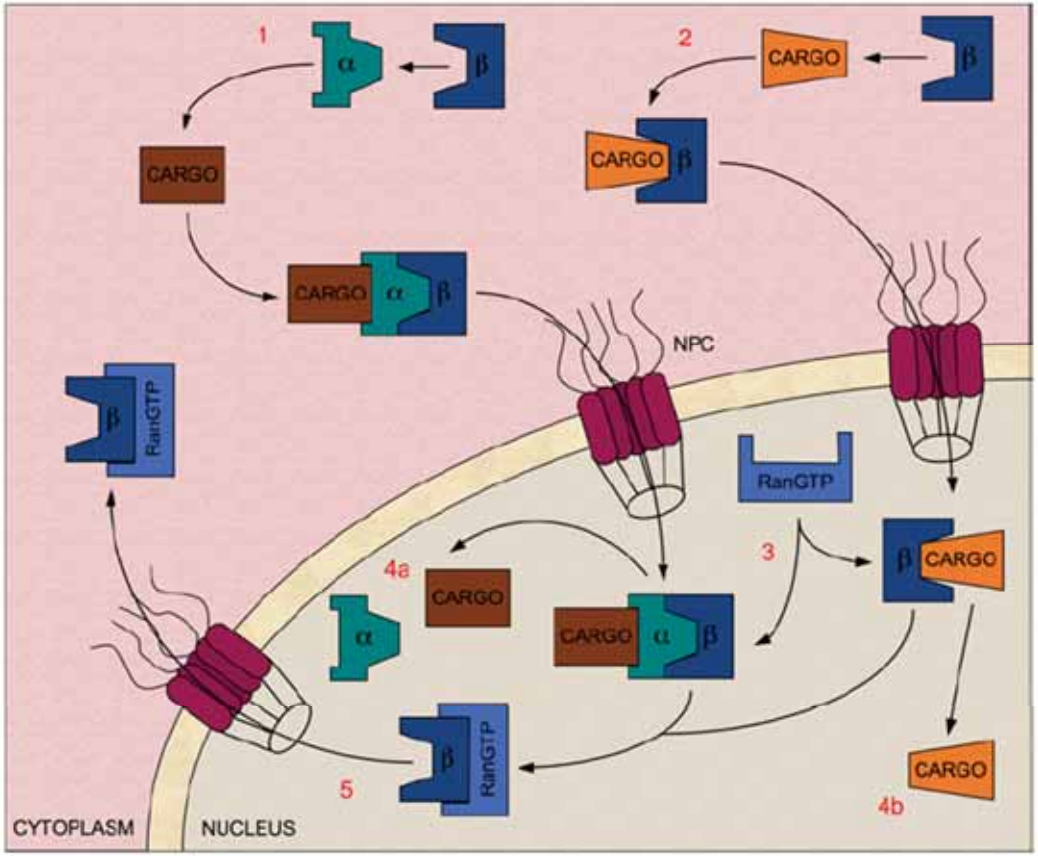

Figure 2 NLS-mediated nuclear import pathways

In classical nuclear import, the NLS found in cargo bound for the nucleus is recognized by the Imp α subunit of the Imp α/β heterodimer (1). However, there are also many examples where Imp β or one of its many homologues can mediate nuclear import or cargo proteins independently of Imp α (2). In both cases, transient interactions between the Imp β and the nucleoporin proteins that line the NE-embedded NPCs mediate translocation into the nucleus. Once inside, RanGTP binds to Imp β (3), releasing Imp α and the cargo into the nucleoplasm (4a and 4b). RanGTP itself is then recycled back to the cytoplasm (5), where it is converted into its RanGDP state (not shown). An animated version of this Figure can be found at http://www.BiochemJ.org/bj/406/0185/bj4060185add.htm

NLS Peptide

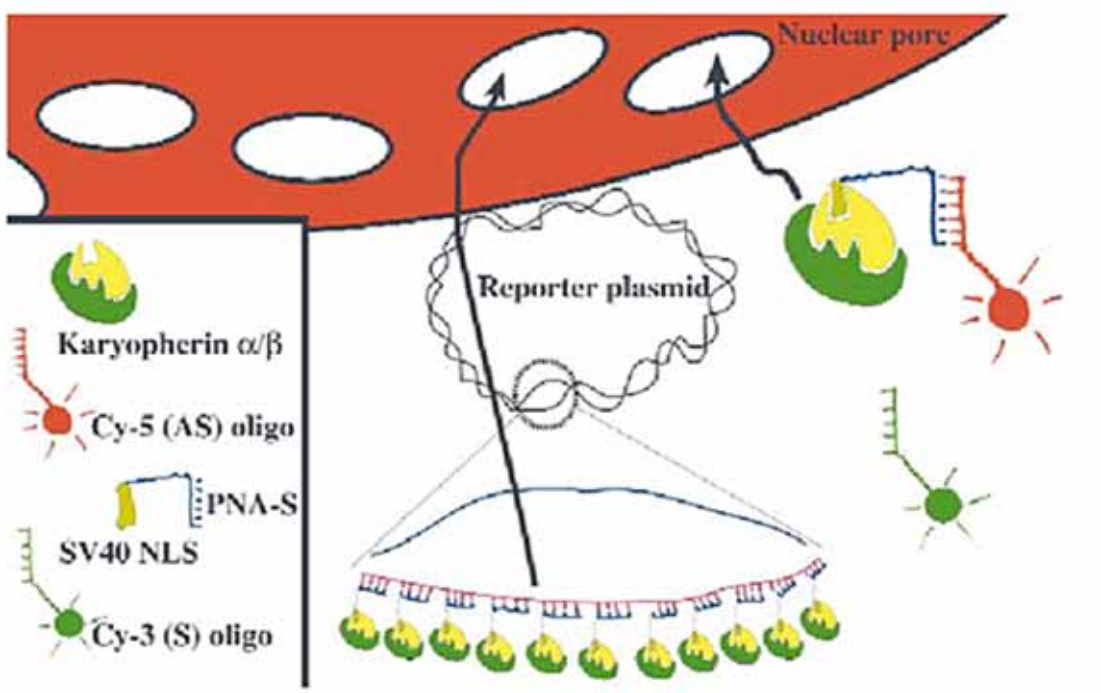
Nuclear pore
Reporter plasmid
Karyopherin α/β
Cy-5 (AS) oligo
PNA-S
SV40 NLS
Cy-3 (S) oligo

Tat Protein

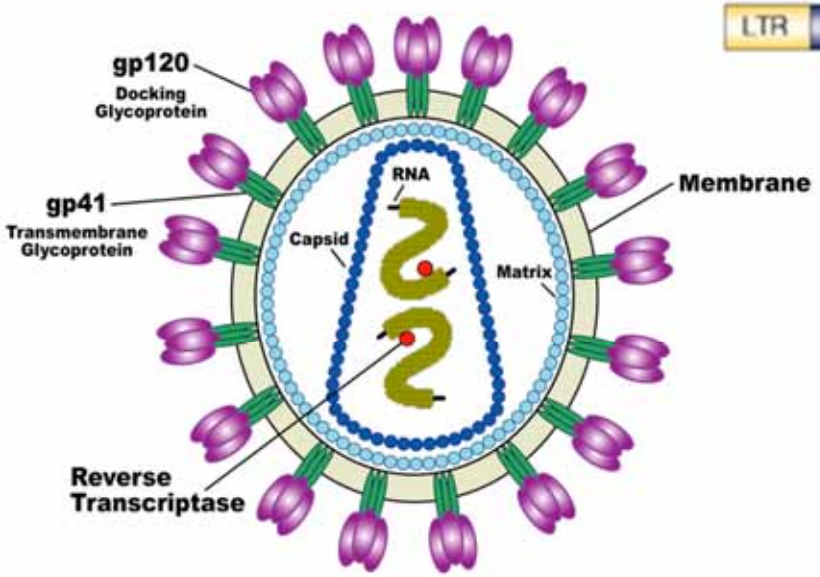
gp120
Docking
Glycoprotein
gp41
Transmembrane
Glycoprotein
RNA
Capsid
Matrix
Membrane
Reverse
Transcriptase

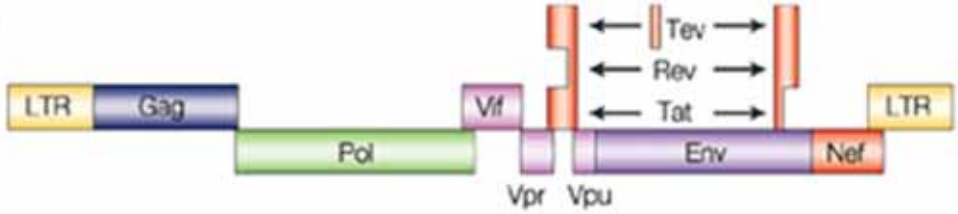
LTR
Gag
Pol
Vif
Vpr
Vpu
Tev
Rev
Tat
Env
Nef
LTR

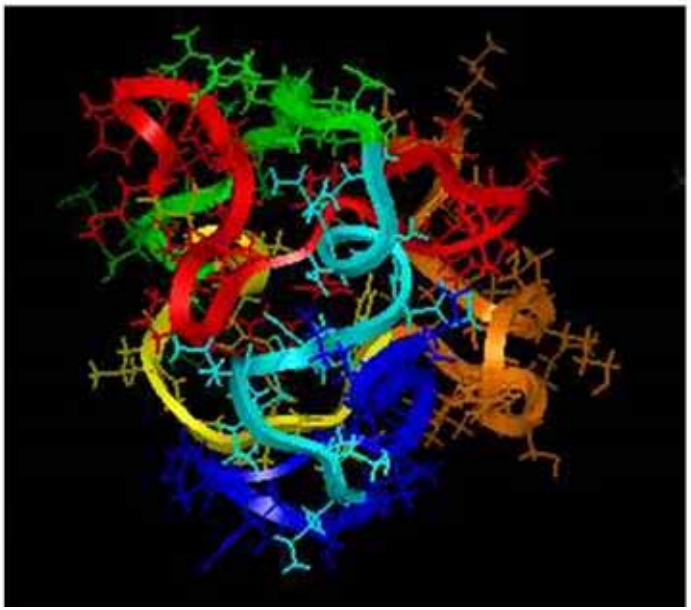

Nanoparticles

- 1-100 nm
- High surface/volume ratio
- Surface charge and size of nanoparticles
- Advantage
  - Large payload
  - Multiple targeting ligands
  - Multiple drug

Table 1 | **Nanoscaled systems for systemic cancer therapy**

Platform	Latest stage of development	Examples
Liposomes	Approved	DaunoXome, Doxil
Albumin-based particles	Approved	Abraxane
PEGylated proteins	Approved	Oncospar, PEG-Intron, PEGASYS, Neulasta
Biodegradable polymer–drug composites	Clinical trials	Doxorubicin Transdrug
Polymeric micelles	Clinical trials	Genexol-PM*, SP1049C, NK911, NK012, NK105, NC-6004
Polymer–drug conjugate-based particles	Clinical trials	XYOTAX (CT-2103), CT-2106, IT-101, AP5280, AP5346, FCE28068 (PK1), FCE28069 (PK2), PNU166148, PNU166945, MAG-CPT, DE-310, Pegamotecan, NKTR-102, EZN-2208
Dendrimers	Preclinical	Polyamidoamine (PAMAM)
Inorganic or other solid particles	Preclinical (except for gold nanoparticle that is clinical)	Carbon nanotubes, silica particles, gold particles (CYT-6091)

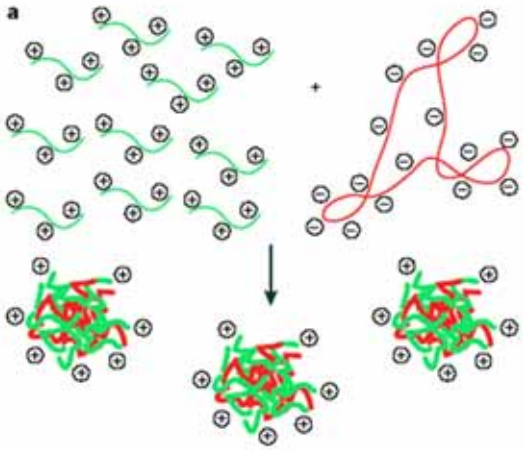

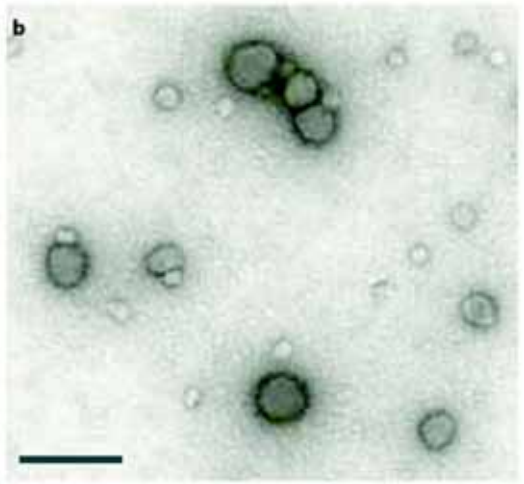

Figure 1 | **Polyplex formation.** Polyplexes are formed by electrostatic interactions between polycations and DNA. **a** | When aqueous solutions of a polycation and DNA are mixed, polyplexes form spontaneously. The interaction is entropically driven. For gene delivery, an excess of polycation is typically used, which generates particles with a positive surface charge. Each particle consists of several plasmid DNA molecules and hundreds of polymer chains and is 100–200 nm in diameter. **b** | Transmission electron micrograph of polyplexes comprising plasmid DNA and a polycation, in this case cyclodextrin-modified, branched polyethylenimine (PEI)[165]. Scale bar = 200 nm.

Box 1 | **Design criteria for non-viral vectors**

- Protection of DNA
- Packaging of large DNA plasmids
- Easy administration
- Serum stability
- Targetability to specific cell types
- Ease of fabrication
- Inexpensive synthesis
- Facile purification
- Robustness/stability
- Internalization
- Endolysosomal escape
- Nuclear transport
- Efficient unpackaging
- Infection of non-dividing cells
- Safety
- Non-toxic
- Non-immunogenic
- Non-pathogenic

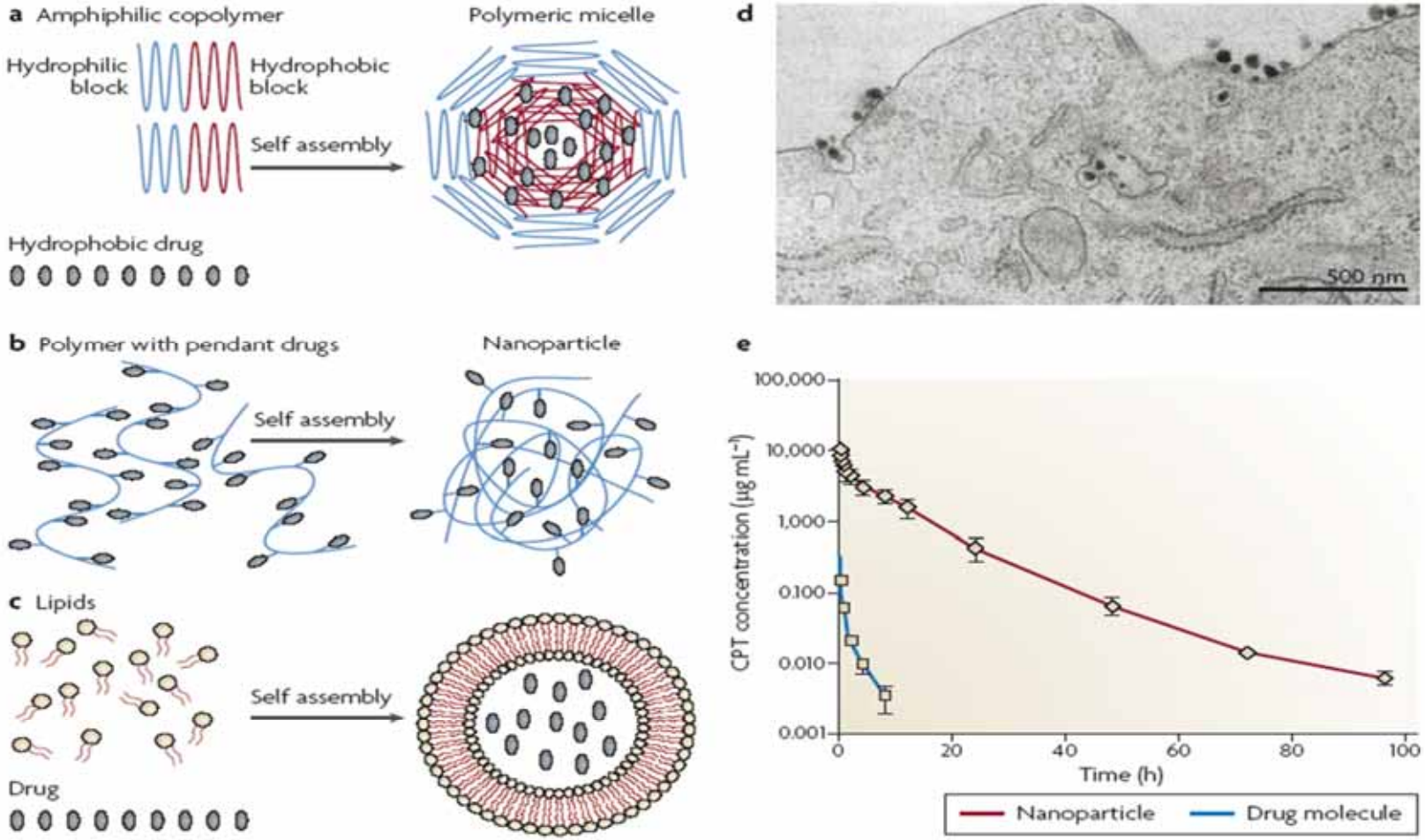

Figure 1 | **Major classes of nanoparticles that are in clinical trials and some of their properties. a** | Nanoparticles formed from therapeutic entities and block copolymers that can form polymeric micelles. **b** | Nanoparticles that form with polymer–drug conjugates. **c** | Nanoparticles formed of liposomes. **d** | Nanoparticles can enter cells via endocytosis. This figure shows a transmission electron micrograph of nanoparticles at the surface of a cancer cell, entering the cell and within endocytic vesicles. **e** | Nanoparticles can have extended pharmacokinetics over the therapeutic entity alone. The data are from a small-molecule drug (CPT) and a nanoparticle containing CPT in rats. Panel (**e**) is adapted with permission from REF. 94 © Springer (2006).

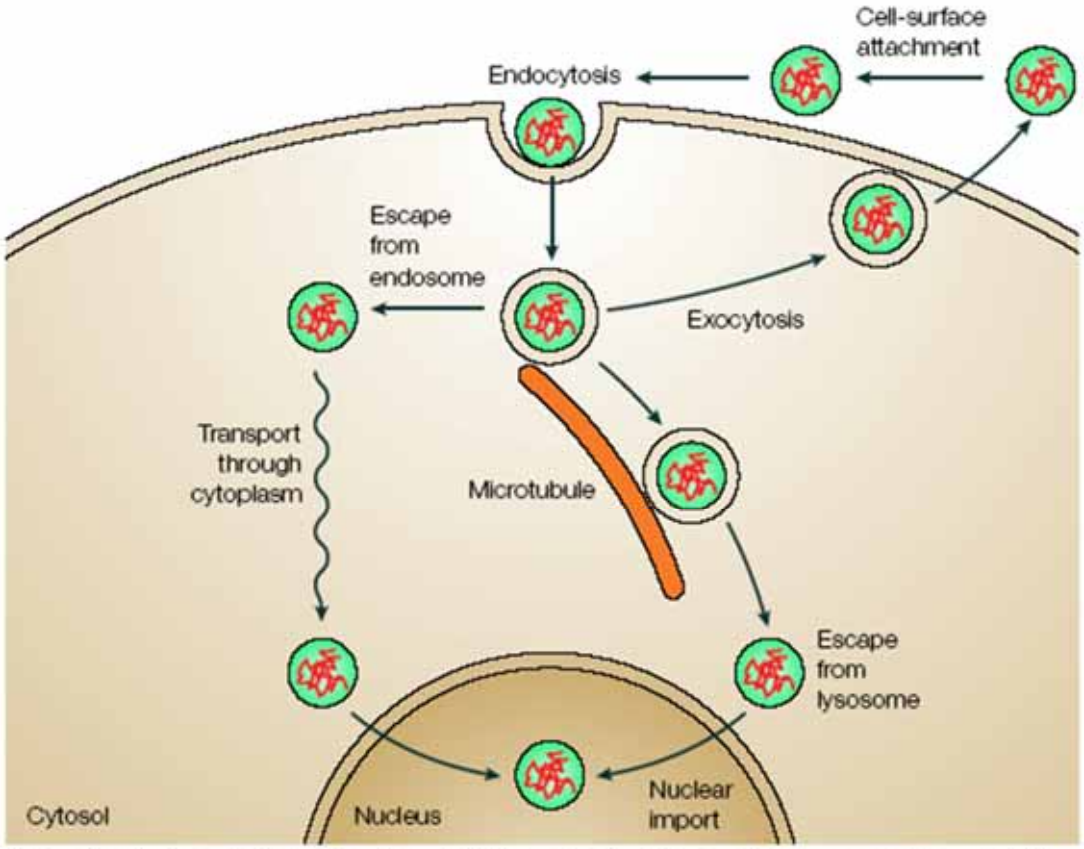

Figure 2 | **Barriers to intracellular trafficking of polyplexes.** Polyplexes must attach to the cell surface, be internalized (by endocytosis), escape from endolysosomes, move through the cytoplasm toward the nucleus and cross the nuclear membrane. Alternative pathways exist for several of these steps. In addition, the polyplexes must unpackage — DNA must be released by the polymer — but where unpackaging occurs is not known.

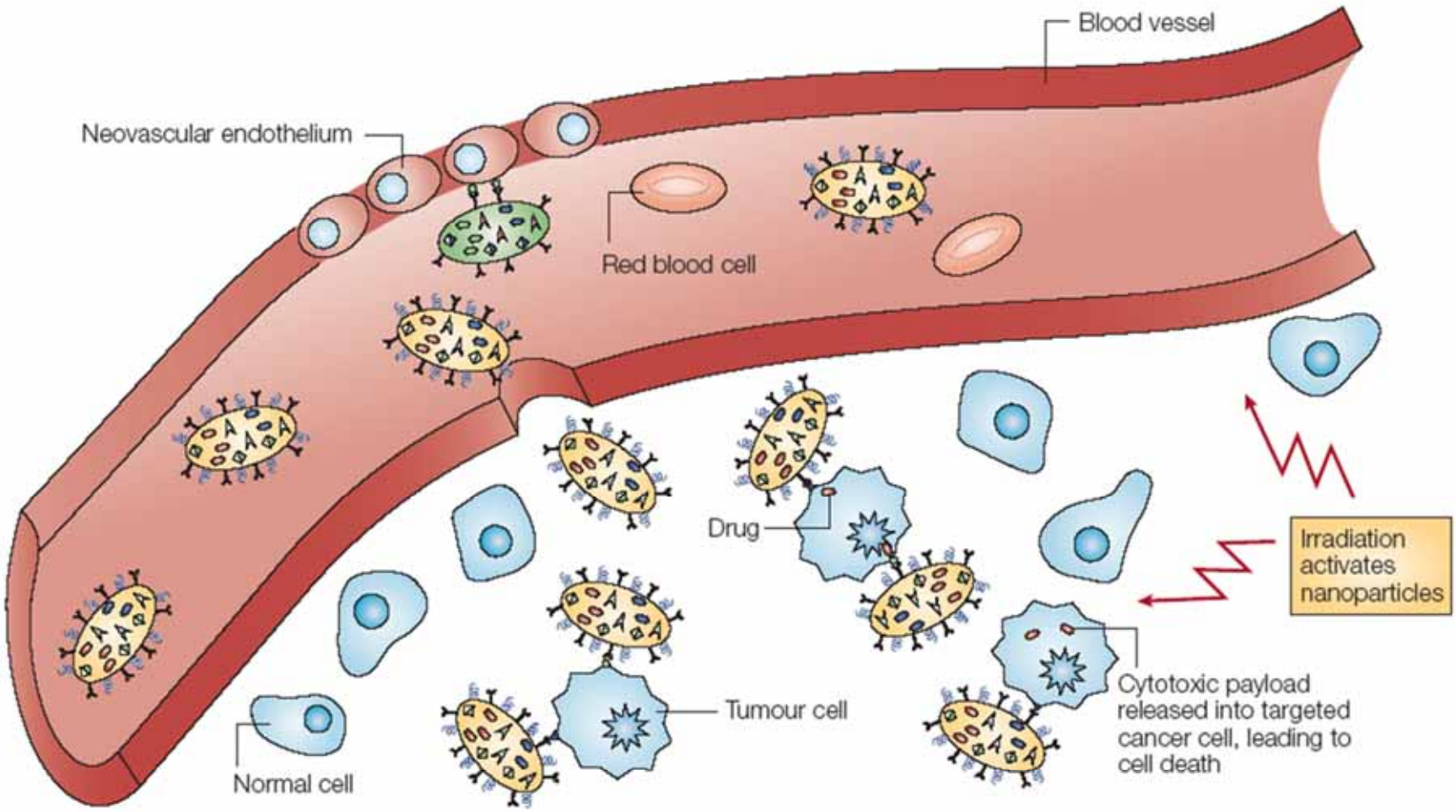

Figure 4 | **Multicomponent targeting strategies.** Nanoparticles extravasate into the tumour stroma through the fenestrations of the angiogenic vasculature, demonstrating targeting by enhanced permeation and retention. The particles carry multiple antibodies, which further target them to epitopes on cancer cells, and direct antitumour action. Nanoparticles are activated and release their cytotoxic action when irradiated by external energy. Not shown: nanoparticles might preferentially adhere to cancer neovasculature and cause it to collapse, providing anti-angiogenic therapy. The red blood cells are not shown to scale; the volume occupied by a red blood cell would suffice to host 1–10 million nanoparticles of 10 nm diameter.

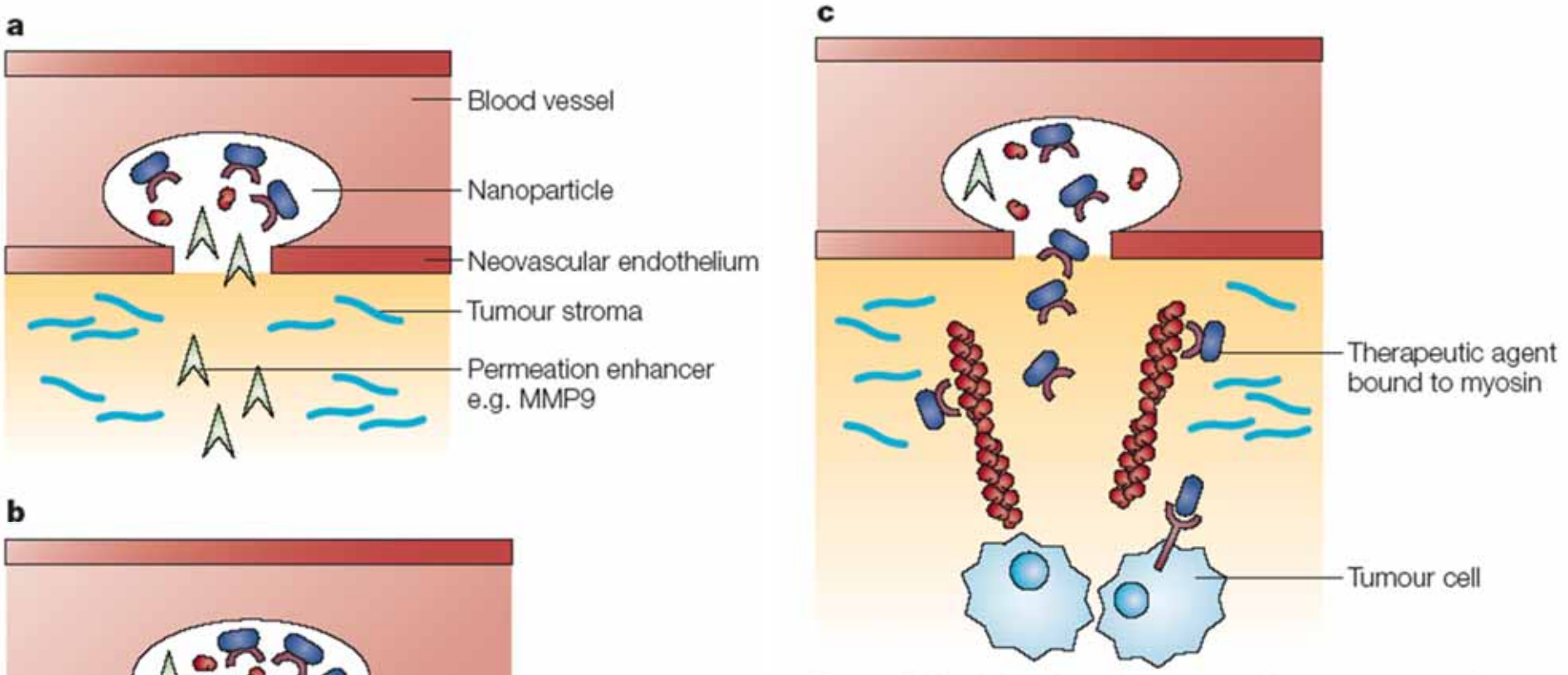

Figure 5 | **A vision for a future multistage nanodevice with multiple-barrier-avoidance capability**. A nanovector selectively binds to the cancer neovascular endothelium, releases a penetration enhancer, generates a fenestration, and deploys through it a track of molecular motor molecules such as actin. Therapeutic agents bound to a conjugate molecule such as myosin are then released by the nanovector, and travel along the 'molecular track' to reach deeply into the cancer lesion, despite the opposing oncotic osmotic pressure.

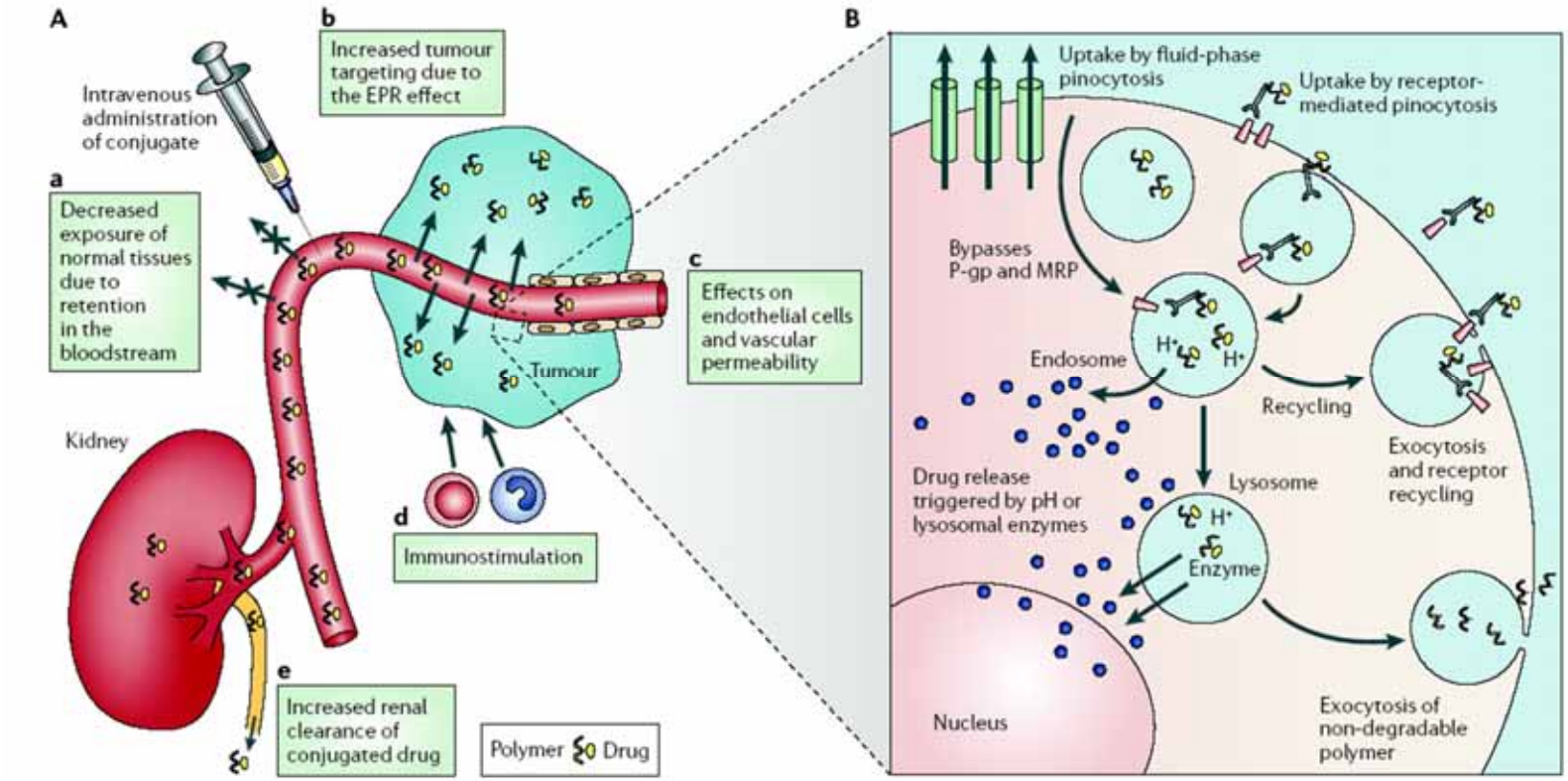

Figure 2 | **Current understanding of the mechanism of action of polymer–drug conjugates. A** | Hydrophilic polymer–drug conjugates administered intravenously can be designed to remain in the circulation — their clearance rate depends on conjugate molecular weight, which governs the rate of renal elimination. **a** | Drug that is covalently bound by a linker that is stable in the circulation is largely prevented fom accessing normal tissues (including sites of potential toxicity), and biodistribution is initially limited to the blood pool. **b** | The blood concentration of drug conjugate drives tumour targeting due to the increased permeability of angiogenic tumour vasculature (compared with normal vessels), providing the opportunity for passive targeting due to the enhanced permeability and retention effect (EPR effect). **c** | Through the incorporation of cell-specific recognition ligands it is possible to bring about the added benefit of receptor-mediated targeting of tumour cells. **d** | It has also been suggested that circulating low levels of conjugate (slow drug release) might additonally lead to immunostimulation. **e** | If the polymer–drug linker is stable in the circulation, for example, *N*-(2-hydroxypropyl)methacrylamide (HPMA) copolymer–Gly-Phe-Leu-Gly–doxorubicin, the relatively high level of renal elimination (whole body $t_{1/2}$ clearance >50% in 24 h) compared with free drug ($t_{1/2}$ clearance ~50% in 4 days) can increase the elimination rate. **B** | On arrival in the tumour interstitium, polymer-conjugated drug is internalized by tumour cells through either fluid-phase pinocytosis (in solution), receptor-mediated pinocytosis following non-specific membrane binding (due to hydrophobic or charge interactions) or ligand–receptor docking. Depending on the linkers used, the drug will usually be released intracellularly on exposure to lysosomal enzymes (for example, Gly-Phe-Leu-Gly and polyglutamic acid (PGA) are cleaved by cathepsin B) or lower pH (for example, a hydrazone linker degrades in endosomes and lysosomes (pH 6.5–<4.0). The active or passive transport of drugs such as doxorubicin and paciltaxel out of these vesicular compartments ensures exposure to their pharmacological targets. Intracellular delivery can bypass mechanisms of resistance associated with membrane efflux pumps such as p-glycoprotein. If >10-fold, EPR-mediated targeting will also enable the circumvention of other mechanisms of drug resistance. Non-biodegradable polymeric platforms must eventually be eliminated from the cell by exocytosis. Rapid exocytic elimination of the conjugated drug before release would be detrimental and prevent access to the therapeutic target. In general, polymeric carriers do not access the cytosol. MRP, multidrug resistance protein.

Barriers to DNA Delivery

BOX 1

A number of challenges and barriers face the successful delivery of therapeutic DNA to target cells in the body. Physicochemical, economic and sterilization challenges complicate formulation; the complex environment of the human body hinders its successful transport to the target cell population; and endocytic pathway barriers hinder its successful transport to the nucleus of the cell (the site of action). Each known and major barrier is listed in Fig. B1, using nanoscale DNA-delivery systems as representative examples. Each barrier exists independent of length scale. L = lysosome. A number of clever systems have been devised to overcome these barriers, the general design criteria of which are given in Tables B1 and B2.

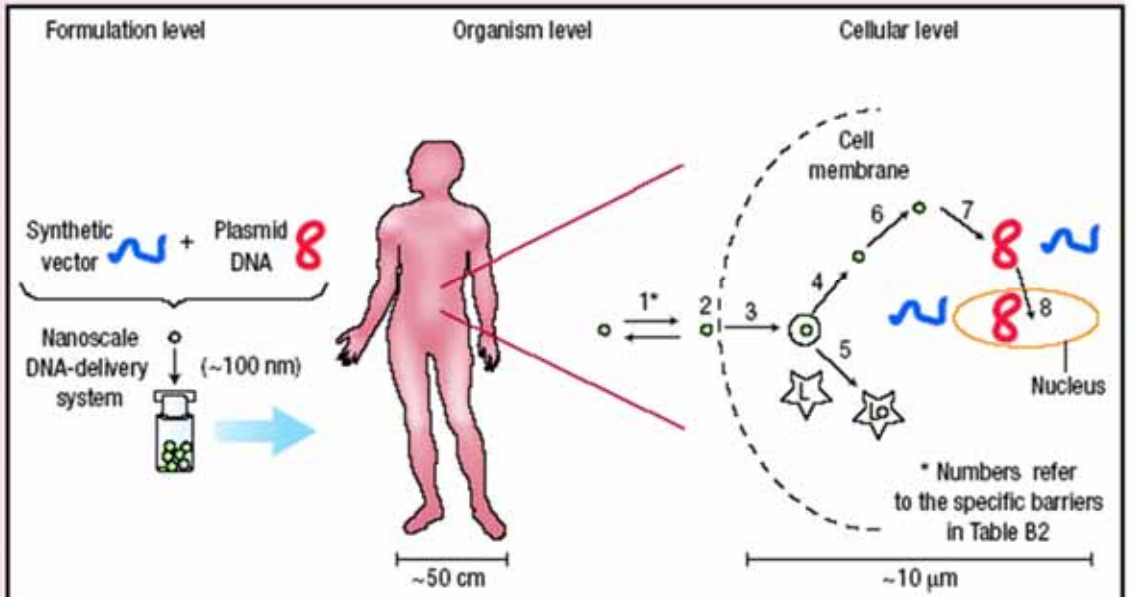

Barriers / challenges / needs

Formulation	Organism	Cellular
Economically viable	Prolonged circulation time	Transport to cell surface
FDA-approvable	Stability in blood circulation	Cellular internalization
Acceptable shelf-life	Access to target tissue/cells	Intracellular transport
	Elimination from body	Enzymatic degradation
	Mininal toxicity	Nuclear entry

Figure B1 Barriers to DNA delivery.

Organism Level			
Barrier/challenge/need	**Rationale**	**Example approaches**	**Materials design criteria**
Prolonged circulation time	Maximize total flux past target cell type	PEG conjugates to minimize interaction with serum proteins	Hydrophilic Uncharged
Stability within blood circulation	Maintenance of designed functionality	Crosslinking to maximize overall stability	Stable crosslinks within bloodstream, but reversible upon entry into target cell
Access to target tissue/cells	Transport from capillary lumen to extracellular space to reach target cell surface	Vaso-active protein conjugates (for example, vascular endothelial growth factor)	Retention of protein activity post conjugation
		Targeting restricted to 'leaky' vessel tissues (for example, tumour, liver, spleen).	Small diameter delivery system (for example, <100 nm)
Elimination from body	Minimal build-up of delivery vector over time	Control over molecular weight	Filterable through kidneys
		Engineered biodegradation sites	Biodegradable
Minimal toxicity and immunogenicity	Safety over treatment duration and beyond that required for FDA-approval	Minimize cation density	Non-cytotoxic
		Avoid protein-based materials/conjugates	Non-immunogenic

Cellular Level			
Barrier number (from Fig. B1)	Barrier/challenge/need	Example approaches	Materials design criteria
1, 2 and 3	Transport to cell surface, association with cell membrane, internalization	Receptor/ligand interaction (for example, antibody/polymer conjugates, recombinant protein–polymer fusions, carbohydrate conjugates)	Cell-type specificity, low cross reactivity, if desired
		Non-specific interaction with cell surface (for example, positive zeta potential, lipid conjugates)	Promiscuous attachment, high cross reactivity, if desired (for example, positive zeta potential, lipid conjugation)
			Endocytic pathway trigger (for example, clathrin-dependent, clathrin-independent, caveolin-dependent)
4 and 5	Escape endosomal vesicle and avoid transport to lysosome	Buffering capacity between pH ~7.2 and ~5.0	Ability to disrupt endosomal membrane and/or fusion of endosome with lysosome
		Fusogenic peptide conjugate	
6	Transport through cytosol to perinuclear space with minimal degradation	'Higher' molecular weight to maintain complex stability within cytosol	Thermodynamic and kinetic stability of complex within cytosol
			Minimize DNA degradation within cytosol
7	Separation of complex to allow nuclear translocation	Hydrolytically or reductively degradable polymers to reduce molecular weight	'Triggered' degradation of polymer to reduce thermodynamic and kinetic stability of complex. Release of intact DNA at or near nuclear envelope
8	Nuclear entry	Nuclear localization sequence conjugates	Facilitate nuclear uptake of DNA using virus-derived signals
		Mitosis	Facilitate nuclear uptake during mitosis when the nuclear envelope is dissolved.

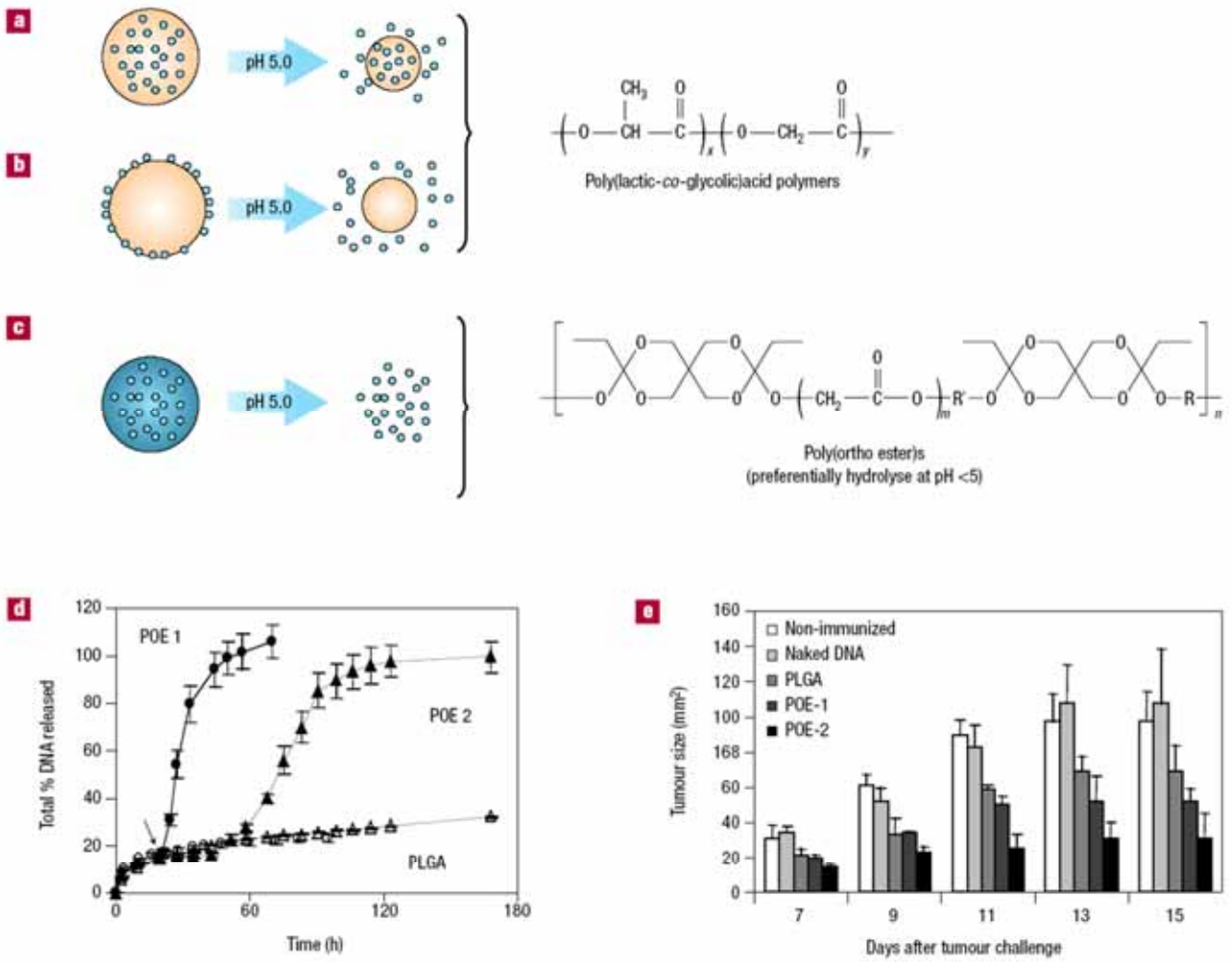

Figure 4 Degradation of polymeric microspheres as a function of pH. Microspheres <10 micrometres in diameter are preferentially internalized by APCs, providing a mechanism by which to target vaccines to the immune system. Following internalization by APCs, the spheres are sequestered within acidic vesicles, providing a mechanism through which to modulate the release of encapsulated DNA intracelluarly. **a**, Poly(lactic-*co*-glycolic)acid (PLGA) microspheres degrade relatively independent of the extracellular and acidic vesicle pH and release DNA as a function of polymer degradation. **b**, DNA adsorbed to the surface of PLGA-based microspheres release DNA more quantitatively than encapsulated DNA, but relatively independent of pH. **c**, Poly(orthoesters) degrade more rapidly at pH ~5.0, allowing triggered release of the DNA in the acidic environment of the phagosome. **d**, The pH-sensitive release of plasmid DNA from microspheres comprised of poly(orthoesters) (POE-1 and POE-2) described in ref. 63 and the pH-independent release of plasmid DNA from PLGA-based microspheres. The arrow shows the time at which the pH was changed from 7.4 to 5.0. The error bars represent the standard deviations over three samples. **e**, The influence that different DNA release kinetics can have on the efficacy of an anticancer DNA-therapeutic (adapted from ref. 63). The error bars represent the standard error from the average over five samples.

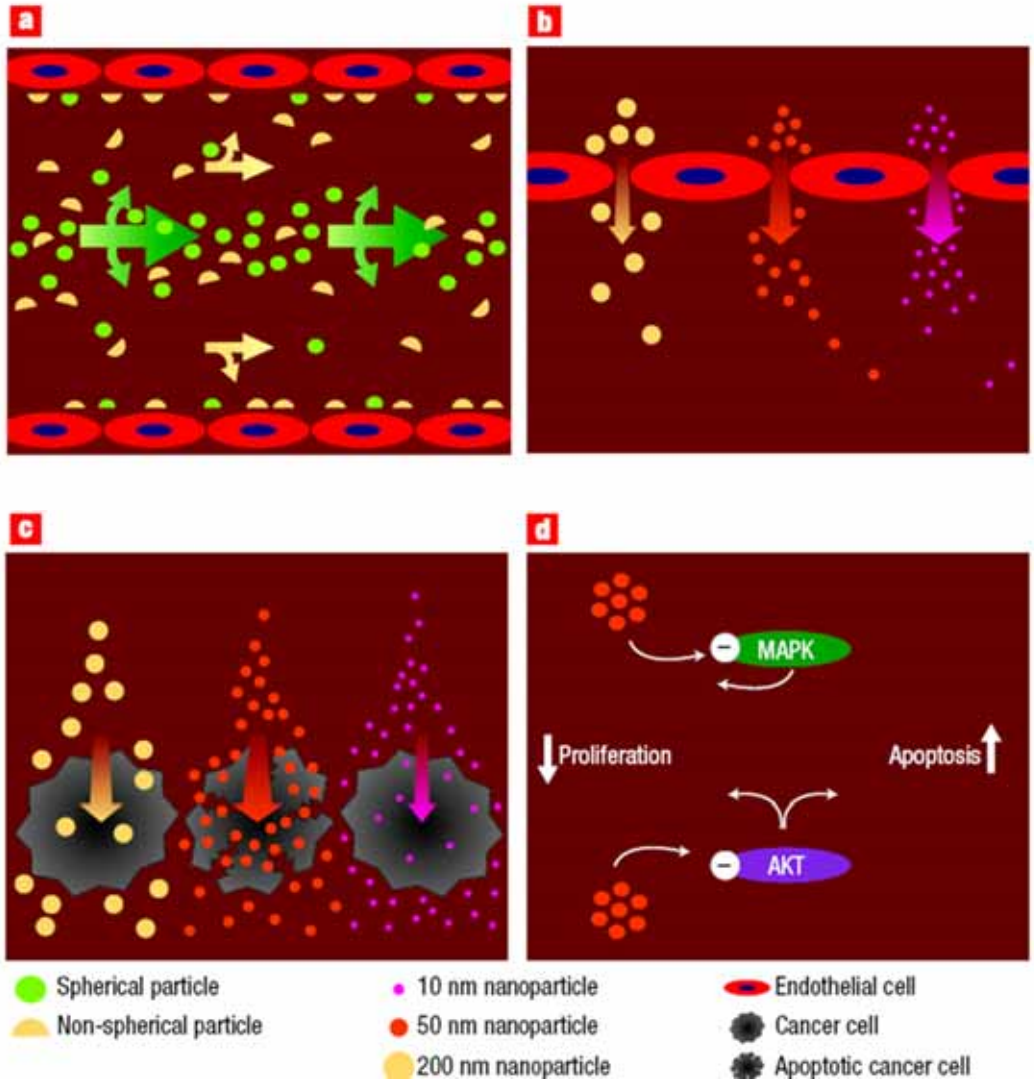

Figure 1 The geometry of a nanoparticle impacts its ability to perform its four basic functions. **a**, Navigation: non-spherical particles are more likely to be near the capillary walls and adhere to the cancer-specific molecules expressed on the vascular walls. **b**, Avoidance of biological barriers: particles of the right size fit through cancer-associated capillary wall fenestrations and localize preferentially in cancer lesions. **c**, Site- and cell-specific localization: nanoparticles of different sizes are taken up by cancer cells with different efficiency. **d**, Targeting of biological pathways. Chan and colleagues[1] showed that nanoparticles of different size can affect two signalling pathways, MAPK and AKT, to decrease proliferation and increase apoptotic cell death. These properties show that nanoparticles themselves can be candidate anticancer agents, even if they do not carry drugs.

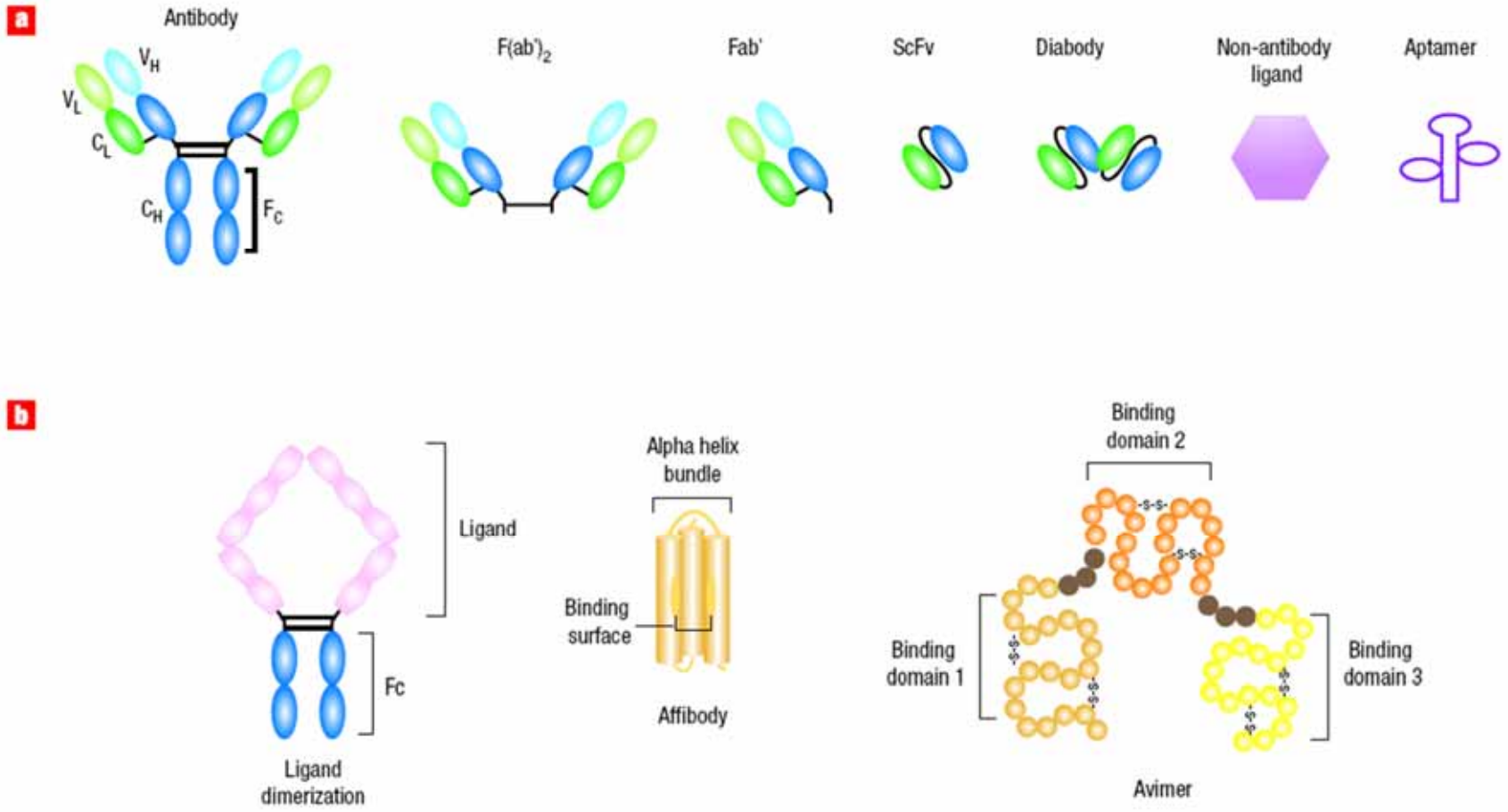

Figure 2 Common targeting agents and ways to improve their affinity and selectivity. **a**, The panel shows a variety of targeting molecules such as a monoclonal antibody or antibodies' fragments, non-antibody ligands, and aptamers. The antibody fragments F(ab)$_2$ and Fab are generated by enzymatic cleavage whereas the Fab , scFv, and bivalent scFv (diabody) fragments are created by molecular biology techniques. V_H: variable heavy chain; V_L: variable light chain; C_H: constant heavy chain; C_L: constant light chain. Non-antibody ligands include vitamins, carbohydrates, peptides, and other proteins. Aptamers can be composed of either DNA or RNA. **b**, Affinity and selectivity can be increased through ligand dimerization or by screening for conformational-sensitive targeting agents such as affibodies, avimers and nanobodies, as well as intact antibodies and their fragments.

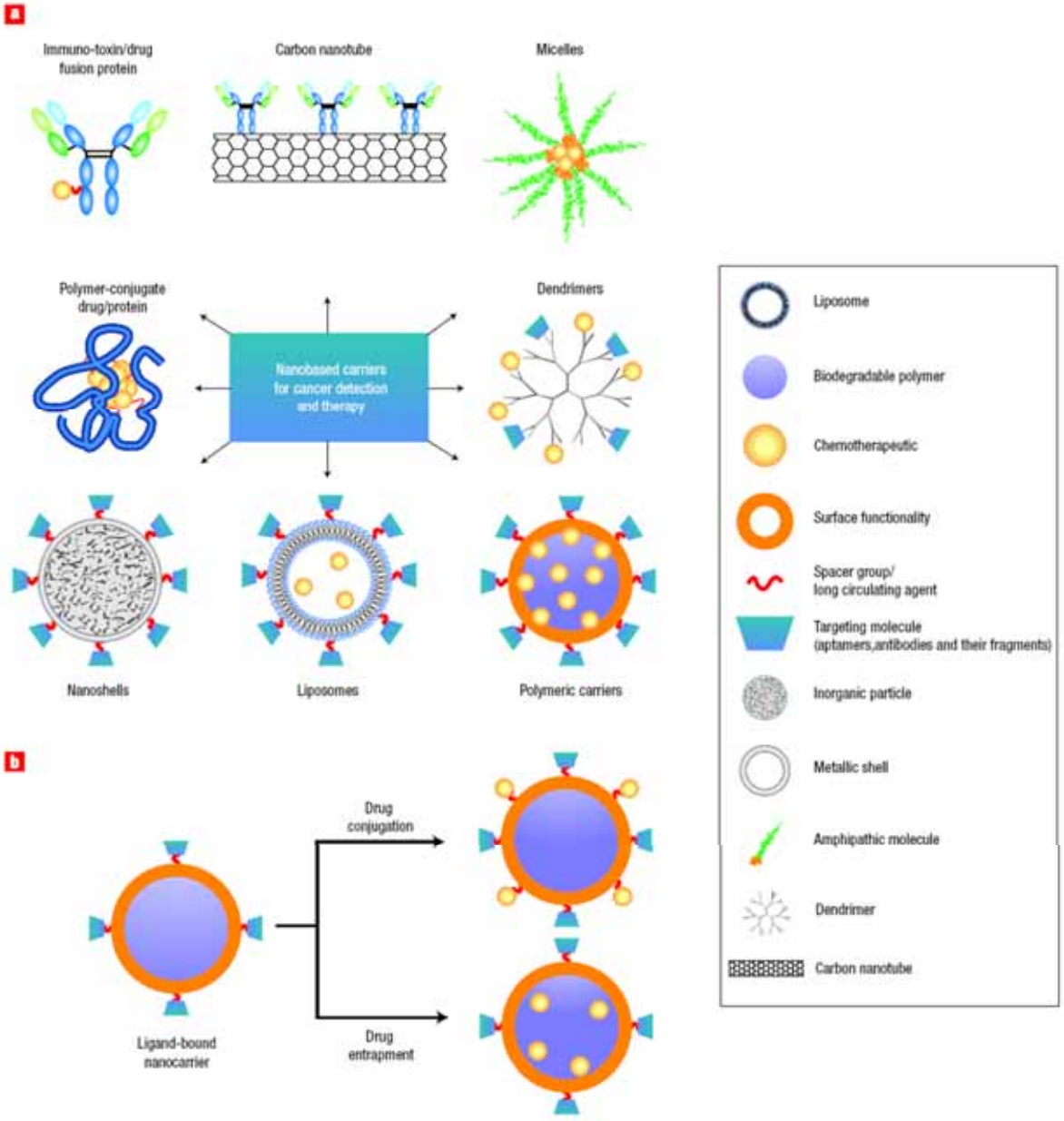

Figure 3 Examples of nanocarriers for targeting cancer. **a**, A whole range of delivery agents are possible but the main components typically include a nanocarrier, a targeting moiety conjugated to the nanocarrier, and a cargo (such as the desired chemotherapeutic drugs). **b**, Schematic diagram of the drug conjugation and entrapment processes. The chemotherapeutics could be bound to the nanocarrier, as in the use of polymer–drug conjugates, dendrimers and some particulate carriers, or they could be entrapped inside the nanocarrier.

Box 2 | **The proton-sponge hypothesis**

'Proton-sponge' polymers[104,114,119], including polyethylenimine (PEI) and polyamidoamine (PAMAM) dendrimers (FIG. 3), which contain a large number of secondary and tertiary amines, exhibit pK_a values between physiological and lysosomal pH. Endolysosomes are acidified by the action of an ATPase enzyme that actively transports protons from the cytosol into the vesicle. These polymers, therefore, undergo large changes in protonation during endocytic trafficking. It has been proposed that proton-sponge polymers prevent acidification of endocytic vesicles, causing the ATPase to transport more protons to reach the desired pH. The accumulation of protons in the vesicle must be balanced by an influx of counter ions. The increased ion concentration ultimately causes osmotic swelling and rupture of the endosome membrane, which releases the polyplexes into the cytosol (FIG. 4)[182].

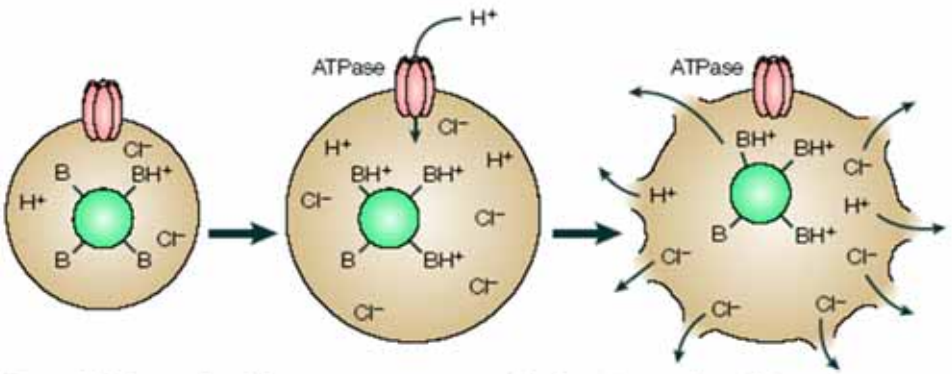

Figure 4 | **Schematic of the proton-sponge mechanism.** Protonation of the proton-sponge polymer (green) causes increased influx of protons (and counter-ions) into endocytic vesicles. Increasing osmotic pressure causes the vesicle to swell and rupture. See BOX 2.

Challenges for nanoparticles

- Escape from the reticulo endothelial system (RES)
  - Polyethylene glycol (PEG)
- Tissue penetration
- Targeting
- Delivered into cells